INFORMATION TO USERS

This manuscript has been reproduced from the microfilm master. UMI films the text directly from the original or copy submitted. Thus, some thesis and dissertation copies are in typewriter face, while others may be from any type of computer printer.

The quality of this reproduction is dependent upon the quality of the copy submitted. Broken or indistinct print, colored or poor quality illustrations and photographs, print bleedthrough, substandard margins, and improper alignment can adversely affect reproduction.

In the unlikely event that the author did not send UMI a complete manuscript and there are missing pages, these will be noted. Also, if unauthorized copyright material had to be removed, a note will indicate the deletion.

Oversize materials (e.g., maps, drawings, charts) are reproduced by sectioning the original, beginning at the upper left-hand corner and continuing from left to right in equal sections with small overlaps.

Photographs included in the original manuscript have been reproduced xerographically in this copy. Higher quality 6" x 9" black and white photographic prints are available for any photographs or illustrations appearing in this copy for an additional charge. Contact UMI directly to order.

Bell & Howell Information and Learning
300 North Zeeb Road, Ann Arbor, MI 48106-1346 USA
800-521-0600

THE COLLOIDAL AND LIQUID CRYSTAL PROPERTIES OF SURFACE MODIFIED CHITIN CRYSTALLITES

by

Jinjiang Li

A thesis submitted to the Faculty of Graduate Studies and Research in partial fulfilment of the requirements of the degree of Doctor of Philosophy

Department of Chemistry
McGill University
Montreal, Quebec, Canada

December 1996

This thesis is dedicated to my newborn daughter, Vivian Li.

"To say you know when you know, and to say you do not when you do not, that is knowledge."

From Lun yu (The Analects, 2.17)
by Confucius (551-479 B.C.)

ABSTRACT

Chitin crystallites were prepared from crab chitin using HCl hydrolysis. On average, the surface charge density of the chitin crystallites was calculated to be 0.5 e/nm^2 based on conductimetric titration data. The formation of a chiral nematic phase in aqueous suspensions of chitin crystallites and the *in situ* texture of the crystallite suspensions were investigated using polarised optical microscopy and freeze-fracture transmission electron microscopy. The effect of the interparticle electrostatic interaction on phase separation has been explored through phase diagrams and the interaction energy was calculated based on experimental zeta potentials. The flow properties of the liquid crystalline phases of chitin crystallites have been studied rheologically. Shear thinning behaviour and a two-regime flow curve were observed for isotropic suspensions and biphasic suspensions respectively. A typical three-regime flow curve for liquid crystalline polymers was found for the anisotropic suspension of chitin crystallites. The maximum in the viscosity- concentration curve was found at the phase transition concentration: isotropic to biphasic. Chitin crystallites were systematically deacetylated using NaOH hydrolysis. It was found that the reaction was pseudo first order. These modified crystallites are highly charged. Their phase behaviour contradicts the theoretical prediction by Stroobants et al. In addition, crystallites with a different extent of N-sulfonation were obtained in an aqueous medium using triethylamine/sulfur trioxide (TEA/SO_3) by controlling the TEA/SO_3 concentration used in the reaction. The colloidal behaviour of the suspension of the N-sulfonated crystallites was studied by plotting the zeta potential of the suspension as a function of the pH. Once the extent of N-sulfonation reached a certain level (80% or above), the chiral nematic phase formed while below this level only the nematic phase was observed. TEM studies showed that the crystallites were well dispersed when the extent of N-sulfonation was above 80%.

RÉSUMÉ

Des cristallites de chitine ont été préparés par hydrolyse à l'acide chlorhydrique en partant de la carapace de crabe. Une titration conductimétrique indique qu'en moyenne la densité de charge en surface était de 0.5 e/nm^2. En utilisant un microscope optique en lumière polarisée et la méthode de cryofracture pour examen par microscopie électronique à transmission (MET) on a pu observer la texture *in situ* de la phase chirale nématique formée à partir de suspensions aqueuses de cristallites de chitine. L'effet des interactions électrostatiques entre particules sur le phénomène de séparation de phase a été examiné et les énergies d'interactions ont été calculées à partir des potentiels zêta observés. Par rhéologie les effets de cisaillement sur les différentes phases des suspensions de cristallites de chitine ont été étudiés.

Les suspensions isotropes ont montré une baisse de viscosité par cisaillement, et les suspensions biphasiques des propriétés d'écoulement à deux régimes. La phase anisotrope, quant à elle, a produit une courbe d'écoulement à trois régimes typique des cristaux liquides de polymère. La courbe viscosité-concentration passait par un maximum à une concentration correspondant à la transition-de phase isotrope-biphasique.

Les cristallites de chitine ont été déacétylés par hydrolyse à la soude et la réaction s'est révélée être d'ordre *pseudo 1*. Les cristallites ainsi modifiés ont une charge plus élevée et leur séparation de phase en suspension aqueuse est en contradiction avec la prédiction théorique de Stroobants *et al.*

Des cristallites avec différents degrés de N-sulphonation ont été obtenus en milieu aqueux avec le triethylamine/trioxide de soufre (TEA/SO_3) à différentes concentrations. Le comportement colloïdal des suspensions de cristallites N-sulphonés a été évalué par le potentiel zêta en fonction du pH. Lorsque le degré de N-sulphonation atteint un certain niveau (80% ou plus) une phase nématique chirale a été observée alors que seulement une phase nématique se formait en dessous de ce niveau de sulphonation. Des observations par MET ont montré que les cristallites étaient parfaitement dispersés quand le degré de N-sulphonation était supérieur de 80%.

PREFACE

This dissertation was prepared according to article B2 of the Guidelines Concerning Thesis Preparation, McGill University, Montreal. This article is quoted as follows:

"Candidates have the option of including, as part of their thesis, copies of the text of a paper(s) submitted for publication, or the clearly duplicated text of a published paper(s), provided that these copies are bound as an integral part of thesis. If this option is chosen, **connecting texts, providing logical bridges between the different papers, are mandatory**.

-The thesis must still conform to all other requirements of the 'Guidelines Concerning Thesis Preparation' and should be in a literary form that is more than a mere collection of manuscripts published or to be published. **The thesis must include, as separate chapters or sections:** (1) a Table of Contents, (2) a general abstract in English and French, (3) an introduction which clearly states the rationale and objectives of the study, (4) a comprehensive general review of the background literature to the subject of the thesis, when this review is appropriate, and (5) a final overall conclusion and/or summary.

-Additional material (procedural and design data, as well as description of equipment used) must be provided where appropriate and in sufficient (eg. In appendices) to allow a clear and precise judgement to be made of the importance and originality of the research reported in the thesis.

-In the case of manuscripts co-authored by the candidate and others, **the candidate is required to make an explicit statement in the thesis of who contributed to such work and to what extent;** the supervisor must attest to the accuracy of such claims at the Ph.D oral defence. Since the task of the examiners is made more difficult in these cases, it is in the candidate's interest to make perfectly clear the responsibilities of the different authors

of co-authored papers"

This thesis has six chapters and three appendices. Chapter 1 is a general introduction providing background information for the thesis. Chapter 2, 3, 4, and 5 present the principal results of the research conducted. Each has been writen in a paper format, with an abstract, an introduction, an experimental, results and discussion, a conclusion, etc. The principles and experimental details of some techniques, the calculation of surface charge density, and the latest FF/FETEM results are described in the appendices.

The following publications were used in this thesis:

1. J. Li, J.-F., Revol, E. Naranjo, R. H. Marchessault, "Effect of electrostatic interaction on phase separation behaviour of chitin crystallite suspensions", *Int. J. Biol. Macrol.*, **18**, 177 (1996). Reprinted by permission of Elsevier Publisher.
2. J. Li, J.-F. Revol, and R. H. Marchessault, " Rheological Properties of Aqueous Suspensions of Chitin Crystallites", *J. Coll. Interface Sci.* **183**, 365 (1996). Reprinted by permission of Academic Press.
3. J. Li, J.-F. Revol and R.H. Marchessault, " Effect of Degree of Deacetylation of Chitin on the Properties of Chitin Crystallites" Accepted for publication by *Journal of Applied Polymer Science*. Reprinted by permission of John-Wiley publisher.
4. J. Li, J.-F. Revol and R. H. Marchessault, " Effect of N-sulfonation on the Colloidal and Liquid Crystal behaviours of Chitin Crystallites" Submitted to *J. Coll. Interface Sci.*

Paper # 1, #2, #3 and #4 are covered in Chapter 2, Chapter 3, Chapter 4, and Chapter 5 respectively. The experimental sections duplicated in papers were only described once based on the sequence that appear and in the following chapters they were refereed to the corresponding chapters.

ACKNOWLEDGEMENTS

I would like to thank my research director, Dr. R. H. Marchessault, for his direction and support during my Ph.D study at McGill, especially for making effort to correct my English. His availability for discussions and encouragement were greatly appreciated.

I also thank my co-director, Dr. J.-F. Revol of PAPRICAN, for many beneficial discussions and the TEM data used in this thesis.

I am very grateful to, Dr. Z. Xu of the Department of Mining and Metallurgical Engineering of McGill University, for encouraging me to engage in colloid science. The computer program for interaction energy calculation was kindly provided by him. I wish him a successful career at the University of Alberta.

The solid state NMR data provided by Dr. F. Morin is indispensable in this thesis. His help is appreciated.

Special thanks go to, Dr. E. Naranjo of the Department of Chemical and Nuclear Engineering of the University of California, Santa Barbara for providing freeze-fracture TEM data (Chapter 2) and Dr. H. Vali of the Department of Earth and Planetary Science of McGill University for conducting freeze-fracture and freeze-etch TEM (Appendix 3) for me.

My gratitude also goes to Dr. A. S. Perlin of McGill for helping me with the N-sulfonation reaction, Dr. Th. van de Ven of PAPRICAN for use of the rheometer and Mrs. S. Poulin of Ecole Polytechnique de Montreal for helping me with interpreting the XPS results.

I also wish to thank my friend, Geoff Nobes, for making this thesis more readable.

At last I would like to thank my wife, Donghua Pei, and my daughter, Fei Li, for support during my study.

TABLE OF CONTENTS

LIST OF FIGURES

LIST OF TABLES

LIST OF SYMBOLS AND ABBREVIATIONS

CN:	Chiral nematic.
TMV:	Tobacco mosaic virus.
TEM:	Transmission electron microscopy.
FFTEM:	Freeze-fracture transmission electron microscopy.
ϕ:	Volume fraction of isotropic phase.
C_i:	Phase boundary concentration for isotropic/biphasic transition.
C_a:	Phase boundary concentration for biphasic/anisotropic transition.
d:	Diameter of chitin crystallites.
L:	Length of chitin crystallites.
κ:	1/Debye length.
d_e:	Effective diameter.
L_R:	The effective repulsive layer thickness.
L_r^d:	Thickness of repulsive layer estimated from interaction energy curves.
m:	Increasing factor of diameter.
β:	Hypothetical linear charge density.
$\phi_{i,e}$:	Effective volume fraction.
Q:	Bjerrum length.
n_s:	Average number density of mobile ions.
z_p:	Univalent charge of the polyion.
c':	Poly ion concentration.
Γ:	Donnan salt exclusion coefficient.
LCPs:	Liquid crystalline polymers.

PBLG:	Poly-γ-benzyl-L-glutamate.
HPC:	Hydroxypropylcellulose.
S:	Order parameter:
D_{20}:	The diffusion coefficient of the suspension at 20°C.
d_e:	Equivalent spherical hydrodynamic diameter.
d_r:	Calculated hydrodynamic diameter of crystallites from D_{20}.
Glu-NH_2:	Glucose amino group.
α:	Degree of neutralization.
$\Delta\psi(\alpha)$:	Electrostatic potential difference between chitin crystallites and reference.
U:	A dimensionless concentration.
σ:	Surface charge density.
DD:	Degree of deacetylation.
SAG:	Surface amino groups.
XRD:	X-ray diffraction.
XPS.	X-ray photoelectron spectroscopy.
TEA/SO_3:	Triethylamine sulfur trioxide.
Pyr./SO_3:	Pyridine sulfur trioxide.
S/N:	N-sulfonated amino group/ amino group.
S_{2p}:	Sulfur 2p peak.
C_{1s}:	carbon 1s peak.
O_{1s}:	Oxygen is peak.
N_{1s}:	Nitrogen 1s peak.
ψ_s:	Surface potential.
τ:	Stress.
η:	Viscosity.
a:	Radius of particles.

E:	Electrical field strength.
V:	Velocity of particles.
F(κa, K'):	A factor depending a double layer thickness and particle shape.
μ:	Electrophoretic mobility of particles.
FF/FETEM	Freeze-fracture and freeze-etch transmission electron microscopy.

Chapter 1
GENERAL INTRODUCTION

1.0 INTRODUCTION

Chitin is a fibrillar crystalline polymer of N-acetylglucosamine which belongs to the family of structural polysaccharides, as shown in Fig. 1.1. Next to cellulose, with which it bears a structural resemblance, chitin is the second most abundant natural polymer (10^9 tons per year). Chitosan, N-deacetylated chitin, is a biodegradable and nontoxic polyelectrolyte. For commercial applications chitosan is defined as at least 75% deacetylated at which point it is soluble in dilute acetic acid.

1.1 HISTORICAL BACKGROUND

Braconnot (1), a professor of natural history in Paris, discovered chitin when he treated mushrooms with warm alkali in 1811. In 1823 Odier (2) isolated a KOH insoluble residue from insects which had a similar structure to that of plants and named this substance chitin from the Greek term χίτὼν (tunic, envelope). Following Odier, Children (3) in 1824 restudied this material, detected nitrogen to be present, and gave an empirical formula of $C_{11}H_{17}O_7N_2$ which was very close to that of the disaccharide fragment from chitosan ($C_{12}H_{22}O_8N_2$). It was Payen in 1843 (4) who started the scientific investigation of the structural difference between cellulose and chitin. In 1878 Ledderhose (5) indicated that chitin was composed of glucosamine, confirmed by Gilson (6), and acetic acid.

Chitosan was discovered in 1859 by Rouget (7) when he boiled chitin using concentrated sodium hydroxide. He named it "modified chitin". In 1894 Hoppe-Seyler reinvestigated this material and renamed it chitosan (8).

At the beginning of this century, the study of chitin mainly focused on the

Fig. 1.1. Structures of chitin, chitosan, and cellulose.

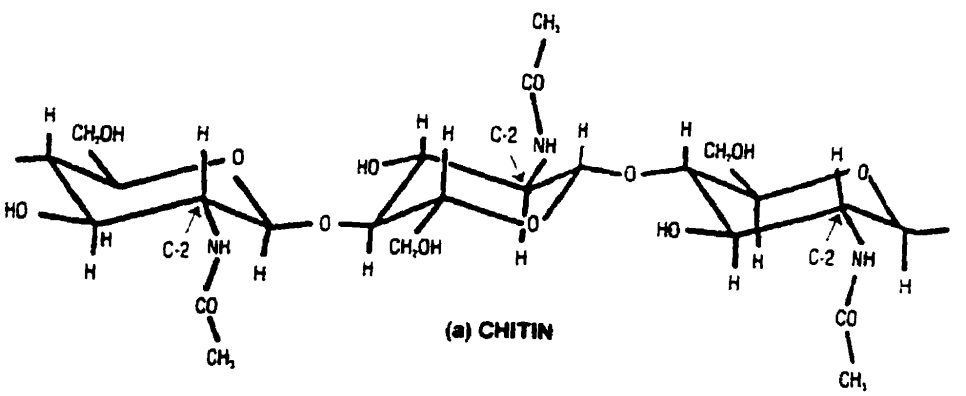

(a) CHITIN

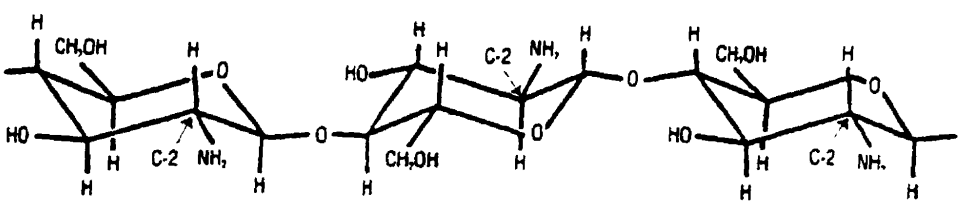

(b) CHITOSAN

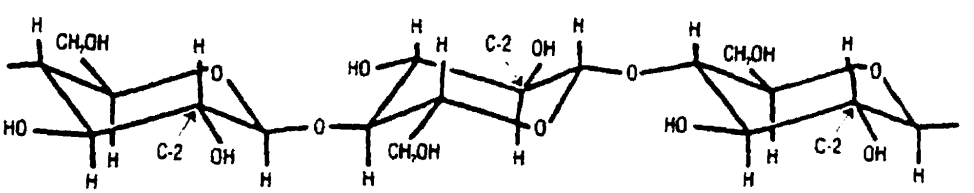

(c) CELLULOSE

occurrence and distribution of the chitinous structure in nature. The breakthrough in the investigation of the chitin structure came when X-ray diffraction and other physical techniques including infrared spectroscopy, NMR, etc. became available. X-ray diffraction is by far the most reliable method for determining the crystalline structure of chitin in cell walls (9). Polarized infrared analysis of the chitin structure by Marchessault et al. (10a, 10b) confirmed the chain conformation and the orientation of interchain amide H bonding. In the 1930s the first patent on producing chitin and chitosan was granted to G. W. Rigby (11), an employee of Du Pont de Nemours & Co. The first book on chitin focusing on biological aspects of chitin was published in the 1950s (12). Around the same time, chitosan was clearly described as a polymer of glucosamine. A comprehensive treatment on this subject was written by Muzzarelli in 1977 (13). With the exception of the 1940s, the number of published papers on chitin or chitosan has increased each decade since the 1930s. Recently, hundreds of papers per year have been published on this topic. A significant number of papers have described the bioapplications of chitin and chitosan, including medical, cosmetic, agricultural, and food-related uses. Industrial activities for chitin and chitosan production started in 1971, led by a Japanese company, Kyowa Oil & Fat Inc. (14). Now more than fifteen companies in Japan are producing chitin or chitosan related materials. In North America chitin and chitosan are produced by several companies including Protan, FMC, Vanson, etc. (14). Although not all chitin is accessible, the abundance of chitin and its unusual properties are factors underlying current interests in developing its commercial potential.

1.2 NATURAL DISTRIBUTION AND PRODUCTION OF CHITIN

1.2.1 DISTRIBUTION

Chitinous structures are widely distributed in nature in marine crustaceans, freshwater arthropods, fungi, algae, etc. They are biosynthesized by invertebrates in

freshwater (arthropods, bryozoans and zooplanktons in eutrophic stagnant water) and by zooplanktons in sea water including copepods, cladocera, mysidaceas, etc. (see Table 1.1). Chitinous structures also exist in molds, fungi, and the cell wall of yeasts (15).

TABLE 1.1 Chitin Production by Some Natural Communities (16)

Community	Chitin production ($g.m^{-2}.year^{-1}$)
Sea water	
Krill (Atlantic Ocean and North Sea)	0.0045
Zooplankton (Calvi Bay, Mediterranean Sea)	1.0014
Benthic communities (Calvi Bay, Mediterranean Sea)	
Depth:-----6 m	0.23
-----18m First year	0.30
Second year	1.00
-----37m	0.34
Spiny Lobster population (Natal Coasts)	1.5
Fresh Water	
Arthropods, eutrophic lake, Japan	51.0
Plankton (Daphnia) eutrophic lake	
----- Holland	0.13-0.30
----- Denmark	3.2
Bryozoans (Plumatella)	21.0

Chitin production is highest in eutrophic freshwater. Bryozoan colonies in organopolluted waters can have a chitin production of about 20 g m^{-2} $year^{-1}$ (17). In freshwater, arthropods are the main chitin producers, with a chitin production of 51 $g.m^{-2}.year^{-1}$ (18).

In marine environments, cladocerans are reported to have a chitin content of 12.22% dry weight (19). The surface zooplankton of the Mediterranean sea is another rich source for chitin. In addition, chitin is produced by crustaceans including North Atlantic ocean krill, crab, shrimp, etc. which belong to the marine benthic communities.

Production of chitin through fermentation is suggested by some researchers to compensate for the seasonal fluctuation of chitin production (20, 21, 22).

1.2.2 SUPPLY OF CHITIN FROM SHELLFISH WASTE AND OTHER SOURCES

The current availability of chitin for industrial uses relies on shellfish waste which depends on the size of the crustacean catch including crab, shrimp, lobster, etc. It is estimated that 1.2×10^5 metric tons of chitin are annually accessible from shell waste on a world wide basis (23), see Table 1.2. It is also estimated that fungi could provide 3.2×10^4 metric tons of chitin annually (23). Some values for chitin concentrations in the mycelia of fungi are given in Table 1.3.

The U.S. has the largest crustacean catch in the world. Shrimp canning plants in the U. S. generally process from 9000 to 18000 kg of raw shrimp per day (19). The Soviet Union was the largest catcher of king crab. Japan is in second place in crustacean catch with a chitin production of 1270 tonnes (24). Polish deep sea fisheries have been engaged in harvesting marine living resources containing chitin (Antarctic krill and squid) since 1975. Approximately 150 kg of chitin per day can be isolated from the shell waste of 5 tonnes of processed krill meat which corresponds to 20-30 tonnes of krill caught by Poland. A total of 357,538 tonnes of Antarctic krill were

TABLE 1.2 Chitin from U.S. Crab and Shrimp Processing Waste and Global Estimates of Potential Chitin Sources

Product	Dry Waste (10^3 tons) Worldwide	Dry Waste (10^3 tons) U. S	Chitin (10^3 tons) Worldwide	Chitin (10^3 tons) U. S.
Shellfish	154		39	
Crab		17		6
Shrimp		78		39
Krill	801		56	
Clam/Oyster	482		22	
Squid	21		1	
total	1458	95	118	45

TABLE 1.3 Relative Amount of Chitin in the Mycelia of Various Fungi

Fungus	Chitin Content (%)
Mucor Rouxii	9.4
Aspergillus Niger	42
Aspergillus phoenicis	23.7
Neurospora Crassa	8.0-11.9
Penicillium chrysogenum	19.5-42
Trichoderma Viridis	12-22
Saccharomycapsis Gutulata	2.3
Blastomyces Dermatitidis	13
Histoplasma capsulatum	25.8
Histoplasma Farciminosum	40
Tremella Mesenterica	3.7
Paracoccidioides brasiliensis	11

caught in southern oceans during the 1990/1991 season. Using the above chitin recovery figure, the practical yield of chitin from krill is between 1788 and 2145 tonnes (24). In addition, Poland harvests up to 100,000 tonnes of squid with a chitin concentration of 40% in the squid pen.

1.3 BIOSYNTHESIS OF CHITIN IN NATURE

The biosynthesis of chitin involves the enzymes, chitin synthetase and deacetylase. The main process of chitin microfibril formation is a transmembrane event (25a). Polymerization and crystallization are the central themes of the process. The synthesis of chitin molecules takes place in chitosomes, which are subcellular organelles, followed by crystallization after secretion (see Fig. 1.2). Rapid crystallization prevents deacetylation and degradation. The pathway of chitin biosynthesis is shown in the *schematic* below, where several enzymes are shown to take part in the biosynthesis together with chitin synthetase, whose official name is uridinediphosphate-2-acetamido-2-deoxy-D-glucose:chitin-4-β-acetamidodeoxyglucosyl transferase [*E.C. 2.4.1.16 (26a)]. It is known that uridinediphosphate-N-acetyl-D-glucosamine (UDPGLcNAc) is the precursor of native chitin in both arthropods and fungi (26b). For arthropods, the epidermal cells have the most important function as they are capable of synthesizing all precursors of chitin, from glucose to uridine diphosphate-N-acetylglucosamine (27). The slight damage of epidermal cells leads to a cessation of biosynthesis. For fungi such as *Mucor rouxii*, N-acetylglucosamine, soluble chitodextrins, N-acetyl-chitodextrins, mannose, glucose, etc. are activators (28).

*E. C. Stands for enzyme commission.

Fig. 1.2. Model depicting the spatial regulation of chitin and chitosan biosynthesis, and three different fates for chitin synthesized at the cell surface of *Mucor rouxii*: Left. Chitin microfibril produced by a tight assembly of chitosome 16 S subunits. Rapid crystallization would prevent the action of deacetylase or chitinase. Middle. Free chitin chains produced by dissociated chitosomes subunits would be highly susceptible to deacetylation. Right. Free chitin chains would be similarly susceptible to degradation by chitinases (25b).

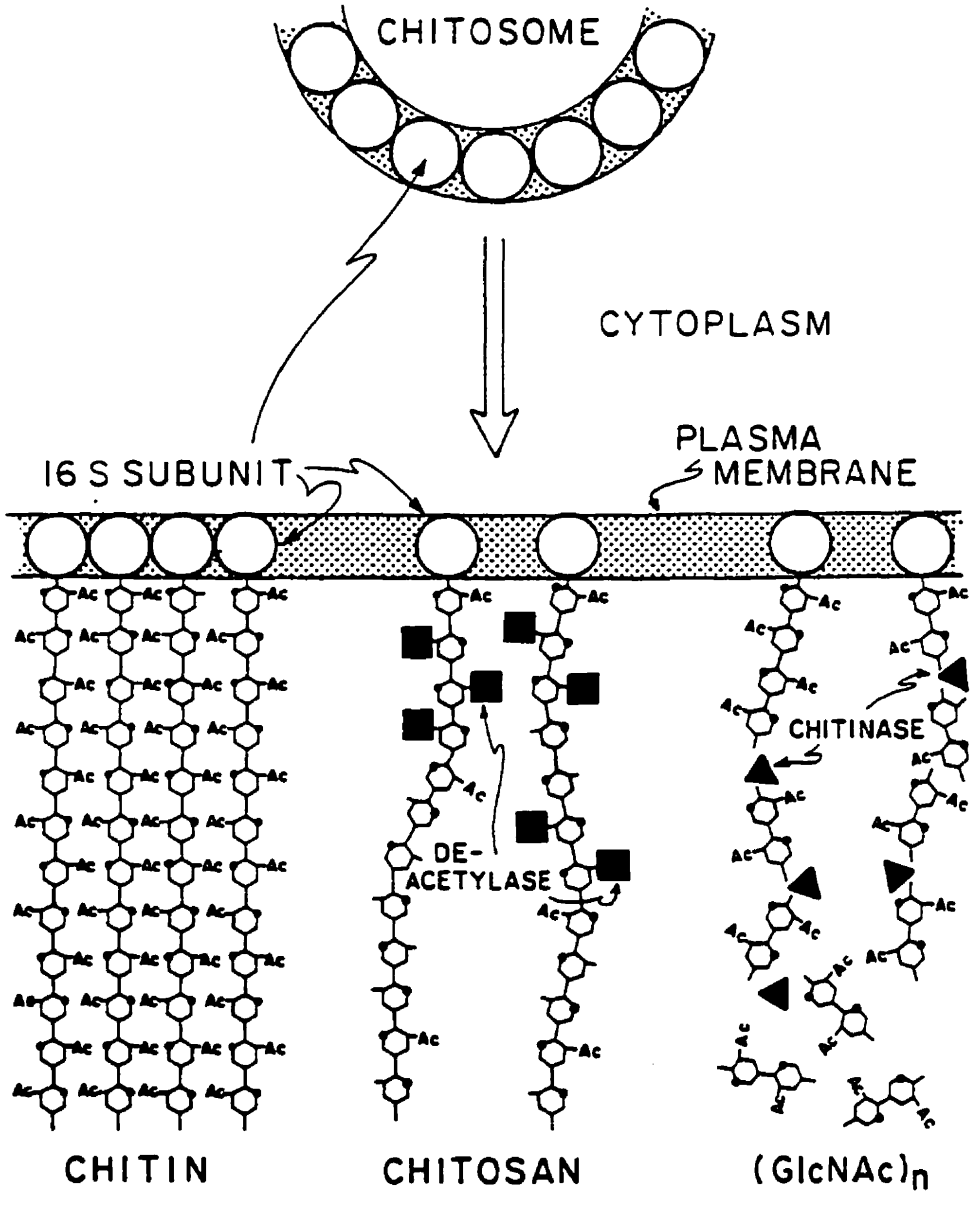
CHITOSOME
CYTOPLASM
PLASMA MEMBRANE
16 S SUBUNIT
CHITINASE
DE-ACETYLASE
CHITIN
CHITOSAN
(GlcNAc)n

Schematic of the Pathway of Chitin Biosynthesis (13)

Trehalose in blood
↓
Glucose
↓ (hexokinase)
Glucose 6-phosphate
↓ (glucose phosphate isomerase, [E. C. 5.3.1.9])
Fructose 6-phosphate
(glutamine-fructose 6-phosphate aminotransferase,
←glutamine [E. C. 2.6.1.16])
→glutamic acid
↓
Glucosamine 6-phosphate
(phosphoglucosamine transacetylase)
←acetyl-Co-A
→Co-A
↓
N-acetylglucosamine 6-phosphate
↓ (phosphoacetylglucosamine mutase)
N-acetylglucosamine 1-phosphate

←UTP (pyrophosphorylase, [E.C.2.7.7.23])
→pyrophosphate
↓
Uridinediphosphate N-acetylglucosamine
(chitin synthetase [E. C. 2.4.1.16])
(chitin synthetase activating factor [E. C. 3.4.22.9])
(and chitin deacetylase)
→UDP
↓
Native chitin (partially deacetylated chitin

*E. C. stands for *enzyme commission.*

1.4 PREPARATION OF CHITIN AND CHITOSAN

Currently all the chitin produced commercially is derived from the shell waste of crab, shrimp and exoskeletons although chitin is widely distributed in nature. Preparation of chitin frequently involves deproteinization using NaOH, demineralization with HCl, and decolouration using acetone. The process schematic is shown below.

SHELLFISH WASTE
↓
GRINDING
↓
DEPROTEINIZATION (5% NaOH)
↓
WASHING
↓
DEMINERALIZATION (2% COLD HCl)
↓
WASHING
↓
DRYING
↓
CHITIN
↓
DEACETYLATION (50% HOT NaOH)
↓
WASHING
↓
DRYING
↓
CHITOSAN

Schematic for Chitin and Chitosan Production Process

A variety of bases including NaOH, Na_2CO_3, $NaHCO_3$, KOH, K_2CO_3, $Ca(OH)_2$, $NaHSO_3$, $CaHSO_3$, etc. are used for deproteinization of shell waste. However, NaOH is the preferred agent in industry. Table 1.4 shows the conditions of deproteinization of shell waste using NaOH. The mildest alkaline treatment reported so far is the use of Na_2CO_3 at concentrations of up to 0.1 M, together with soap, at 100 °C for 4 hours (29); the most severe is treatment of lobster shell with 5 M NaOH at 100 °C for 4 hours (30).

TABLE 1.4 Conditions Employed for Deproteinization of Chitin-containing Waste

Material Source	NaOH Concentration	Temperature (°C)	# of Treatment	Total Time	Ref.
Shrimp	0.25 M	65	1	1 h	31
Crab	0.5 M	65	1	2 h	32
Prawn	0.125 M	100	1	0.5 h	33
Prawn	0.75 M	100	1	NS	33
Krill	0.875 M	90-95	1	2 h	34
Crab	1.0 M	80	1	3 h	35
Crab	1.0	100	1	36 h	36
Lobster	1.0 M	100	5	60 h	37

NS = Not stated in the reference

Demineralization of shell waste using a variety of acids including HCl, HNO_3, H_2SO_4, CH_3COOH and HCOOH was reported in early patents (11, 29). However, most researchers in this field have used HCl for acid demineralization. Conditions vary according to the source of the shell waste and the individual laboratory (see Table 1.5). Extraction using EDTA at alkaline pH has been used as a non-degradative demineralization process (36).

TABLE 1.5 Conditions Employed for Demineralization of Chitin-containing Waste

Material Source	HCl Concentration	Temperature (^{0}C)	Treatment Time (h)	References
Shrimp	0.275 M	RT	16	11, 29
Shrimp	0.5 M	NS	NS	31
Krill	0.6 M	RT	2	34
Crab	0.65 M	RT	24	39
Crab	1.0 M	RT	NS	40
Prawn	1.57 M	20-22	1-3	41
Lobster	1.57 M	RT	11-14	42

RT = Room temperature.

NS = Not stated in the reference.

The exoskeletons of crustacea contain colored matter, principally carotenoids, with the main components being: astacene, astaxanthin, canthaxanthin, lutein and β-carotene (43). These carotenoids can be removed by extracting the shell with acetone or ethanol. In addition, warm 50% acetic acid can demineralize and extract the carotenoids at the same time. Common bleaching reagents destroy the colored matter (29).

Chitosan is produced by deacetylation using alkali (KOH) fusion at high temperature or a concentrated (40-50%) solution of sodium hydroxide at high temperature (100-150°C), excluding air, for about an hour (44). Although complete deacetylation is rarely achieved, highly deacetylated chitin with high molecular weight is usually obtained by intermittently washing the intermediate product in two or more changes of water during the alkali treatment.

In addition, deproteinization of crustacean shells has been achieved using enzymes. Proteolytic enzymes including bacterial proteinase, tuna proteinase, trypsin, papain, etc. were tested by Takeda and Abe (45), Takeda and Katsuura (46), and Broussignac (47) for deproteinization of crustacean shells for production of chitin. The protein level falls to 5% after enzymatic treatment. More recently, Shimahara and Takiguchi (48) used a bacterial protease from *Pseudomonas maltophilia* to treat crustacean shells and observed that after 24 h, the protein content remaining in the shell was only about 1%.

The biosynthesis of chitosan was discovered in microorganisms including *Mucor rouxii*, *Phycomyces blakesleeanus*, etc. (49). The yield of chitosan from these microorganisms is around 30%. Chitin deacetylase was first isolated from *Mucor rouxii* by Araki and Ito (50). This enzyme is active on a glycol chitin and the activity decreased significantly when colloidal chitin and powdered chitin were used as substrates. Recently chitin deacetylase isolated from *Mucor rouxii* was characterized by Kafetzopoulos et al. (51,52).

1.5 PHYSICAL AND CHEMICAL PROPERTIES OF CHITIN AND CHITOSAN

1.5.1 POLYMORPHISM

Chemically, chitin is very similar to cellulose except that the C(2) hydroxyl group of cellulose (Fig. 1.1) is replaced by an acetamido group. Investigation of the structure of chitin has mainly benefited from the structural study of cellulose. Three kinds of polymorphic forms of chitin occur in nature: α-chitin, β-chitin, and γ-chitin. The most abundant is α-chitin, which differs from β-chitin and γ-chitin in the crystalline arrangement of the chains, see Fig. 1.3. α-chitin, the most stable form, has been extensively studied owing to its commercial availability. β-chitin can be converted to α-chitin in 6 N HCl (53a, 53b). The x-ray diffraction study of α-chitin was first reported by Gonell (54), followed by Meyer and Mark (55). However, the generally accepted structure for α-chitin is that presented by Carlstrŏm in 1957 (56). The unit cell of chitin is orthorhombic with a = 4.76Å; b=10.28Å; c=18.85Å, see Fig. 1.4. The fiber repeat distance b is nearly identical to that of cellulose. A major difference in the structure proposed by Carlstrŏm, compared with previous chitin models, is that it is based on a "bent" chain conformation, similar to that proposed by Hermans et al. for cellulose (57). According to Carlstrŏm, the straight chain structure for cellulose, and by analogy for chitin, is unlikely owing to steric hindrance and energetic factors. Furthermore, the bent chain gives a O(3)'···O(5) distance of 2.68 Å, suitable for the formation of an intramolecular hydrogen bond, and a repeat distance along the fiber axis of 10.28 Å which suitably models the x-ray diffraction results. The results of other studies in the following 20 years generally agree with Carlstrŏm's model.

1.5.2 CHEMICAL PROPERTIES

1.5.2.1 ACID AND BASE PROPERTIES OF CHITIN AND CHITOSAN

The dissociation constant of an amine group, K_b, is shown in Eq.1.2,

$$-NH_2 + H_2O \rightleftharpoons NH_3^+ + OH^- \tag{1.1}$$

$$K_b = \frac{[-NH_3^+]\,[OH^-]}{[-NH_2]} \tag{1.2}$$

while the dissociation constant of the conjugate acid is expressed as:

$$-NH_3^+ + H_2O \rightleftharpoons NH_2 + H_3O^+ \tag{1.3}$$

$$K_a = \frac{[-NH_2]\,[H_3O^+]}{[-NH_3^+]} \tag{1.4}$$

For chitosan, which is a polyelectrolyte, K_a is surface charge dependent since the ease of dissociation of the conjugate acid group, NH_3^+, will be increased by the presence of the adjacent $-NH_3^+$ group, thereby increasing K_a and decreasing pK_a. For polyelectrolytes, the pK_0, which is the pK_a at zero charge density, is considered to be the intrinsic pK_a. The pK_a of chitosan is reported to be 6.2. A study by Domard (58) shows that the pK_0 for chitosan is 6.5.

1.5.2.2 SOLUBILITY

Chitin is insoluble in most organic solvents due to its intermolecular and intramolecular hydrogen bonding. However, it is soluble in some neutral salts such as hot CaX_2 (X:F, Br, Cl, I) and LiCNS. Chitin can also be dissolved in concentrated HCl,

Fig. 1.3. Different packing arrangements of the polymer chains of α-chitin, β-chitin, and γ-chitin. Such macromolecules can be: antiparallel, parallel, etc.

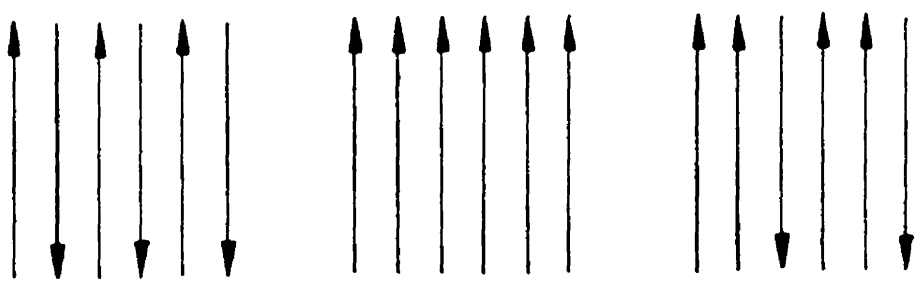

α-chitin β-chitin γ-chitin

Fig. 1.4. The structure of α-chitin proposed by Carlstrŏm. Dotted lines represent the intramolecular hydrogen bonding and interchain hydrogen bonding (13, 56).

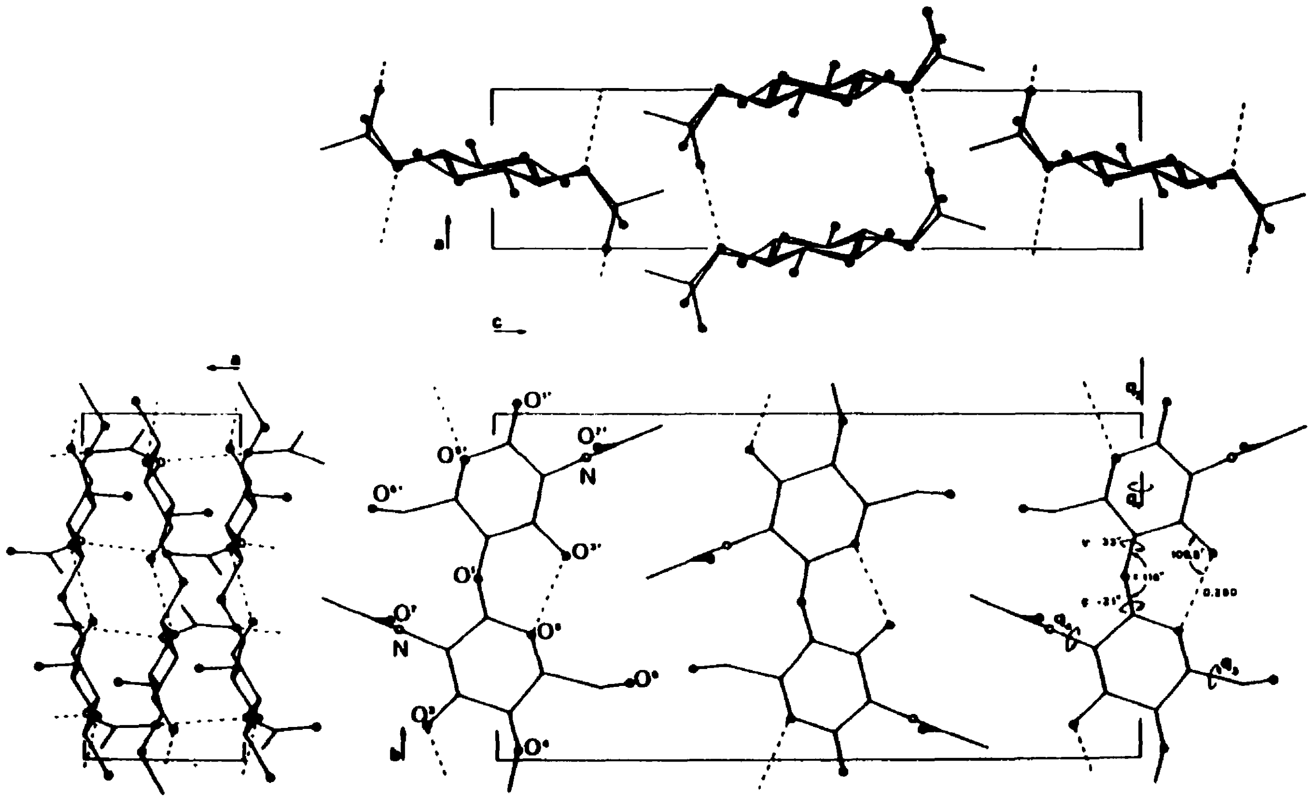
a
c
a
b
N
N
0.280

H_2SO_4 and H_3PO_4, and in some organic acids including formic acid, dichloroacetic acid (DCA), trichloroacetic acid (TCA), etc. However, degradation accompanies dissolution in mineral acids. As for organic solvents, chitin is soluble in a dimethylformamide-N_2O_4 mixture and other systems such as dimethylacetamide-LiCl. Chitosan is soluble in most acids including dilute HCl, HBr, HI, H_2SO_4, carboxylic acids, benzenesulphonic acid, etc.

1.5.2.3 CHELATING PROPERTY

Chitosan is a very effective chelating agent due to the presence of amino groups in its structure. The capacity of forming a complex with metal ions depends on the physical state of chitosan and the oxidation state of metal ions. As a general rule, chitosan forms a complex with transition and post transition metal ions, but does not form a complex with alkali metal ions (59). The adsorption of metal ions by chitosan usually increases with degree of deacetylation (DD) for samples with DD below 60% although the capacity of adsorption depends on the pH and the individual metal ion (60). In spite of the controversy about the structure of the chitosan-metal ion complex, most researchers agree that $-NH_2$ complexes with the metal ion in 1:1 ratio such as the structure proposed by Domard (61).

1.5.2.4 ADSORPTION PROPERTY

Both chitosan and chitin are good substrates for the adsorption of dyes, proteins, aromatic hydrocarbons, and other chemical substances. Giles and co-workers (62) were the first to study the uptake of dyes on chitin. They found that the amount of dye adsorbed depended upon the pH of the suspensions and the molecular weight of the dye. The mechanism of adsorption is as follows:

$$Chi\text{-}NH_3^+X^- + Dye\text{-}SO_3^- \rightleftharpoons Chi\text{-}NH_3^+{}^-O_3S\text{-}Dye + X^- \qquad (1.5)$$

Additional dye ions may be adsorbed through other attractive forces: van der Waals's

force, hydrophobic interaction and hydrogen bonding, depending on the nature of the dye ions. Hackman (63) was the first to demonstrate that chitin can adsorb proteins from aqueous solution. His results indicated that the maximum adsorption occurred at the isoelectric point of the protein. At a given pH, the extent of adsorption decreases with an increase in the ionic strength of the solution. The ability of chitin to adsorb proteins has application in affinity chromatography. Giles and Hassan (64) found that phenol and resorcinol are readily adsorbed on chitin from aqueous solution, in contrast to their non-adsorption on cellulose. The authors concluded that the adsorption from aqueous solution involves hydrogen bonding between phenolic and aminoacetyl groups. Other compounds such as aromatic sulphonic acids, etc. also adsorb on chitin.

1.6 SELF-ASSEMBLY OF CHITIN IN NATURE AND BIOMIMICRY

1.6.1 SELF-ASSEMBLY OF CHITIN IN NATURE

In fungal cells, chitin is associated with other polysaccharides, while in animal forms it is associated with proteins (65). Except in fungi and molds, the chitinous structure is built of a glycoprotein framework, in which chitin is probably covalently linked to proteins. The proteins present in animals are cross-linked by a sclerotization process which is initiated in the cuticle by a phenoloxidase catalyzed oxidation of diphenolic substrates yielding the corresponding O-quinonemethide as a reactive intermediate (66). The chitin-protein complexes can be complemented by the deposition of other substances, such as waxes and lipoproteins, giving the structure impermeability. The chitin-protein complexes provide a framework for mineralization including calcification and silicification.

The chitin-protein complex is morphologically well organized (67). The macromolecular chains of chitin line up in parallel to form a microfibril. The typical size of a microfibril (crystallite) is approximately 3 nm in diameter, consisting of 19 molecular chains hydrogen-bonded in parallel according to Neville. Then, a bundle of such

microfibrils forms a sheet followed by formation of a helicoidal stack layer of microfibrils, see Fig. 1.5. Each layer of crystallites is oriented in a sheet of chains in parallel, thus the direction of the crystallites changes through a small angle from layer to layer in a constant direction of rotation. This was proved by the TEM observation of the arcing pattern from obliquely cut crab shell, see Fig. 1.6. How are large insoluble molecules manipulated precisely into position outside the cells making them? Development of the structure through a mobile phase was proposed by Neville (67). This idea involves two further concepts (1) the matrix is envisaged as self-assembling, and (2) it passes through a liquid crystalline phase to form a plywood arrangement followed by solidification. The orientation of the microfibrils has been proposed to be controlled through three mechanisms:(1) remote control by extracellular self-assembly of a succession of fibre angle changes, giving rise to a helicoid, (2) direct cellular control of a precise fibre direction by directed assembly, (3) reorientation of oriented fibers caused by some physiologically derived forces.

1.6.2 BIOMIMICRY

Biomimicry means to copy biological processes or organizations synthetically. The similarities between the structures in an insect cuticle and in liquid crystals were realized independently by Robinson and Neville. Robinson (68) observed the similarity in optical properties between the two systems and Neville (69) compared the helicoidal structures in both systems. In spite of architectural similarities, the difference between the two systems is that the biological system is made of crystallites whereas the liquid crystals consist of

Fig. 1.5. Diagrams of helicoids and patterns of sections they produce taken from Neville (67): (A) Diagram of a helicoidal stack of microfibril layers. (B) A ranked pattern of nesting arcs generated by the oblique section shown in part A, each part of microfibril is represented by a single line. (C) Another representation of a helicoidal structure.

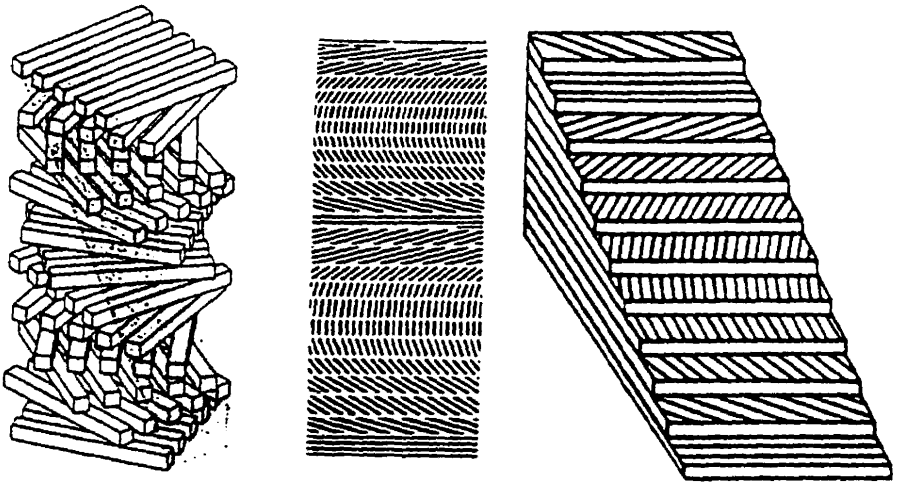
(A)
(B)
(C)

Fig. 1.6. A electron micrograph showing arcing pattern observed in a crab sample (67).

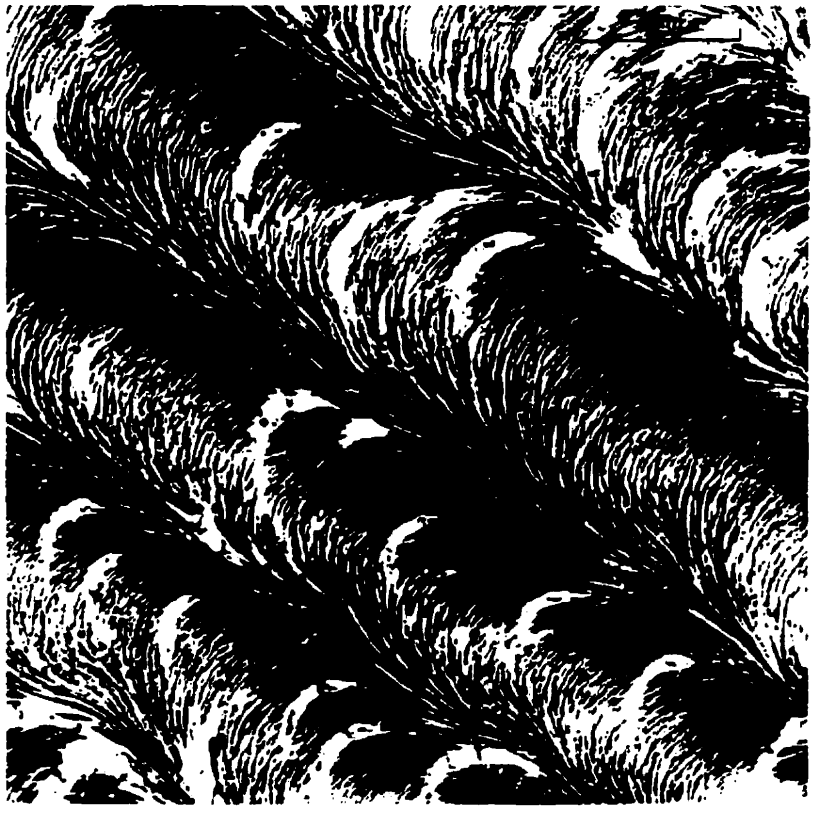

molecular chains.

Liquid crystals represent a fourth state of matter,with properties between those of liquids and solids. There are three different kinds of liquid crystals: nematic, smectic, and chiral-nematic. Chiral nematic, which is regarded as twisted nematic, is also called cholesteric. The factors affecting the self-assembly of chiral-nematic liquid crystals are Brownian motion, the presence of an asymmetric carbon, and the attempt to achieve the lowest free energy. Self-assembly is comparable to crystallization in many respects. Both processes are spontaneous and proceed toward a state of lower free energy, hence toward a structural stability. The difference between the two processes is that crystallization is driven by enthalpy, by a decrease in the heat emitted; self-assembly is entropy driven, by an increase in disorder, usually by the exclusion of ordered water. The theoretical foundation for the formation of nematic liquid crystals was laid down by Onsager (70). Based on a minimization of the Gibbs free energy of the system, Onsager concluded that the critical concentration for the formation of the nematic phase depends on both the axial ratio and the ionic strength. Stroobants (71) extended Onsager' theory by including another factor; the twisting effect due to electrostatic repulsive forces. Examples of biomolecular liquid crystals include hydroxylpropyl cellulose, poly-γ-benzyl-L-glutamate in m-cresol, etc.

Nematic liquid crystals of cellulose and chitin crystallites were first observed to form in concentrated suspensions by Marchessault et al.(72). Recently, formation of a chiral-nematic phase from the suspension of chitin crystallites was found by Revol and Marchessault (73), who prepared suspensions of chitin crystallites by hydrolysing chitin using HCl hydrolysis. An arcing pattern similar to that observed in crab cuticles was observed by TEM after slowly drying the chiral-nematic phase of the crystallites to a film.

1.7 APPLICATIONS

There is an emerging interest in using chitin and chitosan industrially because they are biodegradable and biocompatible. Chitin and its derivative, chitosan, are now widely used as cosmetic additives, food additives, suture materials, etc. In the personal care industry, there is a need for inexpensive polymers to be used as gelation agents, viscosity modifiers, suspension stabilizers, etc. Currently Karaya gum, guar gum, alginate, carrageenin, xanthan gum, cellulose ethers, etc. are used in industry (74). The derivatives of chitin can satisfy many of these applications.

1.7.1 FOOD SCIENCE

In the food industry, chitin can be used as an additive or filler for animal feed that results in normal growth and vigour of the animals. In the food processing industry, chitosan is used to recover proteins from food processing waste. Chitosan can reduce protein suspended solids by 70-98% which replaces traditional electrolytes (75).

1.7.2 BIOTECHNOLOGY

In biotechnology, chitosan is used for immobilizing enzymes and for encapsulation of mammalian cell cultures based on the electrostatic interactions of chitosan as a polycation with other polyanions. FMC Bioproducts Inc. is supporting a study of an encapsulation method that employs chitosan (14). Cells, seeds, or protoplasts are entrapped within chitosan beads, after which the individual chitosan beads are coated with alginate. The chitosan is then dissolved, leaving behind a porous alginate capsule.

1.7.3 FIBER TECHNOLOGY

Von Weimarn (76) first reported that solutions of chitin can be formed into a "ropy-plastic" state in 1926. These solutions were based on readily soluble salts capable of strong

hydration. In order of ease of solubility of chitin, they are:

$$LiCNS > Ca(CNS)_2 > CaI_2 > CaBr_2 > CaCl_2$$

In 1939 Thor and Henderson (75) were first to form fibers from chitin xanthates but no characterization was reported. In 1975 Brine and Austin (78) used trichloroacetic acid (TCA) as a chitin solvent to make fibers. A filament was extruded from a chitin solution of TCA (40%) , chloral hydrate (40%), and methanol (20%) using a hypodermic needle and acetone as the coagulant followed by neutralization with KOH and washing. The tensile strength and breaking elongation were reported to be 72 kg/mm^2 and 13% respectively. Fuji Spinning Company (79) dissolved chitosan in a mixture of water and dichloroacetic acid (DCA). The dope was extruded through a platinum nozzle into a basic $CuCO_3$-$(NH_4)OH$ solution to form fibers. Other solvents including hexafluoroisopropyl alcohol, hexafluroacetone sesquihydrate, and dichloromethane in novel halogenated solvent spin systems were tried for making fibers of chitin. Rutherford and Austin (80) suggested the amide-LiCl system for making fibers of chitin which produced the best dry tenacities although wet tenacity was lacking. Unitika (cf. ref. 2 in Chapter 2) produced its artificial skin from a wet-spinning process based on this system.

1.7.4 AGRICULTURE

The yield of crops including wheat, corn, oats, etc are reported to increase 10-50% when their seeds are treated with chitosan (14). Chitin is used as a nematocide for plants such as cotton, vegetables, orchard trees, etc. because chitin can stimulate the growth of the soil microorganisms including actinomycetes and bacteria which produce chitinase and other enzymes, and these enzymes destroy the eggs of plant pathogenic nematodes.

1.7.5 ENVIRONMENTAL TREATMENT

Chitosan's metal-binding and flocculating properties are useful in the treatment of

drinking water, pools and spas, food processing waste, and other waste streams. A combination of activated carbon and chitosan can be used to purify drinking water (14). Chitosan has two effects: removing organics and chelating heavy metal ions. Chitin derivatives can also flocculate suspended materials including oils, soaps, dirt, and plaster dust from water which is useful for cleaning up pools, ponds, lakes, and other bodies of water. The most successful application of chitosan is the recovery of metals including iron, copper, nickel, cobalt, silver, etc. from electroplating waste.

1.8 FUTURE PERSPECTIVES

Chitin and chitosan as potential materials have increasingly attracted researchers' interests from other disciplines. Currently, research on molecular biological aspects including isolating, sequencing and cloning chitinase, chitin deacetylase, and chitosanases, etc. is very active. This trend will continue. From a materials perspective, the effort to find more applications for chitin, chitosan, and other derivatives in medical science, biotechnology, and health science will be strengthened as more and more research is done in these areas. The potential for chitin and chitosan as environmentally-friendly materials is unlimited as the demand for more biodegradable materials grows.

1.9 THE OBJECTIVES OF THIS THESIS

Following the study of liquid crystals formed from chitin crystallites by Revol and Marchessault (73), this thesis will focus on the effect of electrostatics including surface charge, ionic strength, etc. on phase separation and the formation of anisotropic phases and the properties of the crystallites. In Chapter 2, the effect of the electrostatic forces on phase separation is evaluated through zeta potential measurements, free energy calculations, and freeze-fracture TEM. In Chapter 3, combined with a phase diagram, the rheological properties of crystallites in different phases are investigated under diferent

experimental conditions. In Chapter 4, chitin crystallites are modified using a deacetylation reaction and the phase separation of modified crystallites (high surface charge) is explored. In Chapter 5 the surface N-sulfation of chitin crystallites demostrates that when surface charge is changed from positive to negative, and the formation of an anisotropic phase is modified. Finally, the results and conclusions from biomimetic investigations are compared with the phenomena that occurs in nature (Chaper 6).

1.10 REFERENCES

1. Braconnot, H., *Ann. Chim. Phys.* **79**, 265 (1811).
2. Odier, A., *Mem. Soc. Hist. Nat. Paris* **1**, 29 (1823).
3. Children, J. G., *Zool. J.*, **1**, 101 (1824).
4. Payen, A., *Compt. Rend.*, **17**, 227 (1843).
5. Ledderhose, G., *Zeit. Physiol. Chem.*, **2**, 213 (1878).
6. Gilson, E., *Bull. Soc. Chim.* Paris **3**, 1099 (1894).
7. Rouget, C., *Compt. Rend.* **48**, 792 (1859).
8. Hoppe-Seyler, F., *Ber., Deut. Chem. Gesell.*, **27**, 3329 (1894).
9. Heyn, A. N. J., *Proc. Acad. Sci. Amsterdam*, **39**, 132 (1936).

10a. Marchessault, R. H. and Sarko, A., *Adv. Carb. Chem.*, **22**, 421 (1967).

10b. Pearson, F. G., Marchessault, R. H. and Liang, C. Y., J. Polymer Sci., **43**, 101 (1960).

11. Rigby, G. W., *U. S. Patent* 2,047,226 (1936).
12. Richards, A. G., *The Integument of Arthropods*, Univ. Minnesoda Press, Minneapolis (1951).
13. Muzzarelli, R. A. A., *Chitin*, Pergamon Press, New York (1977).
14. Technical Insight Inc., *Chitin and Chitosan; Specialty Biopolymers for Foods, Medicine, and Industry*, Ford Lee, NJ (1990).

15. Knorr, D., *Food Technology*, January, 114 (1991).

16. Jeuniaux, C., Voss-Foucart, M.-F., Poulicek, M. and Bussers, J.-C., in *Chitin and Chitosan; Sources, Chemistry, Biochemistry, Physical Properties and Applications, Proceedings from the 4th International Conference on Chitin and Chitosan*, pp 3, Ed. by Skjak-Braek, G., Anthonsen, T. and Sandford, P., Elsevier Applied Science, New York (1989).

17. Job, P., *Hydrobiol,* **12**, 257 (1976).

18. Yamamoto, H. and Seki,. H., *Water Air Soil Pollution*, **12**, 519 (1979).

19. Tetteh, A. Y., *Optimization Studies on Chitin Extraction from Crustacean Solid Waste,* pp 8, M.Sc Thesis, Department of Food Science and Agricultural Chemistry, McGill University (1992).

20. Bartnicki-Garcia, S. and Nickerson, W. J., *Biochim. Biophys. Acta*, **58**, 102 (1962).

21. Rane, K. D. and Hoover, D. G., *Food Biotechnology*, **7**(1), 11 (1993).

22. Knorr, D., Beaumont, M. D. and Pandya, Y., in *Chitin and Chitosan; Sources, Chemistry, Biochemistry, Physical properties and Applications, Proceeding from the 4th International Conference on Chitin and Chitosan,* pp 101, Ed. By Skjak-Braek, D., Anthonsen, T. And Sandford, P., Elsevier Applied Science, New York (1989).

23. Knorr, D., *Food Technology*, January, 114 (1991).

24. Nicol, S. and Hosie, G. W., *Biochemical Systematics and Ecology*, **21(2),** 181 (1992).

25a. Badet-Denisot, M.-A., Leriche, C. and Badet, B., in *Chitin Enzymology, Proceedings of the International Symposium on Chitin Enzymology*, pp 161, Ed. by Muzzarelli, R. A. A., Faculty of Medicine, University of Ancona,

IT-60100 Ancona, Italy.

25b. Bartnicki-Garcia, S., *in Chitin and Chitosan; Sources, Chemistry, Biochemistry, Physical Properties, and Applications, Proceedings from the 4th International Conference on Chitin and Chitosan*, pp23, Ed. by Skjak-braek, G., Anthonsen, T., and Sandford, T., Elsevier, New York (1989)

26a. Lunt, M. R. and Kent, P. W., *Bioch. J.* **78,** 128 (1961).

26b. Fevre, M., Gay, L. and Chanzy, H., *Modern Methods of Plant Analysis*, 17, 81 (1996).

27. Surholt, B., *J. Comp. Physiol.* **B-102**, 135 (1975).

28. Keller, F. A. and Cabib, E., *J. Biol. Chem.*, **246**, 160 (1971).

29. Du Pont de Nemours and Co., *UK Patent* 458, 839 (1936).

30. Clark, G. L. and Smith, A. F., *J. Phys. Chem.*, **40**, 863 (1940).

31. Wu, A. C. M. and Bough, W. A., *in Proceedings of 1st International Conference on Chitin/Chitosan*, pp 88, Ed. by Muzzarelli, R. A. A. and Pariser, E. R., MIT Sea Grant Program 78-7 (1977).

32. Muzzarelli, R. A. A., Tanfani, F., Emanuelli, M. and Gentile, S., *J. Appl. Biochem.*, **2,** 380 (1980).

33. Madhavan, P. and Ramachandran Nair, K. G., *Fishery Technol.*, **11**, 50 (1974).

34. Anderson, C. G., Pablo, N. De. and Romo, C. R., in ref 31, p. 54.

35. Mima, S., Miya, M., Iwamoto, R. and Yoshikawa, S., in *Chitin and Chitosan,* pp 21, Ed. by Hirano, S. and Tokura, S., The Japanese Society of Chitin and Chitosan (1982).

36. Shimahara, K., Ohkouchi, K. and Ikeda, M., in ref. 35, pp 10.

37. Hackman, R. H., Aust. *J. Biol. Sci.*, **7**, 168 (1954).

38. Foster, A. B. and Hackman, R. H., *Nature*, **180**, 40 (1957).

39. Broussignac, P., *Chim. Ind. Genie Chim.*, **99**, 1241 (1968).

40. Hackman, R. H. and Goldberg, M., *Carbohyd. Res.*, **38**, 35 (1974).

41. Moorjani, M. N., Achutha, V., Khasim, D. I., *J. Food. Sci. Technol.*, **12**, 187 (1975).

42. Giles, C. H., Hassan, A. S. A., laidlaw, M. and Subramanian, *J. Soc. Dyers Colourists*, **74**, 645 (1958).

43. Simpson, K. L., in ref. 31, pp 253.

44. Jeanloz, R. and Forchielli, E., *Helv. Chim. Acta.*, **33**, 1690 (1950).

45. Takeda, M. and Abe, E., *Norinsho Suisan Koshusho Kenkyu Hokoku*, **11**, 339 (1962).

46. Takeda, M. and Katsuura, H., *Suisan Daigaku Kenkyu Hokoku*, **13**, 109 (1964).

47. Broussignac, P., *Chim. Ind. Genie. Chim.*, **99**, 1241 (1968).

48. Shimahara, K. and Takiguchi, Y., *Methods Enzymol.*, **161**, 417 (1988).

49. Knorr, D. and Klein, J., *Biotechnology Letters*, **8** (10), 69 (1986).

50. Araki, Y. and Ito, E., *Eur. J. Biochem.*, **55**, 71 (1975).

51. Kafetzopoulos, D., Martinou, A. and Bouriotis, V., *Proc. Natl. Acad. Sci.*, USA, **90**, 2564 (1993).

52. Martinou, A., Kafetzopoulos, D. and Bouriotis, V., *J. Chromatography*, **644**, 35 (1993).

53a. Rudall, K. M. and Kenchington, W., *Biol. Rev.*, **49**, 597 (1973).

53b. Rudall, K. M., J. Polymer Sci., **28**, 83, Part C, Polymer Symposia, Proceedings of the Sixth Cellulose Conference, Ed. by Marchessault , R. H., Interscience Publisher (1968).

54. Gonell, H. A., *Zeit. Physiol. Chem.*, **152**, 18 (1926).

55. Meyer, K. H. and Mark, H., *Ber*, **61**, 1936 (1928).

56. Carlstrôm, D., *J. Biophys. Biochem. Cytol.*, **3**, 669 (1957).

57. Hermans, P. H., Booys, J. De. and Maan, C. *J., Kolloid-Zeit*, **102,** 169 (1943). Marchesaault, R. H. and Sundararajan, P. R., in *The Polysaccharides,* Vol 2, pp 12-90, Ed. by Aspinall, G. O., Academic Press, New York (1983).

58. Rinaudo, M. and Domard, A., in *Chitin and Chitosan; Sources, Chemistry, Biochemistry, Physical Properties and Applications, Proceeding from the 4th International Conference on Chitin and Chitosan,* pp 71, Ed. by Skjak-Braek, G., Anthonsen, T. and Sandford, P., Elsevier Applied Science, New York (1989).

59. George, A. F. R., *Chitin Chemistry*, The MacMillan Press Ltd., London (1992).

60. Sannan, T., Kurita, K. and Iwakura, Y., *Makromol. Chem.*, **177**, 3589 (1976).

61. Domard, A., *Int. Biol. Macromol.*, **9,** 98 (1987).

62. Giles, C. H., Hassan, A. S. A. and Subramanian, R, V. R., *J. Soc. Dyers Colourists*, **74**, 685 (1958).

63. Hackman, R. H., *Aust. J. Biol. Sci.*, **8**, 530 (1955).

64. Giles, C. H. and Hassan, A. S. A., *J. Soc. Dyers Colourists*, **74**, 846 (1958).

65. Neville, A. C., *The Biology of the Arthropod Cuticle*, Carolina Biology Readers, no. 103, Carolina Biological Supply Company,Burlington (1978).

66. Peter, M. G., Kegel, G. and Keller, R., in *Chitin in Nature and Technology*, pp 21, Ed. by Muzzarelli, R. A. A., Jeuniaux, C. And Gooday, G. W., Plenum Press, New York (1985).

67. Neville, A. C., *Biology of Fibrous Composites; Development Beyond the*

Cell Membrane, Cambridge University Press, New York (1993).

68. Robinson, C., *Molecular Crystals*, **1**, 467 (1966).
69. Neville, A. C. and Luke, B. M., *Tissue and Cell,* **1**, 689 (1969).
70. Onsager, L., *Ann. N. Y. Acad. Sci.*, **51**, 627 (1949).
71. Stroobants, A., Lekkerkerker, H. N. W. and Odijk, Th., *Macromolecules,* **19**, 2232 (1986).
72. Marchessault, R. H., Morehead, F. F. and Walter, N. M., *Nature*, **184**, 623 (1959).
73. Revol, J.-F. and Marchessault, R. H., *Int. J. Biol. Macromol.* **15**, 329 (1993).
74. Laba, D., *Rheological properties of Cosmetics and Toiletries*, Marcel Dekker Inc., New York (1993).
75. Gagne, N., *Production of Chitin and Chitosan from Crustacean Waste and Their Use As a Food processing Aid*, M.Sc Thesis, Food Science and Agricultural Chemistry, McGill University (1994).
76. Von Weimarn, P. P., *J. Textile Inst.*, **17**, T642 (1926).
77. Thor, C. J. B., *US Patent* 2,168,375 (1939).
78. Brine, C. J. and Austin, P. R., in *American Chemical Society Symposium Series; Marine Chemistry in the Coastal Environment,* Vol. 18, pp505-518, Ed. by Church, T. D. (1975).
79. Fuji Spinning Co., Ltd., *Japanese Patent* 59116418 (1984).
80. Rutherford, F. A. and Austin, P. R., in *Proceedings of the First International Conference on Chitin and Chitosan,* pp 182-192, Boston, Massachusetts, Ed. by Muzzarelli, R. R. A. and Pariser, E. R., MIT Sea Grant Program, Cambridge (1977).

Chapter 2

EFFECT OF ELECTROSTATIC INTERACTIONS ON THE PHASE SEPARATION BEHAVIOUR OF CHITIN CRYSTALLITE SUSPENSIONS

2.0 ABSTRACT

Optical and electron microscopy were used to observe the dynamics of the phase separation in crystallite suspensions prepared by HCl hydrolysis of crab chitin. Freeze-fracture transmission electron microscopy reveals that chitin crystallites are aggregated in parallel in the suspensions and have an average length of 200 nm and an average width of 8 nm. They exhibit a positive surface charge of ~0.5 e/nm^2 when fully protonated. The liquid crystal-forming aqueous suspensions of such crystallites are investigated through phase diagrams and zeta potential measurements for different ionic strengths. Exposure of the suspension to a low concentration of a univalent electrolyte has a negligible effect on the phase separation because of the contribution of the charged crystallites themselves to the ionic strength. The thickness of the effective repulsive layer is estimated both from the phase diagrams according to Onsager's theory and from the computed interaction energy derived from the Poisson-Boltzmann equation using the experimental zeta potential as the surface potential. When the contribution of crystallites to the ionic strength is taken into account and a hypothetical linear charge density close to the Manning limit is assumed, there is a good agreement between the thickness of this layer and the Debye length.

2.1 INTRODUCTION

As discussed in Chapter 1, crab and shrimp shell chitin, and its derivative chitosan are used as industrial biopolymers for waste water treatment, medical applications, cosmetics, etc.(1,2). None of these applications depend on the chiral nematic (CN) structure of chitin microfibrils as found in arthropod shell and cuticles. The arcing

microfibrillar organization observed by electron microscopy, a characteristic feature of CN ordering of chitin microfibrils (3,4), has never been observed in the various commercial products using chitin or chitosan. Yet this CN ordering has now been reported in films of dried chitin crystallite suspensions, demonstrating the self-assembling liquid crystalline character of chitin under certain conditions (5). The formation of an anisotropic gel from a suspension made from the hydrolysis of a purified chitin sample was reported by Marchessault et al. in 1959 (6). At the concentrations then used (12 to 15% w/w), CN order was not observed probably because centrifugation was used to provoke rapid concentration buildup to a non-equilibrium state.

Recently, Revol et al.(5,7, 8) found that in a limited concentration range, aqueous colloidal suspensions of cellulose and chitin crystallites separate spontaneously into a CN phase and an isotropic phase. However, the mechanism of self-organization of the chitin crystallites in suspension and the microstructure of the CN phase require further study. In particular, the importance of the electrostatic repulsive force between particles which is believed to play an important role in the process of self-organization needs to be explored. Some $-NH_2$ groups are always present at the chitin crystallite surface, and in acidic media they are protonated to form $-NH_3^+$, a weak acid. The chitin crystallites thus exhibit a positive charge which depends on the pH of the suspension.

The phase separation of rodlike systems such as tobacco mosaic virus (TMV) and xanthan gum has been studied for many years (9,10). The theoretical foundation of the two-phase equilibrium, isotropic/anisotropic, of rodlike particles was first proposed by Onsager in 1949 (11). He used the second virial approximation to formulate the Helmhotz free energy of solutions. For charged particles, the effect of electrostatic repulsion was treated as an increase of the effective diameter of the rods (11). This theory was later extended by Stroobants et al. (12) to include the orientation effect of the electrostatic repulsion between particles. The effect of the ionic strength of the solution or suspension

on the boundary concentrations for the phase separation of charged rodlike particles has also been studied (13, 14,15).

In the present chapter, the particle size of the suspension is evaluated by transmission electron microscopy (TEM) including freeze fracture TEM. The surface charge density of chitin crystallites is characterized using conductimetric titration. The dependence of the phase separation of the chitin suspension on the ionic strength of the suspension is explored through phase diagrams and by determining the ζ potential under various experimental conditions. A calculation based on ionic strength and the observed ζ potential, using the Poisson-Boltzmann equation, is performed in order to explore the interaction energy change with the separation distance between particles. The results are in keeping with a double layer compression affecting the phase separation of chitin suspensions.

2.2 EXPERIMENTAL

2.2.1 SAMPLE PREPARATION

Suspensions were prepared by hydrolysing purified chitin (purchased from Sigma) with 3 N HCl at the boil for 1.5 h. A typical concentration was 0.1 g/ml of chitin in HCl. After acid hydrolysis, the suspensions were diluted with deionized water followed by centrifugation and decanting of the supernatant. This process was repeated several times until the suspension spontaneously transformed into a colloidal state at which point the pH of the suspension was approximately 2. Next, the suspensions were transferred into a dialysis bag and dialysed against deionized water until a desired pH was reached. Concentration of the sample was achieved by immersing the dialysis bag in a concentrated polyethylene glycol solution (molecular weight 10000). To achieve a better dispersion, the suspensions were ultrasound treated in a Branson Sonifier (Model 350) for about 1 min for each 10 ml aliquot of 5% (w/w) suspension.

2.2.2 OPTICAL MICROSCOPIC STUDY OF AQUEOUS CHITIN SUSPENSION

A suspension with a pH of 3.6 and a concentration of 5% (w/w) was transferred into a rectangular glass capillary cell with a path length of 0.4 mm and a width of 8 mm (Vitro-Dynamics Inc, Rockaway, New Jersey 007866, U.S.A) and sealed. The suspension was left standing for two days before examination in a Nikon Microphot-FXA optical microscope. Micrographs of the isotropic and anisotropic phases were recorded with the sample between cross polars.

2.2.3 FREEZE-FRACTURE TRANSMISSION ELECTRON MICROSCOPY (FFTEM) OF CHITIN SUSPENSIONS

Samples for FFTEM were prepared by trapping 0.25 ml of suspension between two thin (0.1 mm) copper freeze-fracture planchettes (Balzers Union BUO-12056-T, Hudson, NH). The planchettes/sample sandwiches were allowed to equilibrate in an environmental chamber at 25°C and 95% humidity to ensure constant composition and temperature before being quickly frozen in liquid propane cooled by liquid nitrogen (16). This method of specimen preparation has been shown to give excellent artifact-free results for aqueous surfactant mixtures (17). The frozen specimens were stored under liquid nitrogen until their transfer to a Balzers 400 freeze-etch device. The samples were fractured under vacuum (10^{-7} mbar) at -170°C and immediately shadowed with a 1.5 nm thick layer of platinum/carbon at a 45° angle with respect to the fracture surface, followed by a 15 nm thick layer of carbon deposited normal to the surface. The samples were dissolved in chromic acid, leaving the Pt-C films behind. The Pt-C replicas thus obtained were cleaned for five days in a 25% vol/vol ethanol-water mixture. They were collected on 200 mesh copper grids, and observed in a JEOL 100CX II transmission electron microscope at 80 kV. Images were recorded on Kodak SO 163 electron image film. Shadows (absence of

platinum) appear light in the Figures.

2.2.4 CHARACTERIZATION OF THE SURFACE CHARGE DENSITY OF CHITIN CRYSTALLITES BY CONDUCTIMETRIC TITRATION

The suspension samples were titrated with 0.01 N NaOH. Approximately 1 g of a 5% (w/w) chitin suspension was transferred to a three-necked round bottom flask followed by addition of 200 ml of deionized water and 4 ml of 0.1 N HCl which assures an excess of H^+ in the suspension. The titration was performed under N_2 with stirring. A Metrohm automatic titration system consisting of a Metrohm 600 sleeveless immersion cell with built-in temperature probe and a titration burette (Metrohm 665 Dosimat) was used to conduct the titration. The process was controlled by an AT-286 personal computer through an interface. In addition, a dry chitin film was titrated using the method described by Raymond et al.(18) for comparison. The conductance of the suspension was plotted as a function of the volume of 0.01 N NaOH used in titration. The pH of the suspension was plotted concurrently in order to obtain the pK_a of the chitin $-NH_3^+$ groups. The volume of alkali, equivalent to the surface amino groups in the sample, was calculated from the points corresponding to the sharp changes in the slope of the titration curve (18). Calculation of the surface charge density of chitin crystallites will be discussed later.

2.2.5 PHASE SEPARATION AND ZETA POTENTIAL MEASUREMENT

2.2.5.1 PHASE SEPARATION EXPERIMENT

Phase separation of chitin suspensions was observed in cylindrical NMR tubes of 5 mm diameter. Suspensions of a given concentration were first adjusted to the desired pH with 0.1 N HCl. Next, several ml of each suspension were transferred into 10 ml vials and diluted to the desired concentrations with deionized water to which HCl had been added to adjust to the same pH. The NaCl concentrations of the suspensions were adjusted

to 10^{-4} M and 10^{-3} M with 0.1 N NaCl prepared with a solution of HCl at the same pH. After mixing, followed by a 30 second ultrasound treatment, the suspension was transferred into NMR tubes which were then covered with stoppers. The volume fraction of the isotropic phase (top phase) was determined by dividing the height of that phase by the total height after two or more days standing.

2.2.5.2 ZETA POTENTIAL MEASUREMENT

All the ζ potential measurements were done on a Pen Kem Model 501 Lazer Zee Meter. Instead of measuring the time travelled by an individual particle as in most ζ potential apparatus based on electrophoresis, the Lazer Zee Meter adjusts the observed image to produce a stationary "cloud"(see Appendix 1). This particle cloud is made to appear stationary using a patented rotating prism technique. The prism provides a motion equal and opposite to the motion caused by the applied electric field. Samples were prepared by diluting the concentrated sample with a solution of HCl at the same pH. The final concentration was in a range of 0.01% to 0.05% (w/w). The measuring chamber was cleaned several times with deionized water and rinsed with the sample before starting the measurements.

2.2.6 CALCULATION OF INTERACTION ENERGY

The interaction energy was calculated with a computer program written by Chan et al.(19) who used a numerical procedure to solve the Poisson-Boltzmann equation for a 1:1 electrolyte between identical, charged plane-parallel interfaces. A constant surface potential model was used in our calculation and the ζ potential was approximated as a surface potential.

2.3 RESULTS AND DISCUSSION

2.3.1 ORDER IN CHITIN SUSPENSIONS

Fig. 2.1a shows the interfacial region of a two phase chitin suspension as observed in the polarizing microscope. Small "tactoids" in the top phase reorganize into larger domains as they move to the bottom under the influence of gravity to form a CN layer. Tactoids are droplets of the anisotropic phase having an ellipsoidal shape (5) and their structure at crystallite level is shown in Fig. 2.1b. The interfacial boundary layer contains large tactoids that probably result from the coalescence of smaller tactoids. The anisotropic phase with typical CN texture, as already described in a previous paper (5), originates from this coalescence. Birefringent bands, having spacing of 8 μm, correspond to half the pitch of the CN structure. By using a quarter wave plate and rotating the sample, it can be demonstrated that the rodlets lie predominantly parallel to the birefringent bands. They are parallel to the plane of observation in the middle of the birefringent bands, and they are perpendicular to the plane of observation in the dark area, as expected for a CN structure. The CN axis is perpendicular to the long axis of the ellipsoidally shaped tactoids and when the periodic structure is well defined and highly contrasted, it is in, or close to lying in the plane of observation.

Fig. 2.2 represents the apparent isotropic phase seen between crossed polars. Interestingly, small tactoids are still present in this phase, even after several weeks in quiet conditions. These small tactoids, which represent the first evidence for a CN assembly are in equilibrium with the surrounding disordered continuum of rods and are probably stabilized by free energy minimization. With time, these tactoids should sediment to the boundary by gravity. However, they remain suspended probably due to an increase of the viscosity of the suspension with time.

2.3.2 FFTEM STUDY OF CHITIN SUSPENSIONS

Freeze-fracture transmission electron microscopy was used to investigate the microstructure of the suspension in the two phases, isotropic and anisotropic. The micrograph of the isotropic phase (Fig. 2.3) indicates that the suspension is polydisperse with an average particle size of approximately 8 nm in width by 200 nm in length. If some of the observed particles are individual chitin crystallites, there are also parallel aggregates of these crystallites. A similar distribution was previously observed by preparing a dispersion of the chitin crystallites on a carbon supporting film (5). The presence of a certain degree of aggregation could be attributed to the drying process on the support or considered as being already present in the colloidal suspension. The freeze-fracture results shown in Fig. 2.3 and Fig. 2.4 suggest that these small aggregates are indeed present in the aqueous colloidal suspension. These particle aggregates display a preference for parallel orientation over a considerable distance. This may represent the incipient tactoid state or an extensive parallel orientation due to shearing during the sample preparation. Further study will help to clarify this.

Fig. 2.4 shows that rodlike particles in the anisotropic phase also display orientation in a given direction. This oriented state covers fields as large as 10μm. When compared to Fig. 2.3, which corresponds to the isotropic phase, the spacing between particles is similar in both cases, as expected since the concentration in chitin is of the same order, i.e. 6.62% (w/w) for the isotropic suspension and 6.48% (w/w) for the anisotropic suspension.

The fact that no arced patterns are observed in the micrograph obtained from the anisotropic phase, means that the freeze-fracture may have been perpendicular to a CN axis, i.e. along the CN planes in which the crystallites are mostly parallel. An alternative explanation is that during the preparation, the anisotropic suspension may have been sheared to produce a nematic order and that the time was too short to allow reassembly into a CN structure. Further experiments should be done to obtain fractures through a sus

Fig. 2.1a. View of the interfacial region of a 5% chitin suspension at pH 3.6 viewed between crossed polarizers. The upper region is isotropic. The bottom phase is anisotropic. The pitch of the chiral nematic domain is 16 μm. The magnification is 470.

Top

Bottom

Fig. 2.1b. A schematic showing the structure of self-assembled chitin crystallites in anisotropic phases. This organization corresponds to CN order.

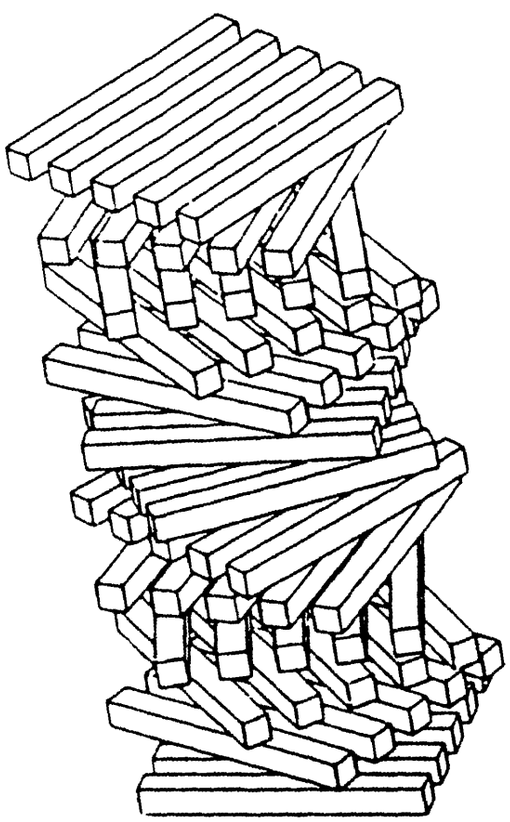

Fig. 2.2. The top phase (isotropic) of a 5% chitin suspension at pH 3.6 showing the presence of a large number of CN tactoids with a pitch of 20 μm. The magnification is 250.

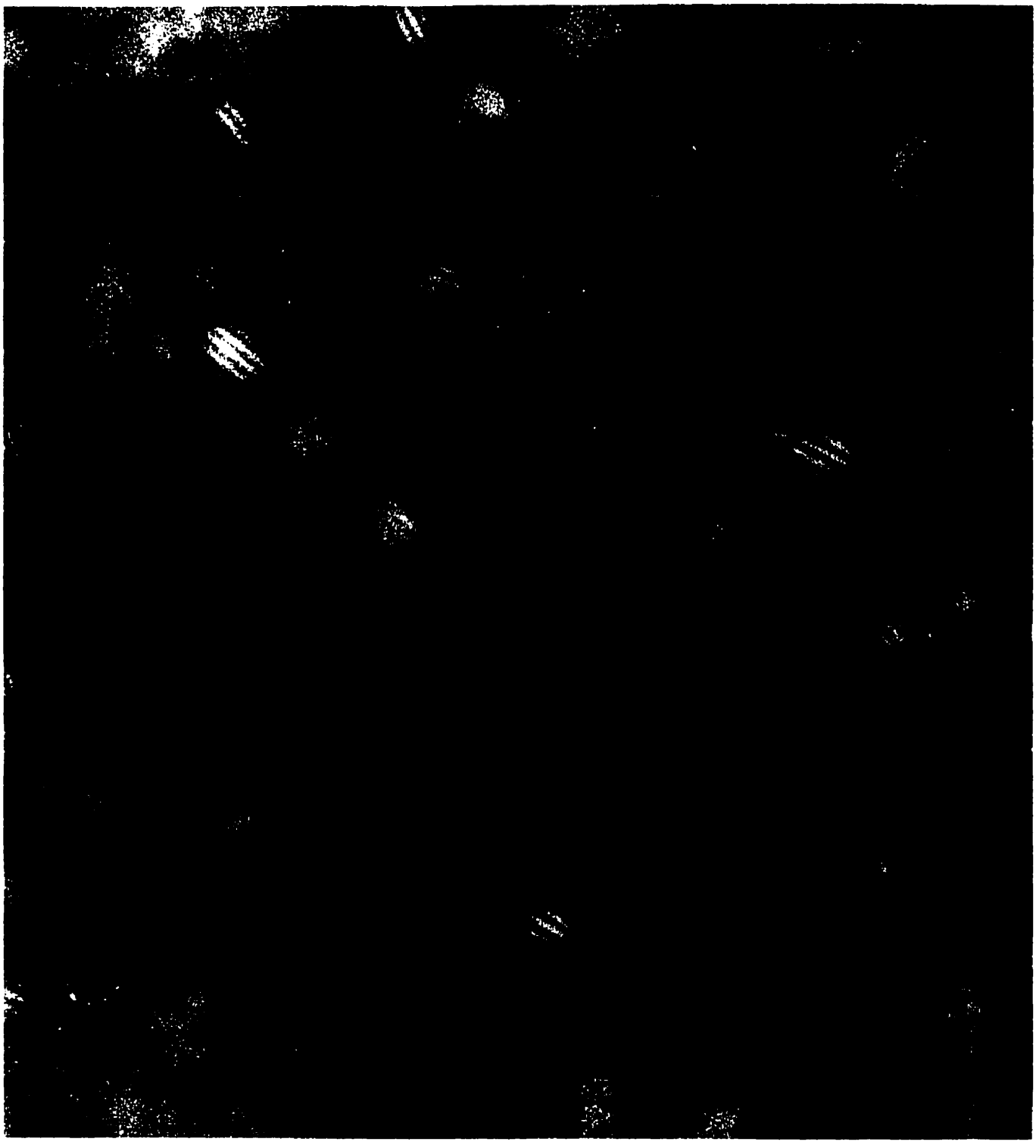

Fig. 2.3. Freeze-fracture electron micrograph of the isotropic phase of 6.62% chitin suspension at pH 4.


0.5 µm

Fig. 2.4. Freeze-fracture electron micrograph of the anisotropic phase of 6.48% chitin suspension at pH 4.44.

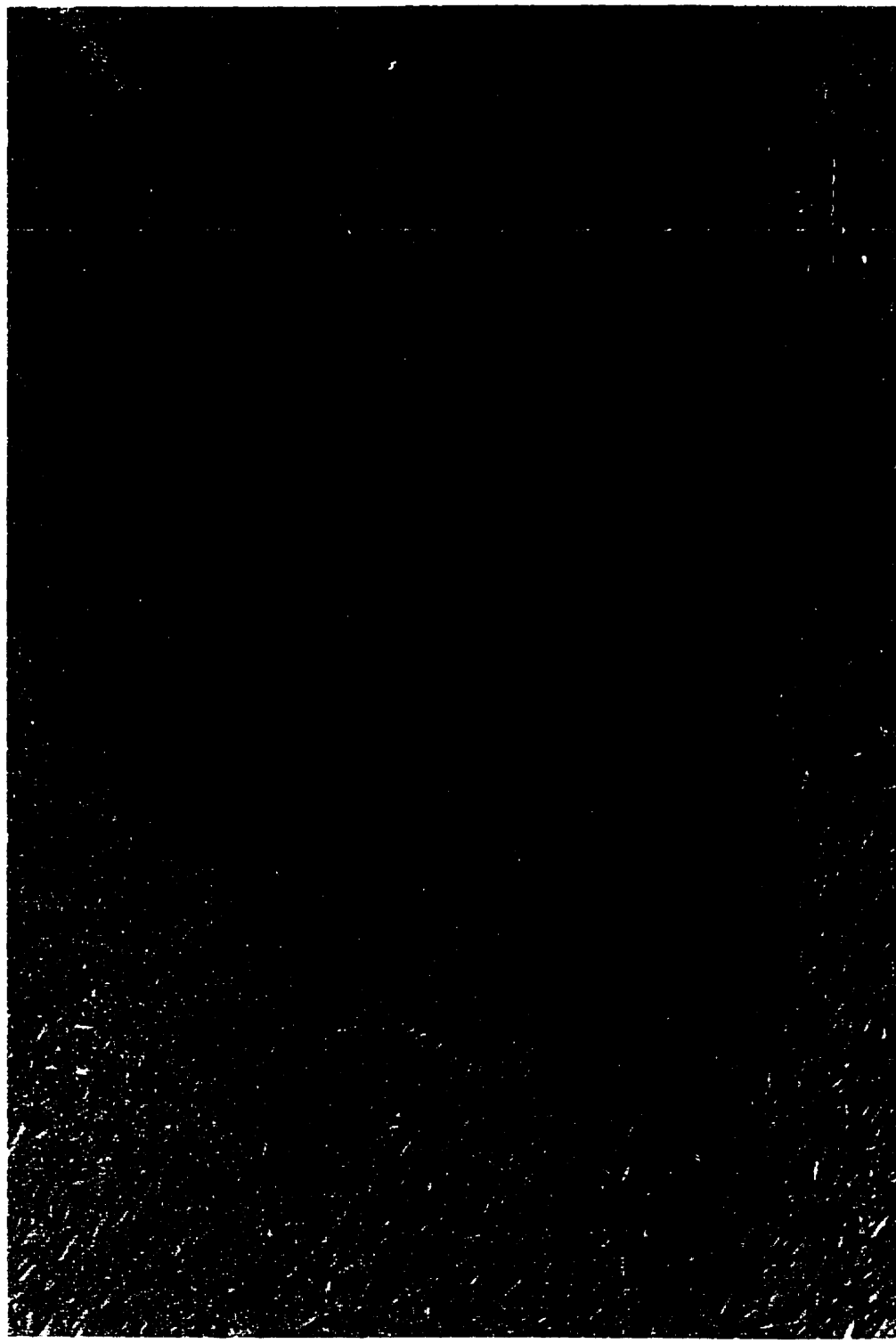

suspension whose CN assemblies have been preserved or recovered.

2.3.3 CHARACTERIZATION OF THE SURFACE CHARGE DENSITY OF CHITIN CRYSTALLITES

Chitin, which is a poly (N-acetyl-D-glucosamine), is never fully acetylated, and some amino groups are present. It is believed that these amino groups are formed during the chitin biosynthesis due to the existence of a chitin deacetylase (20, 21). The surface charge of the chitin crystallites in a suspension of certain pH originates from the protonation of the surface -NH_2 groups, according to Eq. 2.1.

$$Glu\text{-}NH_2 + H^+ \rightleftharpoons Glu\text{-}NH_3^+ \qquad (2.1)$$

Surface -NH_3^+ groups, weak acids are the origin of the electrostatic repulsive force in the suspension. When completely protonated, the total surface charge will be equivalent to the total number of -NH_2 groups present at the surface of the crystallites. If we assume that it is only these groups that can be titrated (18), the maximum surface charge density can be calculated by dividing the total amino groups by the total surface area of the crystallites. The total surface area of the chitin crystallites is derived from the surface area of an individual crystallite and the number of crystallites in the suspension. TEM results indicate that a chitin crystallite is about 200 nm in length and 8 nm in width. A detailed calculation of surface amino group density can thus be undertaken (Appendix 2). The maximum surface charge density from conductimetric titration of the colloidal suspensions for two different samples are tabulated in Table 2.1. The value for the first sample is in good agreement with that derived from the titration of a dried chitin film (18) prepared from the same batch (see Table 2.1). In general, when fully protonated, chitin crystallites made by HCl hydrolysis show a charge which is considered relatively high if converted

to effective linear charge density(12).

Glu-NH_3^+ is a weak acid and its degree of protonation is governed by its pK_a. For chitosan solutions, Glu-NH_3^+ has a pK_a between 6.3 and 7 (22,1). According to the calculations based on pK_a and the surface potential, the surface amino groups are completely protonated at pH 3 or below and they are completely dissociated at pH 7. For the chitin crystallite suspensions, the pH has been monitored during the titration. Apparent pHs of about 3.5 and 7 were found respectively for the beginning and the end of the neutralization of the -NH_3^+. When half of the -NH_3^+ groups were neutralized, the apparent pH was 6.2 $\pm$ 0.1, which corresponds to the apparent pK_a value of Glu-NH_3^+ of the suspensions. The degree of protonation can thus be reasonably estimated from the pH of the suspensions.

TABLE 2.1 Maximum Surface Charge Density of Chitin Crystallites from Conductimetric Titration

Sample name	Charge density ($C/m^{2)}$	Charge density (e/nm^2)
Colloidal suspension 1	0.07862	0.5049
Dry chitin film	0.07800	0.5000
Colloidal suspension 2	0.09410	0.6043

2.3.4 SEPARATION INTO ISOTROPIC/ANISOTROPIC PHASES

The phase separation of chitin suspensions has been investigated at different ionic strengths and pH values. Fig. 2.5 are the phase diagrams of the biphasic region of the chitin suspensions at pH 4.9 for NaCl concentrations of 0, 10^{-4} M and 10^{-3} M. At this pH, about 70% of the surface amino groups are protonated. The curves show the relation between the average chitin concentration and the relative volume fraction of the isotropic phase in the biphasic mixture of the suspension. These curves should be linear for a monodisperse suspension having a constant ionic strength. However, the chitin suspensions made from HCl hydrolysis are polydisperse, see Fig. 2.3. It has been shown that the polydispersity of the length of rodlike particles results in a non-linear relationship between the average concentration and the volume fraction of the isotropic phase ϕ (23). In addition, as will be discussed below, the contribution of the chitin crystallites to ionic strength becomes important as the concentration increases, resulting in an additional effect on the curvature for the concentrated suspensions as seen most evidently in Fig. 2.6. Even though these data do not show a linear relationship, we will nevertheless assume that it is. The extrapolation of the line to $\phi = 1$ and 0 gives the phase boundary concentrations C_i and C_a corresponding respectively to the phase transitions, isotropic/biphasic and biphasic/anisotropic. Fig. 2.5 shows that the critical concentrations for phase separation increase with increasing NaCl concentration, probably due to the compression of the electrical double layer around the crystallites. However, the observed effect is minor.

Fig. 2.5. Diagrams of chitin suspensions at pH 4.9 showing the average concentration vs. the volume fraction of the isotropic phase for different NaCl concentrations: (△) 10^{-3} M NaCl; (▲) 10^{-4} M NaCl; (□) 0 M NaCl.

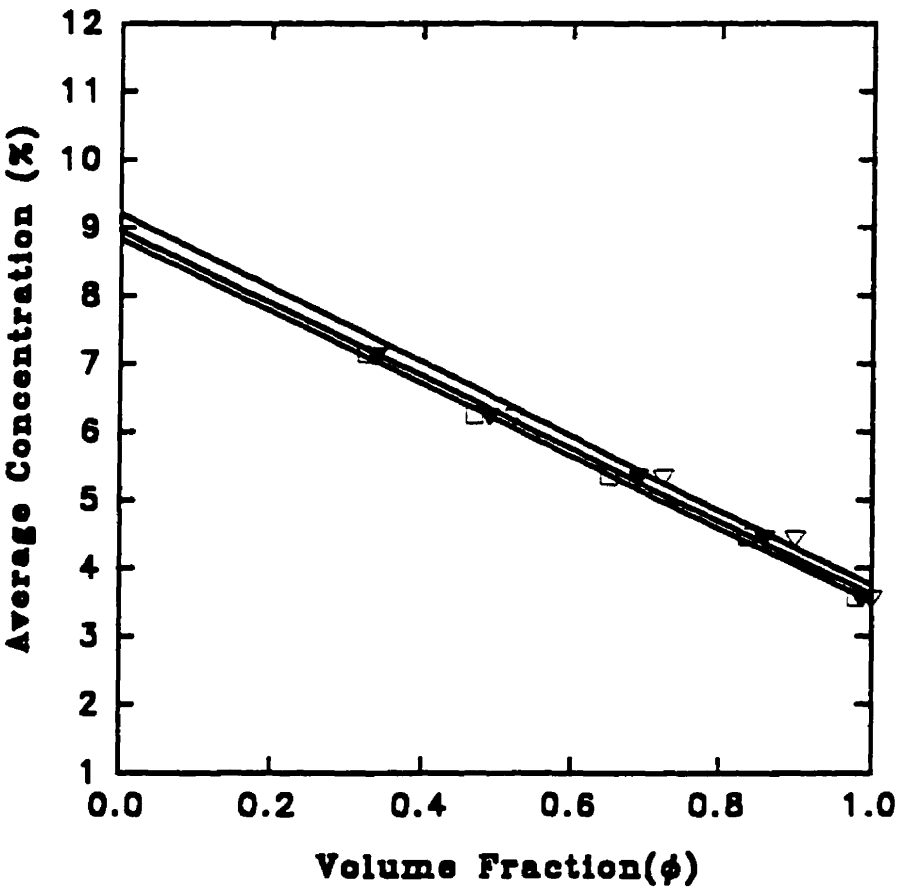
Average Concentration (%)
12
11
10
9
8
7
6
5
4
3
2
1
0.0
0.2
0.4
0.6
0.8
1.0
Volume Fraction(ϕ)

Fig. 2.6. Diagrams of chitin suspensions at pH 3.8 showing the average concentration vs. the volume fraction of the isotropic phase for different NaCl concentrations: (△) 10^{-3} M NaCl; (▲) 10^{-4} M NaCl; (□) 0 M NaCl.

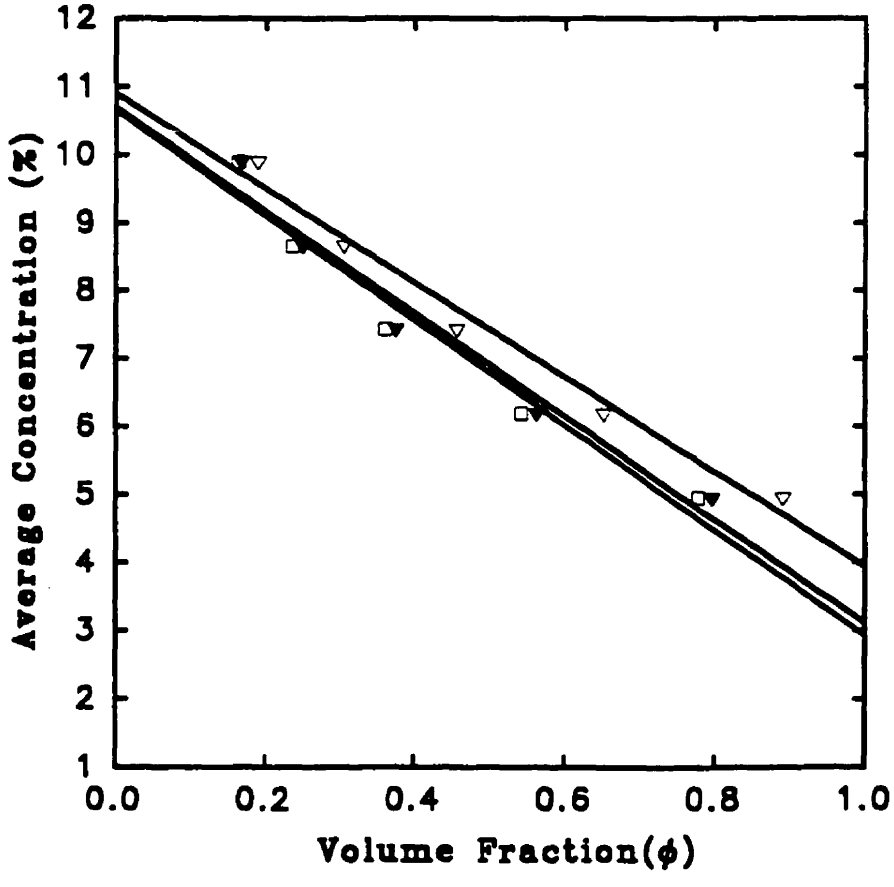
Average Concentration (%)
12
11
10
9
8
7
6
5
4
3
2
1
0.0
0.2
0.4
0.6
0.8
1.0
Volume Fraction(ϕ)

According to both the calculation from pK_a (22) and our experimental results, to have the surface amino groups completely protonated, the pH of the suspension should be around 3.5 or below, whereas at a pH of about 7-8 there are only neutral $-NH_2$. Between these two pH values, the $-NH_2$ groups are only partially protonated. Consequently, when the pH of the suspension decreases, there are two effects acting on the rodlike particles in the suspension. First, the surface equilibrium (see Eq. 2.1) is shifted to the right due to the increase of H^+ concentration and therefore the surface charge density of the suspension increases. Secondly, the ionic strength of the suspension increases as well, which results in double layer compression. Fig. 2.6 shows diagrams of the biphasic region of the suspensions at pH 3.8 (95% protonation at this pH). It is observed that the curve for the suspension with 10^{-4} M NaCl overlaps with that without NaCl due to a similar ionic strength in both suspensions. Increasing [NaCl] to 10^{-3} M results in a further compression of the double layer and the critical concentration for phase separation increases slightly. The diagrams of the biphasic region of the suspension at pH 2.8 show that adding NaCl to the suspension has no effect on the critical concentration of phase separation owing to its negligible effect on ionic strength (see Fig. 3.7). The observed change in the critical concentrations as a function of [NaCl] is thus not significant.

2.3.5 ANALYSIS BASED ON ONSAGER'S THEORY

The Onsager theory predicts that the boundary concentration ϕ_i, being the volume fraction at which phase separation occurs, is given by

$$\phi_i = 3.3(d/L) \qquad (2.2)$$

Fig. 2.7. Diagrams of chitin suspensions at pH 2.8 showing the average concentration vs. the volume fracttion of the isotropic phase for different NaCl concentrations: (△) 10^{-3} M NaCl; (▲) o M NaCl.

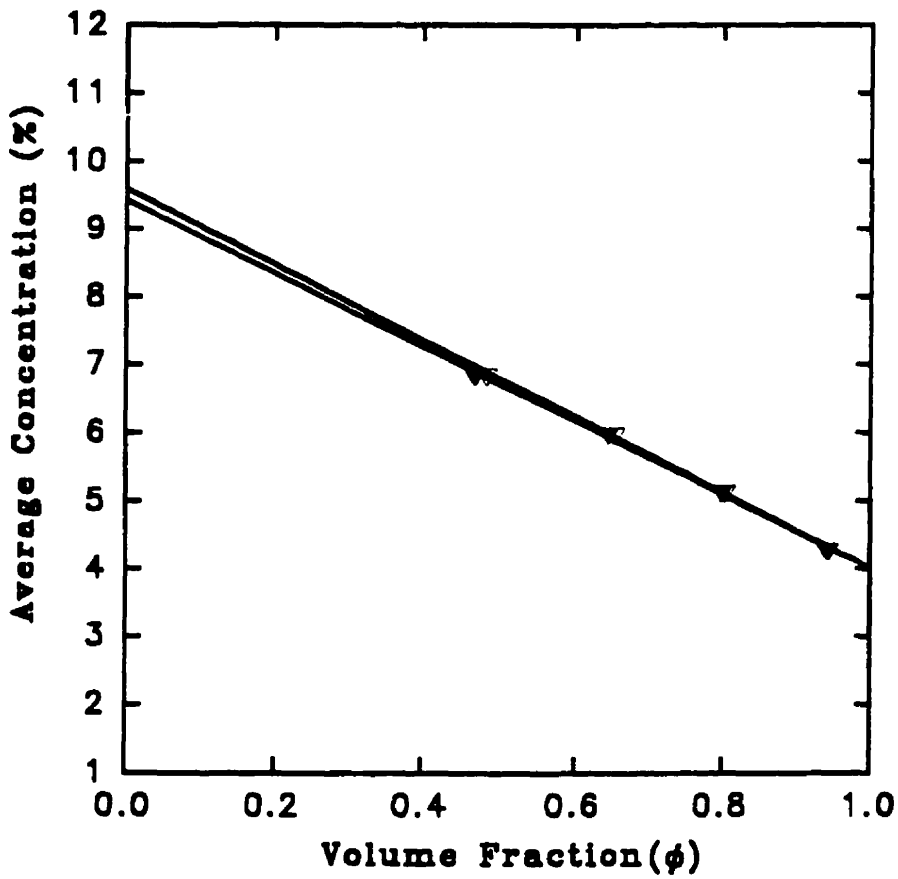
Average Concentration (%)
12
11
10
9
8
7
6
5
4
3
2
1
0.0
0.2
0.4
0.6
0.8
1.0
Volume Fraction(ϕ)

For rodlike particles with length (L) of 200 nm and width (d) of 8 nm , ϕ_i calculated from Eq. 2.2 is 0.132. The boundary concentrations ϕ_i from phase diagrams corresponding to the suspensions with different pH and [NaCl] are around 0.025 (see Table 2.2). This substantial difference indicates the existence of an electrostatic repulsive force between the crystallites.

TABLE 2.2 Boundary Concentrations of Phase Separation of Chitin Suspensions Under Various Experimental Conditions and Calculated κ^{-1}, d_e and L_R

pH	[NaCl] (M)	κ^{-1a} (nm)	κ^{-1b} (nm)	κ^{-1c} (nm)	$\phi \times 100$	d_e (nm)	L_R (nm)	L_r^d (nm)
4.9	0	85.72	18.59	7.061	2.463	43.87	17.94	22.90
4.9	10^{-4}	28.66	15.70	6.787	2.534	42.63	17.32	21.80
4.9	10^{-3}	9.558	8.482	5.568	2.635	41.14	16.57	16.50
3.8	0	24.16	15.79	6.422	2.053	51.45	21.73	21.84
3.8	10^{-4}	18.92	13.82	6.115	2.182	48.40	20.20	20.18
3.8	10^{-3}	8.936	8.001	4.829	2.766	38.16	15.08	16.58
2.8	0	7.639	7.002	4.492	2.807	37.62	14.81	16.05
2.8	10^{-3}	5.982	5.671	4.070	2.807	37.62	14.81	14.08

κ^{-1a} is calculated from the concentration of mobile ions.

κ^{-1b} is calculated based on the contribution of the chitin crystallites to the ionic strength (23) and by using a hypothetical linear charge density derived mathematically (25).

κ^{-1c} is calculated as for b, but with hypothetical linear charge density β = 1.4 e/nm corresponding to Manning limit (24).

L_r^d is estimated from interaction energy curves as discussed in the text.

The presence of surface charge results in the formation of a double layer around the crystallites. This corresponds to an increase of the effective diameter of the rods. If the effective diameter (d_e) of the crystallite is the result of an increase by a factor m of the actual diameter d, the effective volume fraction $\phi_{i,e}$ will be the result of an increase by m^2 of ϕ_i. Thus, we have:

$$d_e = md \quad \text{and} \quad \phi_{i,e} = m^2\phi_i \qquad (2.3)$$

Substituting d_e and $\phi_{i,e}$ into Eq. 2.2, a new relation is derived:

$$m = 3.3d/(L\phi_i) \qquad (2.4)$$

Table 2 summarizes the d_e and L_R values calculated from the experimental ϕ_i values where L_R is the effective repulsive layer thickness and is defined as:

$$L_R = (d_e-d)/2 \qquad (2.5)$$

The κ^{-1} (Debye length) is also calculated to compare it with L_R for each case. The Debye length is defined as the distance from charged surface where the potential has fallen off by a factor 1/e, i.e. approximately half the diffuse layer. For chitin and cellulose crystallite suspensions, the effective repulsive layer thickness should be equivalent to this diffuse layer, where the potential energy starts to exceed the zero level and adjacent crystallites start to interact. It is thus expected that κ^{-1} is of the order of 2 to 3 times less than L_R. For cellulose crystallites, Dong et al. (24) reported values of L_R (derived from d_e) about 3 times larger than κ^{-1}. As a first estimation, we have ignored the contribution of the chitin crystallites to the ionic strength of the suspension. According to Table 2.2, the κ^{-1} obtained is comparable to L_R only for the suspensions of higher ionic strength. It seems obvious that the total ionic strength has been underestimated and the contribution of the crystallites to the ionic strength is not negligible.

For a better estimation, we should therefore consider this contribution. Taking

account of the Donnan salt exclusion effect as was done by Sato et al. (13), thus κ can be expressed as:

$$\kappa^2 = 8\pi Q(n_s + \Gamma z_p c') \qquad (2.6)$$

where Q is the Bjerrum length (It is 0.713 nm for water at 25°C), n_s is the average number density of mobile ions, z_p is the univalent charges of the polyion and c' is the polyion concentration (number density). Γ, the Donnan salt exclusion coefficient, is given by the following equation (25):

$$\Gamma = (4Q\beta)^{-1} \qquad (2.7)$$

where β represents an hypothetical linear charge density that would produce an electrostatic potential similar to the actual surface charge density σ of the crystallites.

Brenner and Parsegian (26) proposed a treatment to evaluate such an hypothetical linear charge density β for large molecules having cylindrical shape. A similar treatment has recently been used for cellulose crystallites (7 nm wide) having a surface charge density of 0.155 e/nm^2 (24). This latter system is similar to ours, with comparable crystallite size and ionic strength. Accordingly, the estimation of β for the chitin crystallite was simply done by correcting the value from the difference in surface charge density σ between chitin and cellulose crystallites (24). The value of β so obtained is about 12 e/nm. κ^{-1} derived from such hypothetical linear charge density are shown in Table 2.2. When compared to L_R (effective repulsive layer thickness), the values of κ^{-1} are now more reasonable, but are still too high for the suspensions of lower ionic strength.

We also note that for the sample at pH 4.9, the values of L_R derived from the phase diagrams are lower than that for the sample at pH 3.8. We have seen that at pH 4.9, the degree of protonation is only about 70% of the total surface amino groups whereas it is ~ 95% at a pH of 3.8. It is thus possible that this lower surface charge is responsible for this discrepancy, and if so it would mean that at this level of surface charge, the electric double layer thickness varies with the surface charge density, i.e. the system is below the

Manning limit (25). This corresponds to a linear charge density β of 1.4 e/nm. Above this value there is condensation of counterions on the polyion to lower the apparent charge density parameter $Q\beta$ to the value one. So, for similar ionic strength the effective double layer should be the same.

It seems that the estimated charge density of about 12 e/nm is too high. This is perhaps because the mathematical treatment is not valid for large crystallites (24). A reasonable assumption can be made in our system by assuming that the value of β should be such that the system is close to the Manning limit (25). With such an assumption κ^{-1} is now in a range that is rational when compared to L_R (see Table 2.2).

2.3.6 ZETA POTENTIAL

The ζ potential is a universal parameter to characterize an electrical double layer. By adding NaCl, the electrical double layer compression increases the boundary concentration for phase separation of a polyelectrolyte solution. In other words, electrostatic repulsive forces are the dominant stabilizing forces. Experimentally, the surface potential of a chitin crystallite is approximated by the ζ potential,i.e. the potential at the slip plane which is the interface between the immobilized layer and the mobile fluid (27). For a suspension of pH 4.9, the ζ potential data corresponding to different NaCl concentrations are shown in Table 2.3. The ζ potential decreases by 5 mV with a 10 fold increase in NaCl concentration. This result is consistent with that for clay particles (28). The relationship between Log ζ and κ is shown in Fig. 2.8. A close-to linear relationship between log ζ and κ (Reciprocal Debye length) suggests that the ζ potential decrease with ionic strength is mostly due to the double layer compression (29). At pH 3.8, the ζ potentials are the same for the suspension with 10^{-4} M NaCl and that without NaCl due to a similar ionic strength (see Table 2.3). Further increase of the NaCl concentration to 10^{-3} M decreases the ζ potential by 5 mV. Similarly, in the case of pH 2.8 , the Zeta

TABLE 2.3 Zeta Potential of Chitin Suspensions at Different pH and NaCl Concentrations

pH	[NaCl] (M)	Specific conductance (ms cm^{-1})	Zeta potential (mV)
4.9	0	0.045	60
4.9	10^{-4}	0.048	55
4.9	10^{-3}	0.155	50
3.8	0	0.109	52
3.8	10^{-4}	0.112	52
3.8	10^{-3}	0.219	47
2.8	0	0.699	44
2.8	10^{-3}	0.899	43.7

Fig. 2.8. The relationship between log ζ vs. κ for the chitin suspension at pH 4.9; ζ is the zeta potential and κ is 1/Debye length.

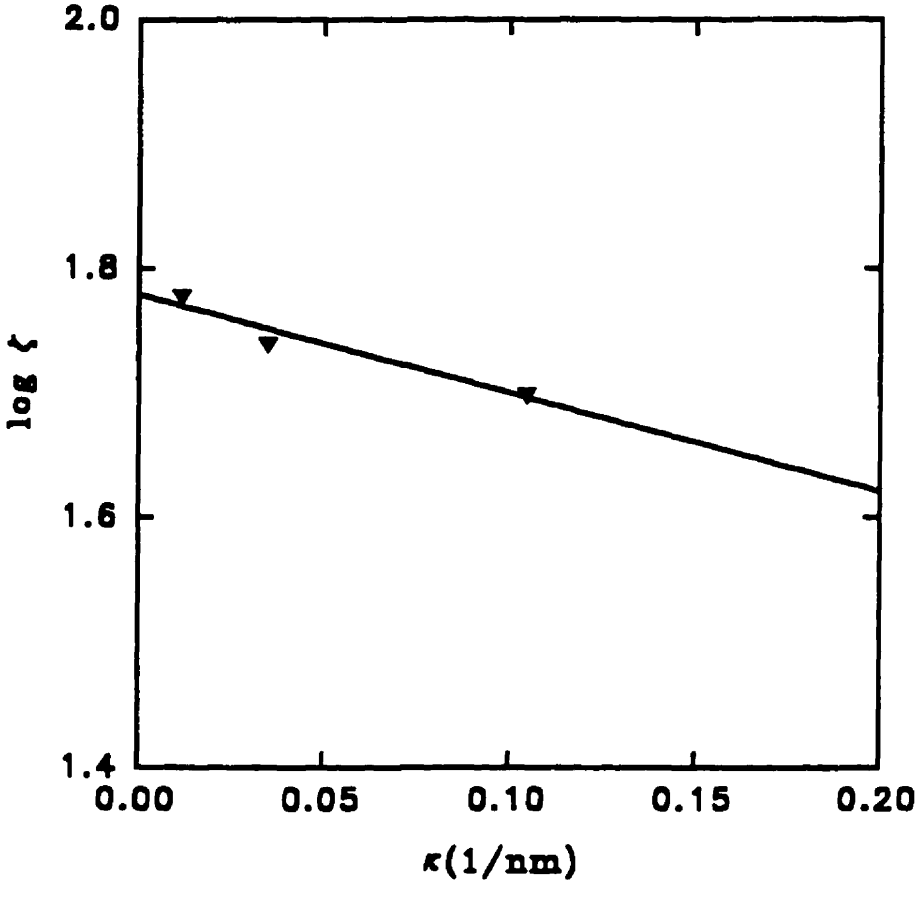
2.0
1.8
1.6
1.4
log ζ
0.00
0.05
0.10
0.15
0.20
κ(1/nm)

potential for the suspension with 10^{-3} M NaCl and without is the same. Overall, the zeta potential data support the assumption that the variation of the critical concentration with ionic strength is predominantly due to double layer compression when there is a significant change in ionic strength.

2.3.7 INTERACTION ENERGY

Based on the ζ potential values, the interaction energies between two rods was calculated as indicated in the experimental part. The calculation was done for suspensions with different pH values(4.9, 3.8 and 2.8) and different concentrations in NaCl (10^{-3} M, 10^{-4} M and 0). The curves representing the interaction energy as a function of the separation distance are shown in Fig. 2.9, 2.10 and 2.11. For the suspension at pH 4.9, the interaction energies vs the separation distance is shown in Fig. 2.9. At any given interaction energy, the separation distance is shorter for the suspension with the high NaCl concentration compared to that of the suspension with the low NaCl concentration. This implies that when NaCl concentration increases, the electrical double layer is compressed and the particles can be packed more closely. Therefore, the critical concentration for phase separation is increased. In the case of the suspension at pH 3.8 (see Fig. 2.10), there is overlap between the curve with 10^{-4} M NaCl and that without NaCl, which is consistent with that from the phase diagram. Increasing the NaCl concentration to 10^{-3} M results in a shorter separation distance for a given interaction energy. The same argument is applied to the pH 2.8 suspension (see Fig. 2.11), when all the curves overlap more or less since the ionic strength remains practically the same. Fig. 2.9 and Fig. 2.10 also show that the double layer compression effect due to the increase of [NaCl] is not very significant. This is in line with the change in critical concentrations observed from phase diagrams.

If we assume, as already mentioned, that the effective repulsive layer thickness (L_R)

Fig. 2.9. Calculated interaction energies at different separation distances for pH 4.9 chitin suspensions using the Poisson-Boltzmann equation: (△) 10^{-3} M NaCl; (▲) 10^{-4} M NaCl; (•) 0 M NaCl.

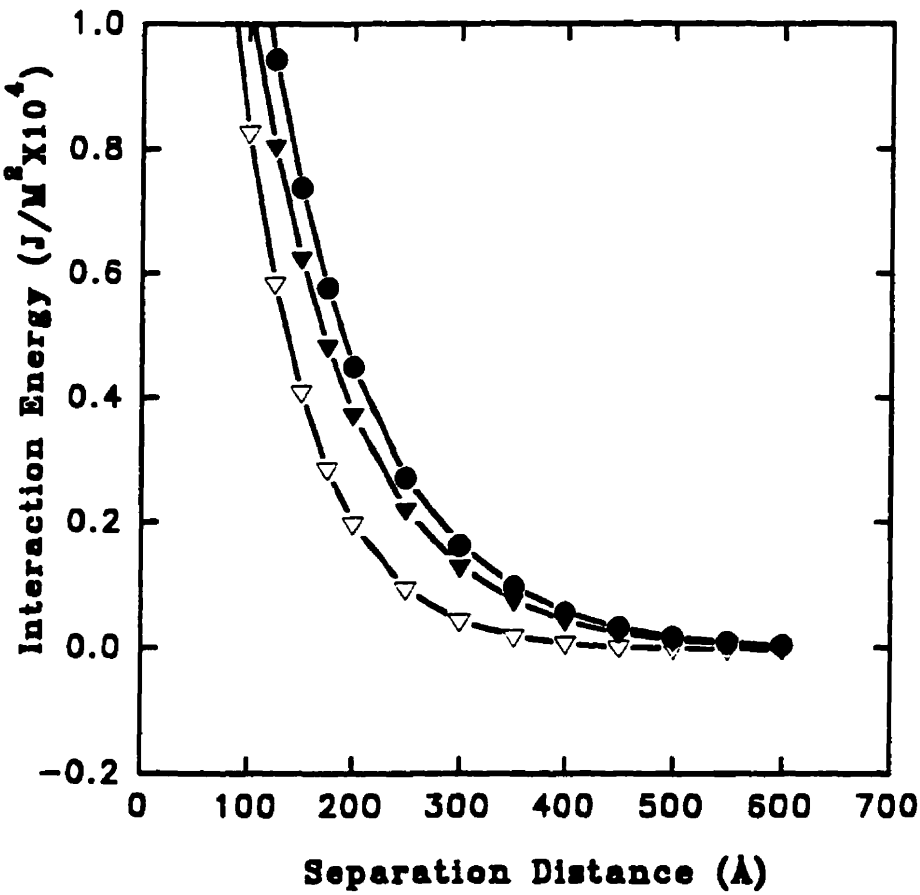
1.0
0.8
0.6
0.4
0.2
0.0
−0.2
0
100
200
300
400
500
600
700
Interaction Energy (J/M^{2}X10^4)
Separation Distance (Å)

Fig. 2.10. Calculated interaction energies at different separation distances for pH 3.8 chitin suspensions using the Poisson-Boltzmann equation: (▲) 10^{-3} M NaCl; (△) 10^{-4} M NaCl; (•) 0 M NaCl.

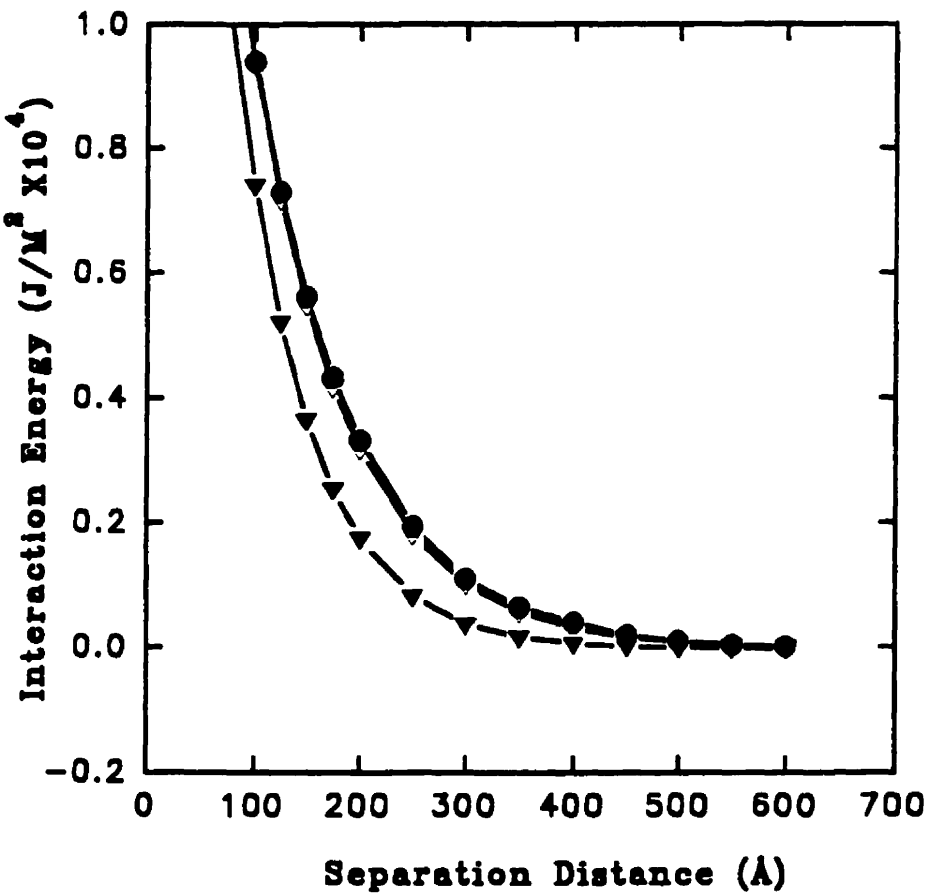
1.0
0.8
0.6
0.4
0.2
0.0
−0.2
Interaction Energy (J/M² X10⁴)
0
100
200
300
400
500
600
700
Separation Distance (Å)

Fig. 2.11. Calculated interaction energies at different separation distances for pH 2.8 chitin suspensions using the Poisson-Boltzmann equation: (□) 10^{-3} M NaCl; (▲) 0 M NaCl.

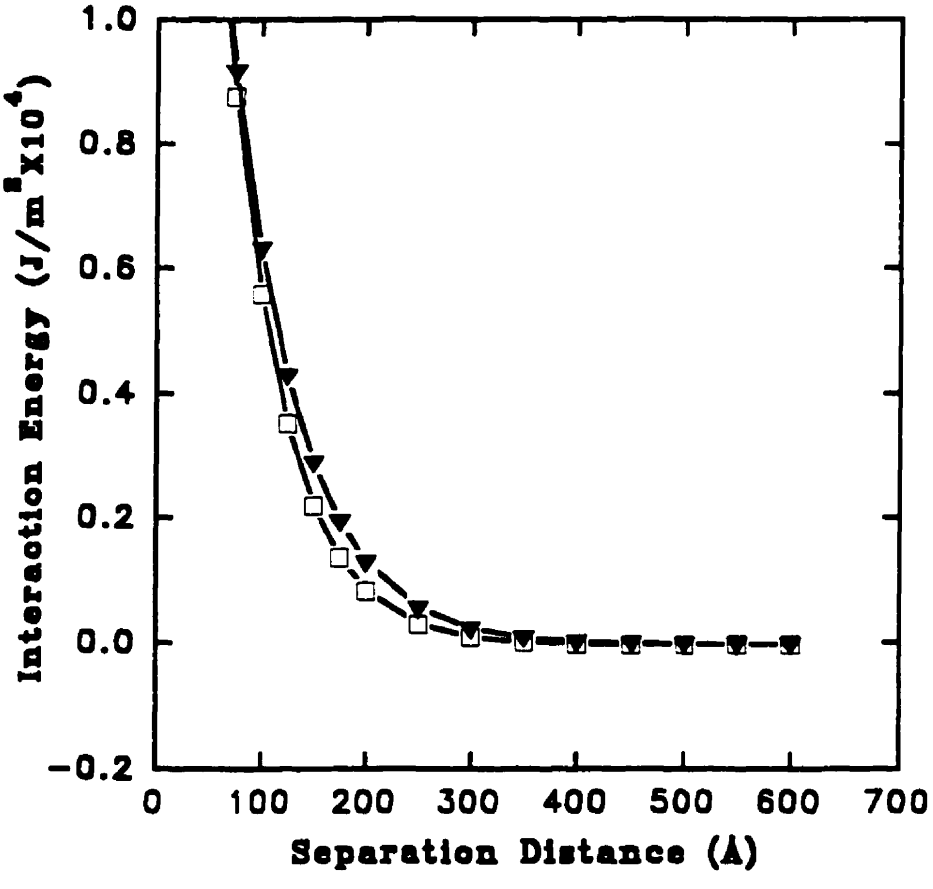
1.0
0.8
0.6
0.4
0.2
0.0
−0.2
Interaction Energy (J/m²X10⁴)
0
100
200
300
400
500
600
700
Separation Distance (Å)

corresponds to the distance between adjacent crystallites at which the interaction energy just starts to exceed the zero energy level, and we have arbitrarily fixed this energy level at 0.01×10^{-4} J/m^2, L_R values can be estimated from the interaction energy curves (see Table 2.2). When compared to the values derived from the phase diagrams according to Onsager's treatment (see Table 2.2), we can see that the values obtained from the phase diagrams at pH 4.9 are lower, even though they are of same order. The reason for this might be that the ζ potential has been measured in dilute conditions whereas the phase diagrams are obtained at a relatively high concentration of chitin. As already mentioned, at this concentration level, the contribution of the polyelectrolyte (chitin crystallites) to the ionic strength is certainly not negligible, and the ζ potential measured in the condition of phase separation would be probably lower than in dilute conditions. Moreover, this discrepancy is less pronounced for the sample suspensions having a higher total ionic strength, when the contribution of the polyeletrolyte is less.

2.4 CONCLUSIONS

Chitin crystallites prepared from HCl hydrolysis of crab shell are found to be positively charged by conductimetric titration and ζ potential measurement. FFTEM shows that the suspension from HCl hydrolysis is polydisperse with an average particle size of 200 nm in length and 8 nm in width which is consistent with previous results (5). FFTEM reveals also that there is a certain degree of aggregation in the chitin suspensions.

The Zeta potential measurements which are made in relatively dilute conditions clearly show the screening effect due to the double layer compression when the acid and salt concentrations are increased. The phase diagrams, however, which are obtained with concentrated liquid crystalline suspensions do not show significant change with added NaCl. This is attributed mainly to the contribution of the chitin crystallites themselves to the ionic strength. To be able to see the effect of electrolytes on phase separation, i.e. on

the double layer compression, the concentration in 1:1 electrolyte should be higher than 10^{-3} M, but above this critical concentration there is flocculation of the chitin suspensions. This limits our experiments to an electrolyte concentration level which doesn't significantly affect the total ionic strength.

The interaction energy calculated from the Zeta potential measurements indicate that the effective repulsive layer thickness L_R derived from energy curves are comparable with the values derived from the phase diagrams according to Onsager. This method is thus valid for charged rod-like particles if the electrostatic repulsion is treated as an increase of the effective diameter of the rods.

The Debye length κ^{-1} has also been compared to L_R. The best fit was found when κ^{-1} was estimated by taking into account the contribution of the chitin crystallites to the total ionic strength as well as by assuming an hypothetical linear charge density close to the Manning limit.

2.5 REFERENCES

1. Muzzarelli, R. A. A., *Chitin,* Pergamon Press, Oxford, (1977).
2. Hougu, T. and Phillips, G., *New fibres*, pp 122-123, Ellis Horwood (1990).
3. Neville, A. C., *Biology of Fibrous Composite-development Beyond the Cell Membrane*, Cambridge university press (1993).
4. Bouligand, Y. C. r. *Acad.Sci. Paris* 1965, **44**, 531
5. Revol, J.-F. and Marchessault, R. H. *Int. J. Biol. Macromol.*, **15**, 329-335 (1993).
6. Marchessault, R. H., Morehead, F. F. and Walter, N. M. *Nature*, **184**, 632 (1959).
7. Revol, J.-F., Godbout, L, Dong, X., Gray, D.G., Chanzy, H. and Maret, G. *Liquid Crystals*, **16**, 1, 127 (1994).

8. Revol, J.-F., Bradford, H., Giasson, J., Marchessault, R. H., and Gray. D.G., *Int. J. Biol. Macromol.*, 1992, **14**, 170-172.

9. Bawden, F. C. and Pirie, N. W. *Proc. R. Soc. Lond.* (b) **123**, 274 (1937).

10. Maret, G., Milas, M. and Rinaudo, M. *Polym.Bull.*,**4**, 291 (1982).

11. Onsager, L., *Ann. N. Y. Acad.Sci.*, **51**, 627 (1949).

12. Stroobants, A., Lekkerkerker, H. N. W. and Odijk. Th., *Macromolecules,* **19**, 2232-2238 (1986).

13. Sato, T., Kakishi, T. and Teramoto, A., *Polymer*, **31**, 824 (1990).

14. Fraden, S., "*In observation and Prediction of phase transitions in complex fluids*" NATO-ASI-Course CXXIX, 26 july-5 August 1994 Eds: M.Baus, L.F.Rull, J.P.Ryckaert.

15. Fraden, S., Maret, G., Caspar, D.L.D., and Meyer, R. B., *Physical Review Letters*, 63, 19, 2068 (1989).

16. Bellare, J. R., Davis, H. T., Scriven, L. E. and Talmon, Y., J. *Eletron Microsc. Tech.*, **10**, 87 (1988).

17. Zasadzinski, J.A.N., Bailey, S.M.J. *Electron Microsc.Tech.*, **13**, 309 (1989).

18. Raymond, L., Morin, F. G. and Marchessault, R. H., *Carbohydrate Research,* **246**, 331(1993).

19. Chan, D. Y. C., Pashley, R. M. and white, L. R., *J. colloid and interface science*, **77(1)**, 283 (1990).

20. Araki, Y. and Ito, E., *Eur. J. Biochem.* **55**, 71-78 (1975).

21. Kafetzopoulos, D., Martinou, A. and Bouriotis, V., *Proc. Natl. Acad. Sci.* USA, **90**, pp. 2564-2568 (1993).

22. Rinaudo, M. and Domard, A., *Proceedings from the 4th International*

Conference on Chitin and Chitosan, Ed. Skjak-Braek, G., Anthonsen, T. and Sandford, P., pp 71-86 (1988).

23. Moscicki, J. K. and Williams, G. *Polymer*. **23**, 558-568 (1982).
24. Dong.X., Kimura, T., Revol, J-F. and Gray, D. G., *Langmuir*, **12** (8), 2076 (1996).
25. Manning, G. S., *J. Chem. Phys*. **51,** 924 (1969).
26. Brenner, S. L. and Parsegian, V. A., *Biophys. J.* **14**, 327 (1974).
27. Myers, D., *Surfaces, Interfaces and Colloids*: principles and applications, VCH Publisher Inc., New York (1990).
28. Delgado, A., Gonzalez-caballero, F. and Bruque, J.M., *J. coll. and Interface Sci.*, **113**, 1, 203-210.
29. Van Oss, C.J., *Interfacial Forces in Aqueous Media*, Marcel Dekker, New york (1994).

Chapter 3

RHEOLOGICAL PROPERTIES OF AQUEOUS SUSPENSIONS OF CHITIN CRYSTALLITES

3.0 ABSTRACT

Rheologically, suspensions of chitin crystallites are found to behave as other molecular liquid crystalline polymers (LCPs). The average hydrodynamic diameter of the crystallites in the suspension at pH 4 is determined to be approximately 80 nm using dynamic light scattering. Conductimetric and pH titration results show that the pK_a of the crystallites is 6.3 ± 0.1, which is the same as that reported for chitosan. In comparision with phase diagrams, the flow properties of isotropic, biphasic, and anisotropic suspensions were investigated. For isotropic suspensions, a classical shear thinning behaviour of rodlike particles is observed. In the case of biphasic suspensions, a two-regime curve is observed where tactoids first orient, deform, and then break up under the shear force. Similar to other LCPs, a three-regime flow curve is found for the anisotropic suspensions. The viscosity-concentration curve exhibits a maximum at the phase separation concentration, and this maximum is less distinct with a decrease of the ionic strength. A secondary electroviscous effect due to strong particle-particle interaction influences the viscosity of the suspensions at higher concentration.

3.1 INTRODUCTION

In Chapter 2, the phase diagram of the crystallite suspension in water was determined, the effect of the ionic strength in the suspensions on phase separation was studied, and the microstructure of films obtained by drying the helicoidal phases was characterized using FFTEM. In this chapter, we report on the rheological properties of

these aqueous chitin crystallite suspensions as a function of shear, pH and concentration. Recently, chitin has been used for making artificial skin (1) since it stimulates the growth of epithelial cells. The process of preparing the artificial skin requires understanding of the flow properties of chitin crystallites. Rheological properties of a suspension are a function of both the shape of the particles and the interparticle forces: dispersion and electrostatic repulsive forces. The viscosity of dilute suspensions of rodlike particles has been treated theoretically for the case of very low shear stress (2). The theoretical treatment has been confirmed in experiments using model rod systems such as poly-γ-benzyl-L-glutamate (PBLG) in m-cresol (3) and dilute suspensions of charged cellulose microfibril fragments (4). Hermans (3) reported that the viscosity of PBLG in m-cresol reached a maximum at the concentration where the phase transition of isotropic to anisotropic occurred. This was confirmed by Kiss and Porter for the same polymer (5). Similar observations were made by other workers, such as Papkov, in their study of poly-p-benzamide solutions (6). Aharoni (7) and Balbi et al. (8) suggested that the onset of liquid crystallinity was not related to the concentration at the maximum viscosity but rather to a shoulder in the viscosity-concentration curve. Aharoni (7) described the entire viscosity-concentration curve covering the isotropic, biphasic and anisotropic phases in terms of axial ratio . Nevertheless, there was no successful theoretical interpretation of this viscosity-concentration curve until Doi (9) extended the Doi-Edward rigid rod solution theory to the entire concentration range and formulated a molecular basis for the relationship between viscosity and the order parameter (S). In addition, the flow behaviour of liquid crystalline polymers (LCPs) such as PBLG and hydroxypropylcellulose (HPC) has been investigated by several authors (10,11). Typically, flow curves of LCP solutions display three regions: shear thinning, a Newtonian plateau and shear thinning, as was proposed by Onogi and Asada (12). This result has become a scaffold for interpreting the flow behaviour of LCPs (13,14).

In a shear flow, the viscosity of charged particles is affected by distortion of the electrical double layer surrounding them and the electrostatic interaction between neighbouring particles. This effect was first investigated by Smoluchowski (15) who called it "electroviscous effect". Extensive theoretical and experimental investigations have shown how the electroviscous effect influences the viscosity (16, 17, 18, 19).

In the present study, the flow behaviour of isotropic, biphasic and anisotropic suspensions of chitin crystallites in water is reported. The effect of solution anisotropy on the viscosity of the suspension is studied by relating the phase diagrams to the viscosity-concentration curves. The electrostatic interaction of the electrical double layer around particles was studied by measuring the viscosity and zeta potential of the suspensions with or without NaCl.

3.2 EXPERIMENTAL

3.2.1 SAMPLE PURIFICATION

Chitin samples purchased from Fluka (practical grade) were first disintegrated to pass through a 20-mesh screen using a Wiley mill. This was followed by washing the samples several times with deionized water and drying in a fume hood. Then, the samples were boiled in a 5% KOH solution for several hours to remove residual protein. Following this, the chitin samples were bleached using 8.5 g of $NaClO_2$ in one liter of water containing ~0.3 M sodium acetate buffer in a ratio of 0.5 kg to one liter bleaching solution, for 6 hours at 80°C. The bleaching solution was changed every 2 hours followed by rinsing the samples with deionized water and decanting the top aqueous layer. Finally, the bleached samples were washed several times with deionized water prior to an acetone rinse and subsequent air-drying in a fume hood.

3.2.2 RHEOLOGICAL AND ZETA POTENTIAL MEASUREMENTS

The chitin suspensions prepared from purified chitin samples as described in Chapter 2 were first concentrated to approximately 9% (w/w) using polyethylene glycol. A series of samples for rheological measurements were prepared by diluting the concentrated sample with a solution of HCl at the same pH. Rheological measurements of the suspensions were made using a Bohlin (VOR) rheometer at 25 $\pm$ 0.5C^0 with Couette geometry in the viscometry mode. An ethylene glycol water bath was used to assure a constant temperature for all the measurements. The double gap sample cell (24/27) was used, and a 1.90 g·cm torque bar was selected. The calibration reading was first made against a silicon oil standard of 8.9 cP (Brookfield) at a shear rate of 46.16 (1/s) and 25 ^{0}C prior to the actual measurements. For the rheological measurements, an aliquot (7.5 ml) of the suspension was pipetted into the 10 ml sample cell and the end effect was eliminated by controlling the sample level. The measuring process was controlled via an IBM 486 PC through an interface whereby the viscosities of the suspensions at different shear rates were automatically recorded. For each set of measurements an "up-down" shear-rate cycle was recorded immediately after the sample was transferred into the sample cell. Only the "up" parts of curves are presented here. The lowest shear rate in our measurements was always 0.185 (1/s) and the highest shear rate varied from sample to sample. For isotropic suspensions, the maximum was typically 581 (1/s).

The procedure of zeta potential measurement of the suspensions was the same as described in Chapter 2.

3.2.3 PHASE DIAGRAMS

For each series of suspensions at a given pH, a corresponding phase diagram was constructed. As described in Chapter 2, the ratio of two phases in the suspension was

observed in stoppered cylindrical NMR tubes of 5 mm diameter. The volume fraction of the upper phase was determined from the observed height of the two menisci displayed in the column viewed through crossed polarized films with back illumination after the NMR tubes stood for one week at room temperature.

3.2.4 ELECTROVISCOUS EFFECT IN CHITIN SUSPENSIONS

A concentrated chitin suspension (8%, w/w) was first adjusted to pH 4 with HCl followed by ultrasound treatment. Then, 1.01 ml of 0.1 N NaCl was added to 100 ml of suspension. A series of samples covering the concentration range of isotropic, biphasic and anisotropic were prepared by diluting the concentrated suspension with 10^{-3} N NaCl solution of pH 4. The viscosity measurements of these suspensions were performed as described above.

3.2.5 DYNAMIC LIGHT SCATTERING

A Brookhaven Bi-2030 AT dynamic light scattering instrument was used in our study. A concentrated suspension at pH 4 was diluted to approximately 0.05% (w/w) with water of pH 4. Similarly, the suspension at pH 4 with 10^{-3} M NaCl was also diluted to 0.05% with water having the same pH and ionic strength. The measurements were carried out at $20^{0}C \pm 0.1$ with ten repetitions.

3.3 RESULTS

The chitin crystallites from HCl hydrolysis were characterized using freeze-fracture TEM and the results were presented in Chapter 2. A typical average size of chitin crystallite was found to be 200 $\pm$ 20 nm in length and 8 $\pm$ 1 nm in width. The presence of a certain degree of aggregation was also observed in the suspension. In this chapter, dynamic light scattering (20) was used to characterize the particle size in the suspension

at pH 4 (see Table 3.1). The difference between the results from TEM and dynamic light scattering in terms of diameter is due to the fact that the latter gives equivalent size information including the electrical double layer around crystallites. The existence of an electrical double layer around particles was also demonstrated by dynamic light scattering since adding NaCl reduced the diameter of the particles (see Table 3.1). This conclusion is also supported by the data in the following sections.

TABLE 3.1 The Diffusion Coefficient, Equivalent Spherical Diameter, and Hydrodynamic Diameter of Chitin Crystallites from Light Scattering*

pH	[NaCl] (M)	D_{20}[a] (10^{-8} cm^2/s)	d_e (nm)[b]	d_r (nm)[c]
4	0	1.8	123	89
4	10^{-3}	1.9	113	83

[a] D_{20} is the diffusion coefficient of the suspension at 20°C.

[b] d_e is the equivalent spherical hydrodynamic diameter of the crystallites.

[C] d_r is the calculated hydrodynamic diameter of the crystallite from D_{20}, assuming the length of the crystallite is 200 nm (20).

*Note: No special effort was made to fractionate the suspensions which literature shows that it is polydisperse and readers should not expect a good agreement between the values from dynamic light scattering and electron microscopy dimensions.

3.3.1 CONDUCTIMETRIC AND pH TITRATION OF CHITIN SUSPENIONS

According to the last chapter, chitin crystallites are present as positively charged particles due to the protonation of glucosamine present at the crystallite surface in acidic media according to the following equation:

$$Glu\text{-}NH_2 + H^+ \rightleftharpoons Glu\text{-}NH_3^+ \qquad (3.1)$$

The average surface charge density of the crystallites was shown to be approximately 0.5 e/nm^2 (see Chapter 2) when the accessible surface amino groups are completely protonated. The surface charge density of crystallites depends on the pK_a of $Glu\text{-}NH_3^+$, which determines the dissociation of this acid, and on the pH of the suspension. Muzzarelli has reported a pK_a of 6.3 for chitosan and 7.5 for 2-amino-2-deoxy-β-D-glucose (21). As described in the experimental section, both the observed pH and the conductimetric titration results are used to determine pK_a based on Eq. 3.2 and 3.3:

$$Glu\text{-}NH_3^+ + OH^- \rightarrow Glu\text{-}NH_2 + H_2O \qquad (3.2)$$

This method is recommended for its accuracy in establishing the pK_a i.e. the point where half the amount of NH_3^+ is consumed in the titration. A typical pH and conductimetric titration curve is shown in Fig. 3.1. Based on the Katchalsky-Spitinik equation (22):

$$pH = pK_a + \log[\alpha/(1-\alpha)] = pK_0 - \epsilon\Delta\Psi(\alpha)/KT \qquad (3.3)$$

where α is the degree of neutralization, $pK_a = pH$ when α is 0.5, pK_0 is the pK_a at zero surface charge and $\Delta\Psi(\alpha)$ is the difference of the electrostatic potential between the crystallite surface and the reference. From the titration curve shown in Fig. 3.1, the pK_a of the chitin crystallites is found to be 6.3 ± 0.1, which is the same as that reported for chitosan (21). Considering chitin crystallites as a polyelectrolyte, the pK_0, the intrinsic pK_a for charged particles, is calculated (23) to be 8.2 ± 0.1 which is close to the pK_a of 2-amino-2-deoxy-β-D-glucose (21).

Fig. 3.1. Conductimetric and pH titration curves of chitin crystallites.

Titration of Chitin Suspension

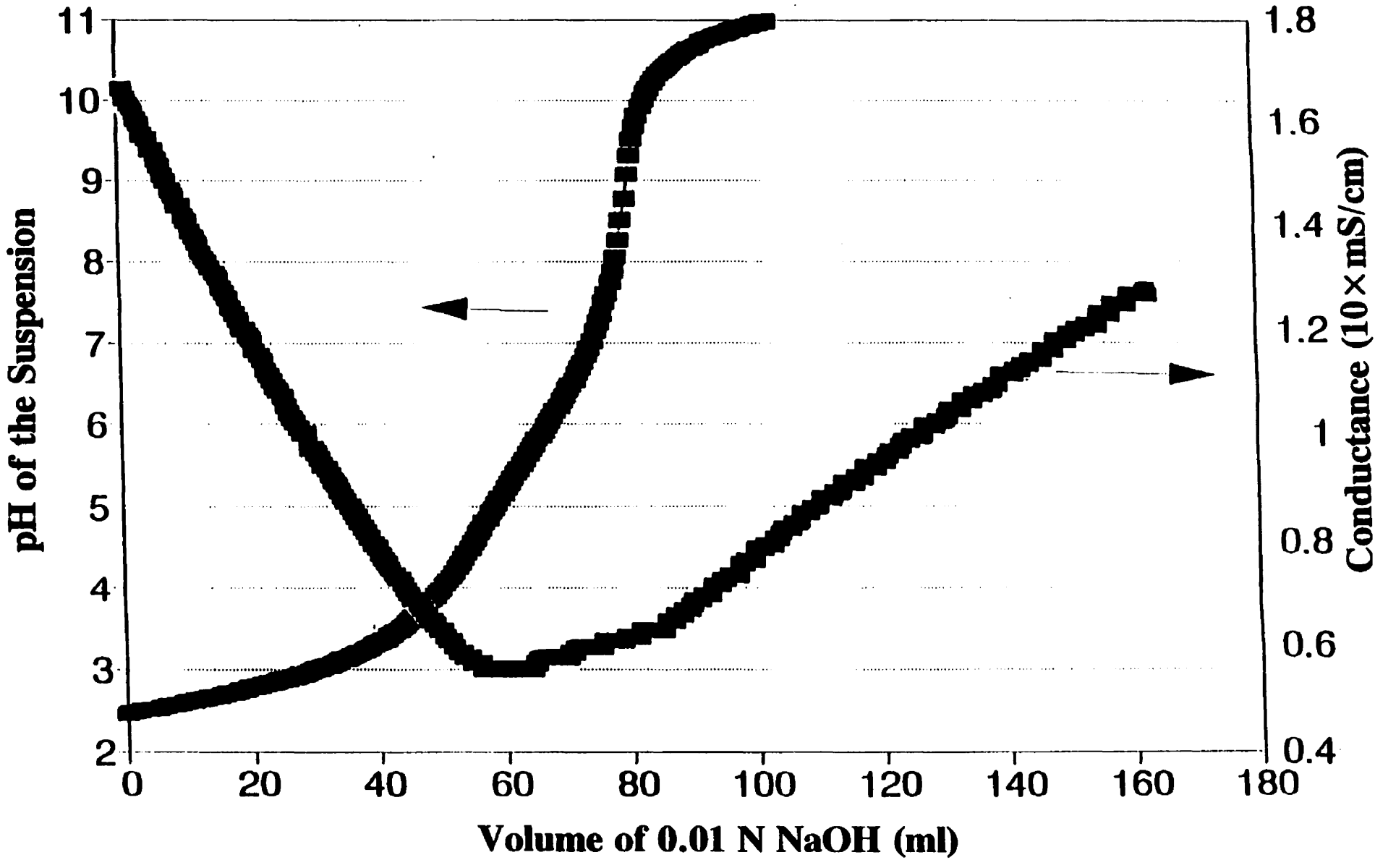

3.3.2 PHASE SEPARATION OF CHITIN CRYSTALLITE SUSPENSIONS

As shown in Chapter 2, an aqueous suspension of chitin crystallites formed by acid hydrolysis will separate into two phases above a certain concentration. Fig. 3.2 shows the phase diagrams of the suspensions at pH 2.8 and pH 3.6, including a schematic of the average texture of the isotropic, biphasic and anisotropic phases. The boundary concentrations for the phase transitions: isotropic-biphasic and biphasic-anisotropic, were found to be dependent on the ionic strength which in turn depends on the pH of the suspension. The curvature shown in Fig. 3.2 is due to the contribution of the charged chitin crystallites to the ionic strength and to the polydispersity of the suspension. As illustrated in the schematic (see the top part of Fig. 3.2), rodlike particles (crystallites) are randomly distributed in the isotropic region, some anisotropic domains (tactoids) are formed in the biphasic region and the rodlike particles are almost completely organized in the anisotropic region (9). In the biphasic region, the anisotropic fraction increases with increasing concentration. The presence of an ordered phase in the chitin suspension affects the viscosity behaviour. In the following sections, the relation between viscosity and volume fraction of the anisotropic phase is explored.

3.3.3 THE FLOW PROPERTIES OF CHITIN CRYSTALLITE SUSPENSIONS

The plots of the viscosity versus shear rate for isotropic chitin suspensions at pH 2.8, 3.6 and 4.5 having corresponding concentrations of 2.2%, 1.9% and 1.97% (w/w) are shown in Fig. 3.3. The viscosity of the suspensions decreases monotonically with an increase of shear rate until it approaches the shear thickening point. The effect of pH on the viscosity of the isotropic suspensions is minor and the same is true for a range of particle concentrations. This behaviour is predictable for the isotropic suspensions because there is sufficient room for the rodlike particles to tumble with little interaction between particles at these dilutions, (see **Schematic *a*** in Fig. 3.2 and next section). The particle

Fig. 3.2. Diagrams of phase separation of the suspensions at pH 2.8 and 3.6 and the schematics showing rodlike particles and tactoids in the (a) isotropic, (b) biphasic, and (c) anisotropic regions of chitin suspensions. The size of tactoids is of the order of 1μm or more, and the size of a rodlike particle is 200 nm in length and 8 nm in width.

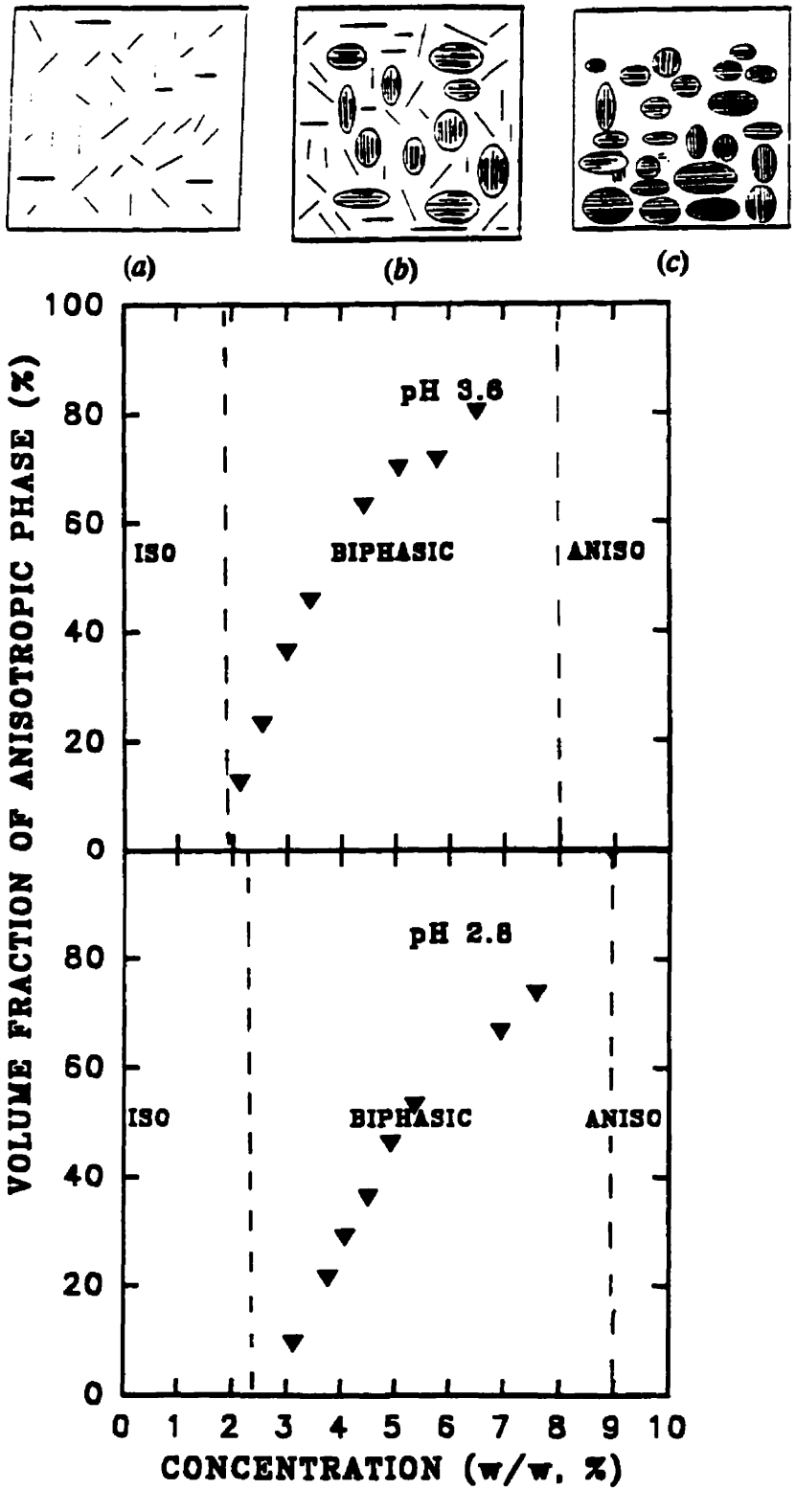
(a)
(b)
(c)
pH 3.6
ISO
BIPHASIC
ANISO
pH 2.8
ISO
BIPHASIC
ANISO
VOLUME FRACTION OF ANISOTROPIC PHASE (%)
0
20
40
60
80
100
0 1 2 3 4 5 6 7 8 9 10
CONCENTRATION (w/w, %)

Fig. 3.3. Rheograms for isotropic suspensions of pH 2.8 (◂), pH 3.6 (■), and pH 4.5 (□) with corresponding concentrations of 2.20, 1.90, and 1.97%.

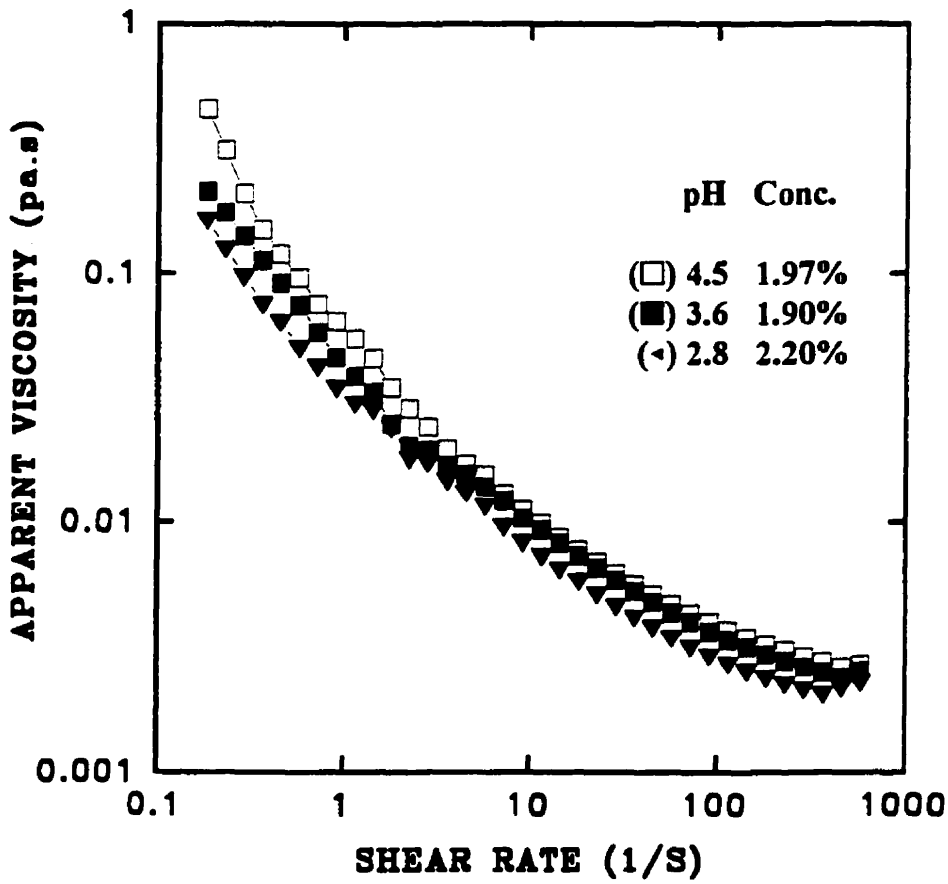
1
0.1
0.01
0.001
APPARENT VISCOSITY (pa.s)
0.1
1
10
100
1000
SHEAR RATE (1/S)
pH Conc.
(□) 4.5 1.97%
(■) 3.6 1.90%
(◂) 2.8 2.20%

tumbling results in a high viscosity at low shear rates because of a large excluded volume (7). With increasing shear rate, particles are aligned and the viscosity drops rapidly (see Fig. 3.3).

The viscosity of biphasic suspensions at pH 2.8, pH 3.6 and pH 4.5 with corresponding concentrations of 5.1%, 5.3% and 5.0% (w/w) is plotted as a function of shear rate in Fig. 3.4. Clearly the flow curves exhibit two regimes with a sharp transition point. The viscosity decreases rapidly with increasing shear at low shear rates in the first regime and then decreases more gradually in the second regime. In this case, the rodlike particles and ellipsoidal anisotropic domains coexist (see **Schematic *b*** in Fig. 3.2). It is believed that both domains shear orient at the low shear rate (14). The tactoids probably undergo plastic deformation. When the shear rate increases further, the tactoids are broken down and partially dispersed into rodlike particles which in turn orient further under the influence of the increasing shear forces. This corresponds to the second regime in Fig. 3.4. The overall viscosity of the system is the sum of the contribution of the low viscosity ordered phase and of the high viscosity disordered phase. The effect of pH on the viscosity is not pronounced in this region because the distance between particles in the biphasic suspension is too large to produce strong particle-particle interactions.

For the suspensions which are nearly 100% anisotropic, a three-regime flow behaviour is observed. Fig. 3.5 shows that the viscosity first decreases with increasing shear rate with a slope of between -1 and -1/2, followed by a plateau in which the viscosity is almost constant, and then decreases again with increasing shear rate. Based on the Onogi and Asada model (12), the viscosity dependency can be interpreted in terms of the response of the tactoids to the shear forces (see **Schematic *c*** in Fig. 3.2). In regime I the structure of tactoids is not altered, but they flow over each other with some deformation. Regime II describes when the tactoids start to break up due to shearing. The residual tactoids are probably highly deformed. Regime III begins when the shear rate becomes strong enough

Fig. 3.4. Rheograms for biphasic suspensions of pH 2.8 (◂), pH 3.6 (□), and pH 4.5 (■) with corresponding concentrations of 5.00, 5.33, and 5.10%.

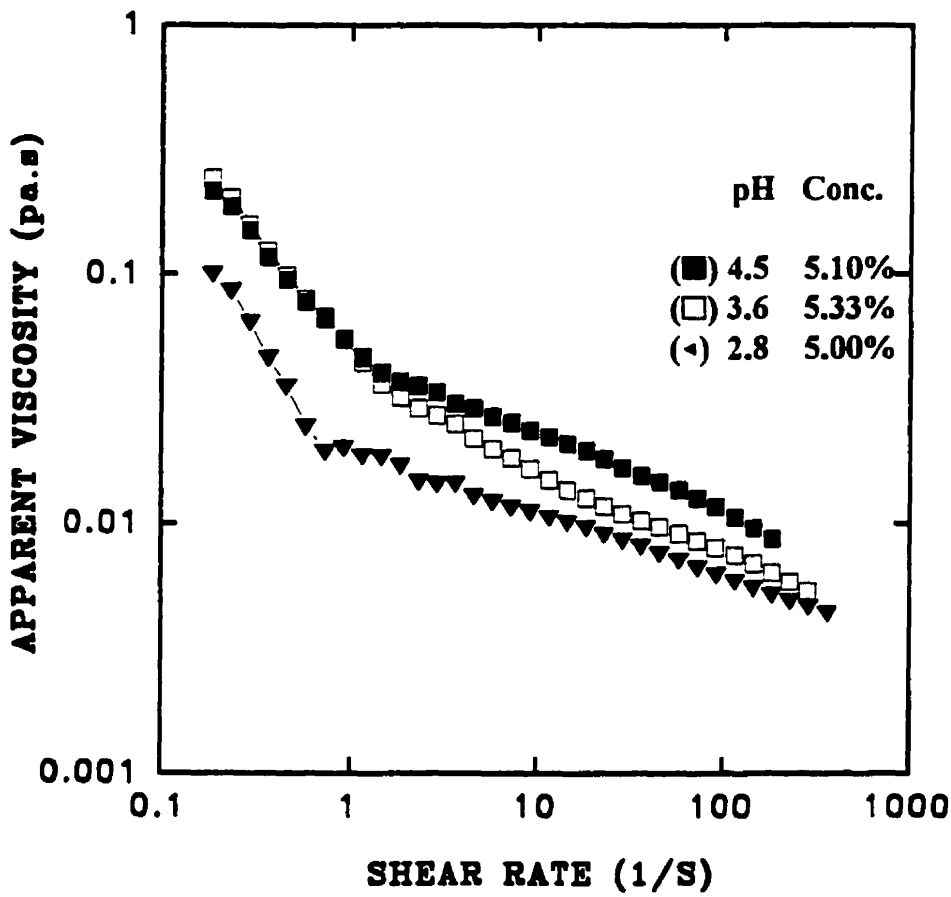
APPARENT VISCOSITY (pa.s)
1
0.1
0.01
0.001
0.1
1
10
100
1000
SHEAR RATE (1/S)
pH Conc.
(■) 4.5 5.10%
(□) 3.6 5.33%
(◂) 2.8 5.00%

Fig. 3.5. Rheograms for anisotropic suspensions of pH 2.8 (△) and pH 4.5 (◂) with corresponding concentrations of 7.00 and 7.70%.

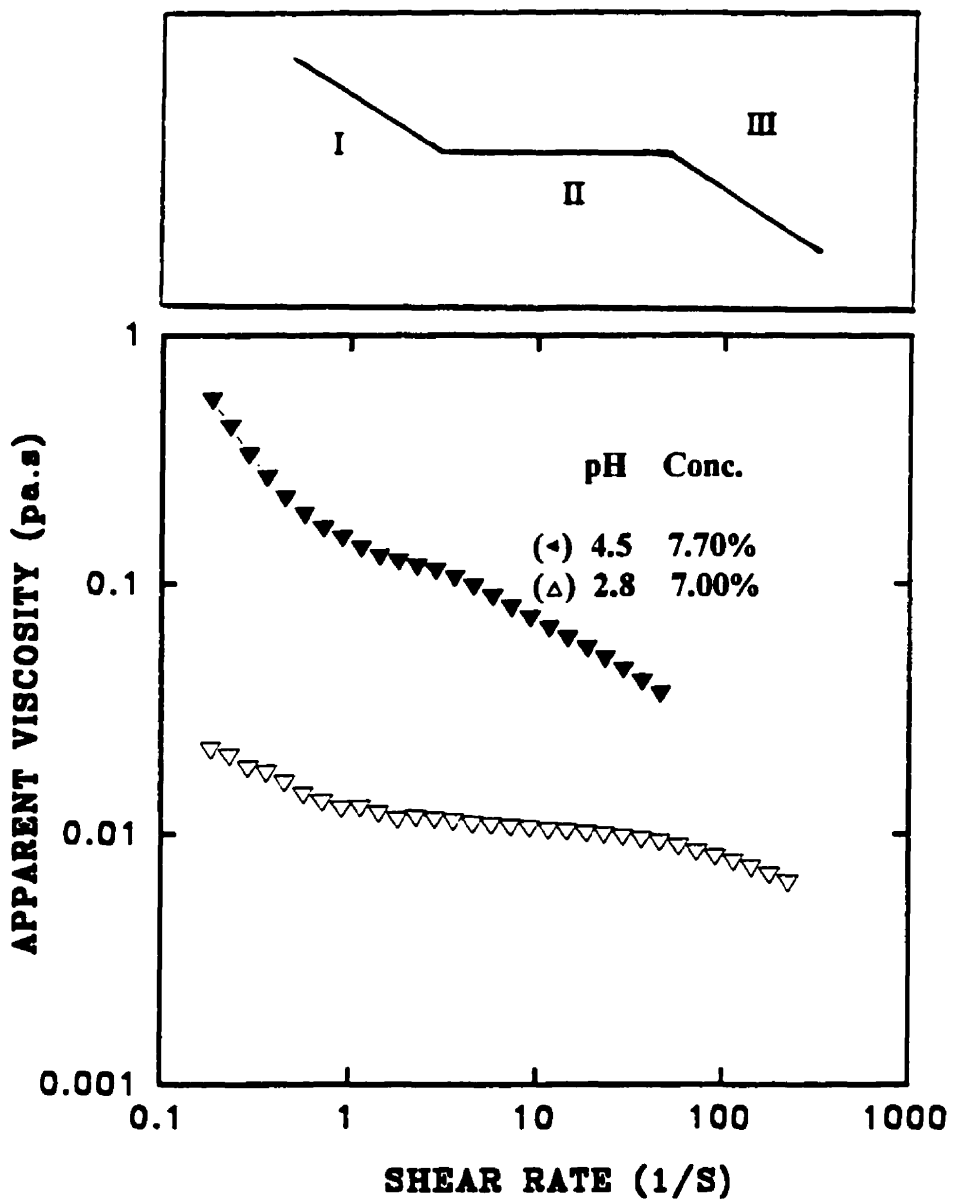
I
II
III
1
0.1
0.01
0.001
APPARENT VISCOSITY (pa.s)
pH Conc.
(◂) 4.5 7.70%
(△) 2.8 7.00%
0.1
1
10
100
1000
SHEAR RATE (1/S)

to break up all the tactoids and create some single particles and/or small aggregates. At this point, the directors of the particles are aligning with the shear direction (14, 24). A large difference between the viscosities of suspensions at pH 4.5 (7.7%, w/w) and pH 2.8 (7.0%, w/w) is found. This is attributed to the contribution of the electrostatic interaction from the electrical double layer around particles since as seen in Fig. 3.6, the concentration variation has a rather limited effect on the viscosity. In general, the effect of pH on the viscosity is a consequence of the variation of the double layer thickness around the particles (often referred as a screening effect). Increasing pH (for pH < 7) decreases the ionic strength of the suspension. Consequently, the double layer thickness increases and the hydrodynamic volume occupied by the rodlike particles is larger. Accordingly the viscosity is higher. In addition, the interaction between the crystallites which strongly depends on the ionic strength of the suspension contributes significantly to the viscosity of the suspensions of higher concentration.

3.3.4 MODEL ANALYSIS

According to Onsager's theory (25), U, a dimensionless concentration, is defined as:

$$U = 2cdL^2 \tag{3.4}$$

where d is the rod diameter, L is its length, and c is the number of particles per unit volume. When $U \leq U_1 = 8.38$, the equilibrium phase is isotropic, that is $S^{eq} = 0$. S is the *scalar order parameter* ranging from 0 (completely isotropic) to 1 (all rods are aligned in the same direction) and is defined as:

$$S = (3/2\mathbf{S}:\mathbf{S})^{1/2} \tag{3.5}$$

Where **S** is the *order parameter tensor*. Similarly, when $U \geq U_2 = 10.67$, the equilibrium phase is nematic where $S^{eq} > 0$. If U is between 8.38 and 10.67, the solution exists as a biphasic solution. For the chitin crystallite suspensions, the phase transition concentration

Fig. 3.6. Rheograms for anisotropic suspensions with concentrations of 7.77% (◂) and 8.70% (□) at pH 4.5.

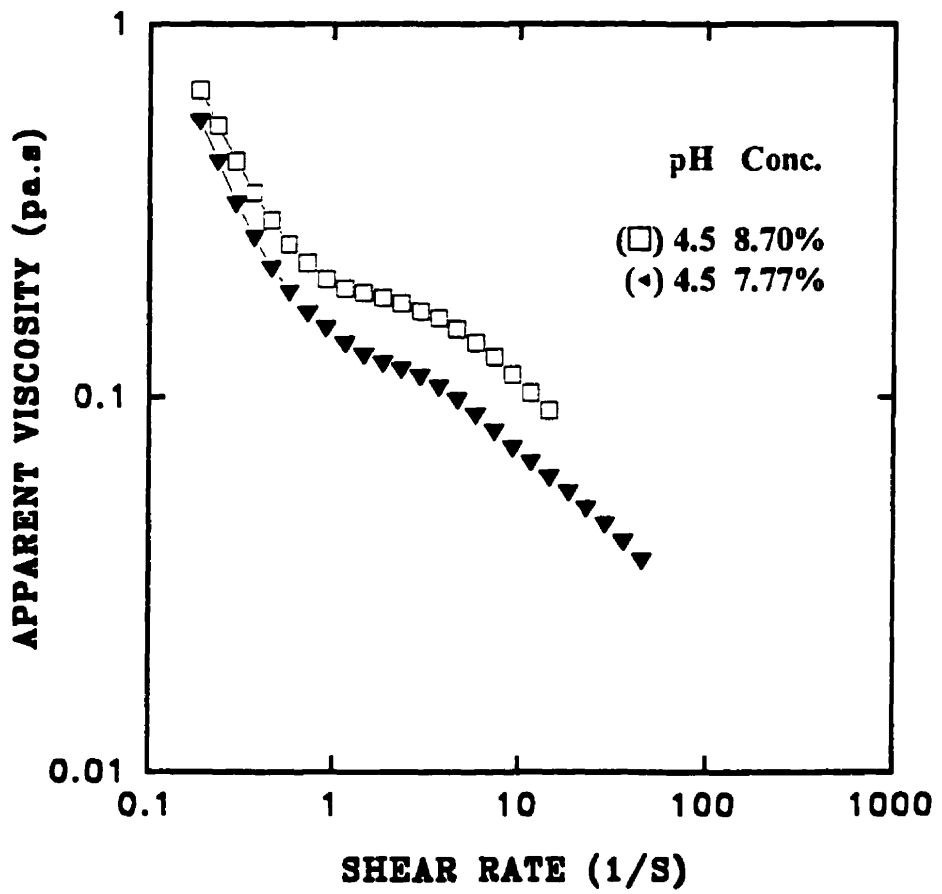
1
0.1
0.01
APPARENT VISCOSITY (pa.s)
0.1
1
10
100
1000
SHEAR RATE (1/S)
pH Conc.
(□) 4.5 8.70%
(◂) 4.5 7.77%

is ionic strength dependent as described in Chapter 2. Typical phase transition concentrations for suspensions at pH 3.8 and 2.8 are shown in Table 3.2. The number of particles per unit volume is calculated based on rods having dimensions of 200 nm in length and 8 nm in width. Considering the formation of electric double layer around particles, the apparent diameter of rod in the suspension is:

$$d_{apparent} = 2/\kappa + 8 \qquad (3.6)$$

where $1/\kappa$ is the double layer thickness from Debye theory

The values of U for these suspensions can be calculated according to eq. 3.4. and are shown in Table 3.2. The deviation of U values from 8.38 is due to the polydispersity of the system and the inaccurate determination of the apparent diameter from the Debye theory (see Chapter 2). The flow curves for isotropic suspensions having U values of 2.3, 3.9 and 10.0, corresponding to pHs of 2.8, 3.6 and 4.5 respectively, are shown in Fig. 3.3. The curves are very similar to that obtained from simulation by Larson using Doi's Model (26) except that the low shear rate part can not be obtained experimentally. Above the phase transition concentration, the chiral nematic phase forms. The flow curves of biphasic suspensions with U values of 5.2, 10.8 and 25.5, corresponding to pHs of 2.8, 3.6 and 4.5 respectively, are shown in Fig. 3.4. Larson (26) proposed that the simulated curve obtained with a biphasic system, which exhibited a very sharp transition, is due to a discontinuous phase transition as the metastable isotropic phase is oriented by shearing in the first regime. For the anisotropic suspensions at pH 2.8 and 4.5, the U values are 7.14 and 39.2 respectively. Under shear, Larson proposed that the directors of particles in the anisotropic suspensions experience tumbling, wagging and aligning motions. However, this theory needs to be confirmed. In our present work, the Onsager theory does not apply because the ordered phase is chiral nematic rather than nematic, the rod-like particles are polydsiperse in length and the electrical double layer is formed around the particles. For biphasic and anisotropic suspensions, it is difficult to compare the Larson's

conclusion with our experimental results due to similar reasons. The U value is extremely high at pH 4.5 because at high pH the contribution of crystallites to ionic strength is significant and our calculation did not take account of this contribution.

TABLE 3.2 The U Values of the Suspenions at pH 2.8 and 3.8 at the Phase Separation Transition Concentration

pH	κ^{-1} (nm)	C (g/100 ml)	C $\times 10^{14}$ (1/ml)	$d_{apparent}$ (nm)	U
3.8	24.15	3.030	16.61	56.30	7.5
2.8	7.636	4.050	22.20	23.27	4.1

3.3.5 VISCOSITY AS A FUNCTION OF CHITIN CRYSTALLITE CONCENTRATION

In Fig. 3.7, the viscosity of the suspension at pH 2.8 is plotted as a function of the concentration at shear rate 1.16 (1/s). As Hermans found for PBLG (3) viscosity reaches a maximum at the phase separation concentration, see Fig. 3.2. Prior to phase separation, rodlike particles occupy a large excluded volume leading to high viscosity whereas beyond this critical concentration, the minimization of free energy requires that particles align spontaneously to produce a high degree of local order leading to anisotropic domain formation. Since the particles no longer tumble freely in the anisotropic domains, a slip motion with less friction develops. As the concentration increases, the volume fraction of the anisotropic phase increases and the overall viscosity decreases to a minimum. When the volume fraction of the anisotropic phase approaches 50%, the viscosity changes more gradually. From the viscosity minimum onward, the concentration effect becomes dominant which results in "contact" between particles and accounts for the rapid increase in viscosity. This behaviour is like "gelation".

Fig. 3.7. Steady shear viscosity vs. concentration for the suspension of pH 2.8.

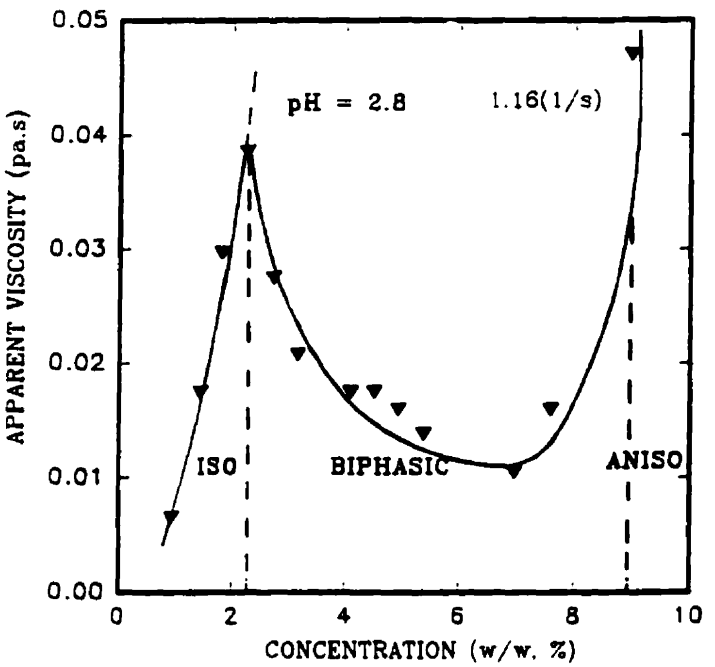
0.05
0.04
0.03
0.02
0.01
0.00
APPARENT VISCOSITY (pa.s)
pH = 2.8
1.16(1/s)
ISO
BIPHASIC
ANISO
0
2
4
6
8
10
CONCENTRATION (w/w. %)

Fig. 3.8 shows a plot of viscosity vs the concentration of the suspension at pH 3.6. It is evident that the change in viscosity with concentration is more gradual than for the suspension at pH 2.8, especially in the biphasic region. In other words, the ordering effect due to the increasing presence of the anisotropic phase is less than that for pH 2.8 suspensions. At a pH of 3.6, the ionic strength being less than at a pH of 2.8, the electrical double layer is less compressed leading to a larger apparent diameter and consequently to a reduced effective axial ratio of the particles (see Table 3.3). This results in a decrease of rodlike characteristic of the particles.

TABLE 3.3 Calculated Double Layer Thickness, Apparent Diameter, and Axial Ratio for Suspensions at pH 2.8, pH 3.6, and 4 with 10^{-3} M NaCl Present

pH	[NaCl] (M)	Double-layer thickness (κ^{-1}) (nm)	Apparent diameter of rod (nm)	Axial ratio
2.8	0	7.6	23.3	8.7
3.6	0	19.2	46.4	4.3
4	10^{-3}	9.6	27.2	7.3

Fig. 3.8. Steady shear viscosity vs. concentration for the suspension of pH 3.6

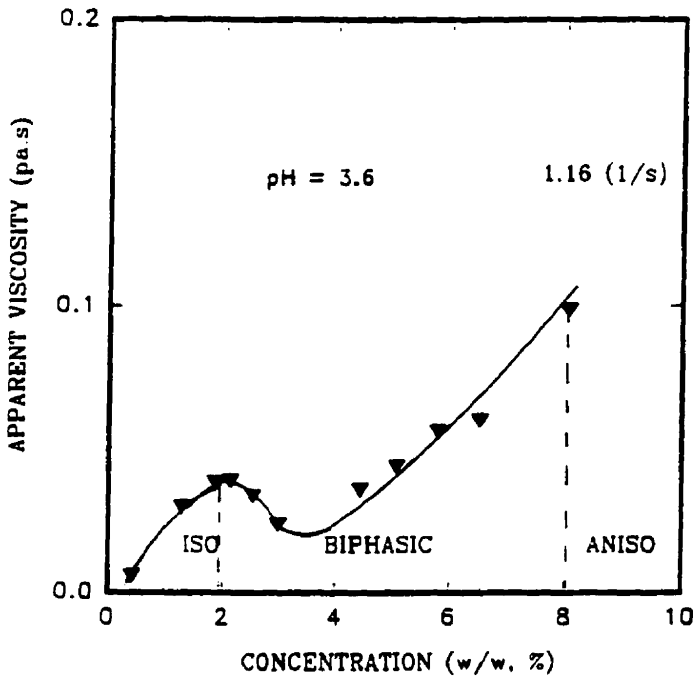
0.2
0.1
0.0
APPARENT VISCOSITY (pa.s)
pH = 3.6
1.16 (1/s)
ISO
BIPHASIC
ANISO
0
2
4
6
8
10
CONCENTRATION (w/w, %)

3.3.6 ELECTROVISCOUS EFFECT

Since chitin crystallites are positively charged in the suspension, the electrical double layer and, as a consequence, the electrostatic interactions significantly contribute to the viscosity of the suspension. This effect includes three factors: (a) the resistance to distortion of the diffuse layer of ions surrounding each particle (b) the electrostatic repulsion between neighbouring particles, and (c) the intraparticle repulsion which affects macromolecular conformation of linear chains. For chitin suspensions the effect (a) is not pronounced, as shown by the small viscosity difference for dilute suspensions at different pHs (Fig. 3.3). The effect (c) does not influence the behaviour of rigid rods. Therefore, only the secondary electroviscous effect influences the viscosity of chitin suspensions. As shown by several authors (16 and 17), secondary electroviscous effects are pronounced in relatively concentrated suspensions since this interaction becomes important when the distance between particles is sufficiently small. In the present work, such an effect is clearly demonstrated in Fig. 3.5.

Another demonstration of the electroviscous effect is shown by comparing Fig. 3.7 and Fig. 3.9 where the viscosities of the suspensions at pH 2.8 without NaCl and pH 4 with NaCl (10^{-3} M) are plotted as a function of the concentration. The curves show similar viscosity properties because the ionic strength and, as a consequence, the apparent axial ratio is of the same order, see Table 3.3. For the suspension at pH 4 with NaCl (10^{-3}), the electrical double layer around the particles is compressed. This effect (screening effect) reduces the electrostatic interaction and thereby decreases viscosity. The screening effect of a surface charge is also reflected in the zeta potential data, see Table 3.4. Table 3.4 shows that the zeta potential of a pH 4 suspension with NaCl (10^{-3} M) is of same order as at pH 2.8. The conductance difference is due the conductivity difference between H^+ and Na^+.

Fig. 3.9. Steady shear viscosity vs. concentration for the suspension of pH 4 with 10^{-3} M NaCl

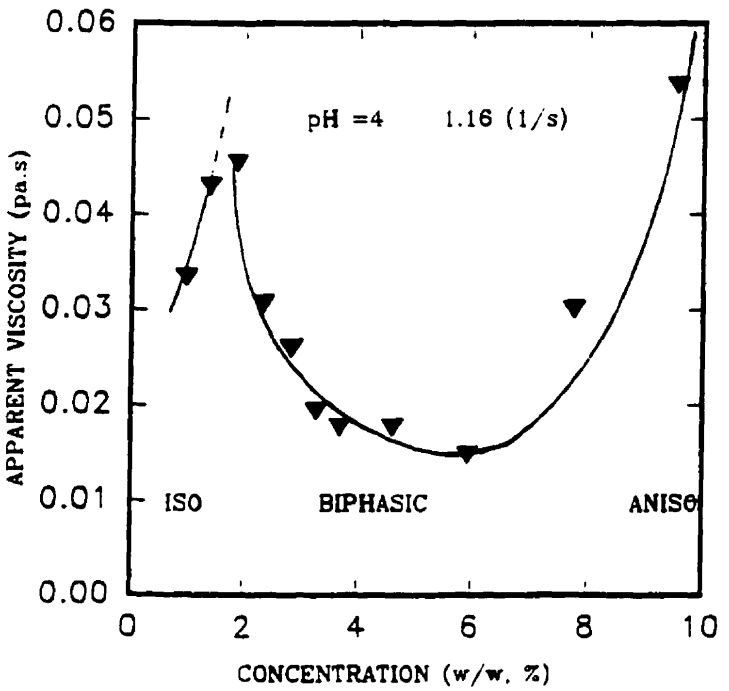
0.06
0.05
0.04
0.03
0.02
0.01
0.00
APPARENT VISCOSITY (pa.s)
pH =4
1.16 (1/s)
ISO
BIPHASIC
ANISO
0
2
4
6
8
10
CONCENTRATION (w/w, %)

TABLE 3.4 Zeta Potentials of the Chitin Crystallites in Suspensions of pH 2.8 and pH 4 with 10^{-3} M NaCl Present

pH	[NaCl] (M)	Zeta potential (mV)	Specific conductance (ms/cm)
2.8	0	44	0.699
4.0	10^{-3}	47	0.180

3.4 CONCLUSIONS

The experimental results show that the viscosity of chitin suspensions is strongly shear rate dependent. For isotropic suspensions, rodlike particles are present in the suspension as individual particles undergoing Brownian motion. Under shear force, particles orient along shear lines producing a decrease in viscosity (3). At a very low shear rate , the suspension should behave as a Newtonian fluid. Unfortunately, we are unable to demonstrate this due to the instrument limitation, but such a behaviour was detected by Marchessault et al. using a special Ubbelohde viscometer (4).

For biphasic suspensions, a two-regime flow curve was observed. This is due to the presence of tactoids in the suspension. For a nearly 100% anisotropic suspension, a three-regime flow curve described as shear thinning, Newtonian and shear thinning again is operative (see Fig. 3.5 and Fig. 3.6). This behaviour is attributed to tactoid orientation/deformation, rodlike particles sliding in tactoids and completely breaking up. It is also speculated that the chiral nematic structure of tactoids could first change to

nematic under shear force before the rodlike particles actually start to slide. The contribution of rodlike particles to the flow curve is less significant for nearly 100% anisotropic suspensions.

A viscosity maximum at the phase separation concentration is observed in the viscosity-concentration curve. This is consistent with the results of other molecular LCPs. It is evident that electrostatic interactions significantly increase the suspension viscosity at higher concentration. This is consistent with theoretical predictions.

3.5 REFERENCES

1. Hongu, T. and Phillips, G., *New Fibres*, Ellis Horwood Limited, West Sussex, England (1990).
2. Simha, R., *J. Phys. Chem.* **44**, 25 (1940).
3. Hermans, J. Jr., *J. Colloid Sci.*, **17**, 638-648 (1962).
4. Marchessault, R. H., Morehead, F. F. and Joan Koch, M., *J. Colloid Science*, **16**, 327-344 (1961).
5. Kiss, G. and Porter, R., *J. Polym. Sci., Polym. Phys. Ed.*, **18**, 361(1980).
6. Papkov, S. P., Kulichikhim, V. G., Kalmykova, V. D. and Malkin, A. Ya., *J. Polym. Sci., Polym. Phys. Ed.*, **12**, 1753 (1974).
7. Aharoni, S. M., *Polymer*, **21** 1413 (1980).
8. Balbi, E., Bianchi, E., Ciferri, A., Tealdi, A. and Krigbaum, W. R., *J. Polym. Sci. Polym. Phys. Ed.*, **18**, 2037 (1980).
9. Doi, M. and Edwards, S. F., *The Theory of Polymer Dynamics*, Oxford University Press, New York (1986).
10. Sigillo, I. and Grizzuti, N., *J. Rheol.* **38**(3), 589 (1994).
11. Wissbrun, K. F., J. Rheol. **25**(6), 619 (1981).

12. Onogi, S. and Asada, T., pp. 127-147 *in Rheology,* Vol. I, Astarita, G., Marrucci, G. and Nicolais, L., Eds., Plenum, New York (1980).

13. Walker, L. and wagner, N., *J. Rheol.*, **38**(5), 1525 (1994).

14. Dadmun, M. and Han, C. C., *Macromolecules*, **27**, 7522 (1994).

15. Smoluchowski, M. von. Kolloidzeit. **18**, 190.

16. Watterson, I. G. and White, L. R., *J. Chem. Soc. Faraday Trans.* II, 77, 1115 (1981).

17. Russel, W. B., *J. Colloid and Interface Sci.*, **55**, 590 (1976).

18. McDough, R. W. and Hunter, R. J., *J. Rheol.*, **27**(3), 189 (1983).

19. Honig, E. P., Pünt, W. F. J. and Offermans, P. H. G., *J. Colloid and Interface Sci.*, 134, 169 (1990).

20. Schmitz, K. S., *An Introduction to Dynamic Light Scattering by Macromolecules,* Academic Press, New York (1990).

21. Muzzarelli, R. A. A., *Chitin*, Pergamon Press, Oxford, England (1977).

22. Domard, A., *Int. J. Biol. Macromol.*, **9**, 98- 104 (1987).

23. Kawaguchi, S., Yekta, A. and Winnik, M. A., *J. Colloid and Interface Science,* **176**, 362-369 (1995).

24. Orts, W. J., Godbout, L., Marchessault, R. H. and Revol, J.-F., *Flow-Induced Structure in Polymers*, presented at the 208th National Meeting of the American Chemical Society, Washington, D. C., August 21-25 (1994).

25. Onsager, L. *Ann. N.Y. Acad.Sci.* **51**, 627 (1949).

26. Larson, R. G., *Macromolecules* **23**, 3983-3992 (1990).

Chapter 4

EFFECT OF DEGREE OF THE DEACETYLATION ON THE PROPERTIES OF CHITIN CRYSTALLITES

4.0 ABSTRACT

Chitin from crab shell was systematically modified using NaOH treatment with control of the reaction time. The degree of deacetylation, monitored using solid state NMR, revealed that the reaction was pseudo first order. Based on this, swollen and NaOH saturated particles are proposed as the reaction system. The weight loss of the partially saponified and neutralized samples after HCl hydrolysis increased linearly with the degree of deacetylation. The crystallinity of the samples was found to increase after acid hydrolysis. According to conductimetric titration, the surface charge density of the crystallites, after acid hydrolysis, was found to increase with base treatment time. The effect of surface charge on the formation of a chiral nematic phase due to the rod-like nature of the crystallites was explored. These results show that because the contribution of charged particles to the ionic strength was significant, the double layer compression was affected and so was the phase separation of the suspension, especially since the surface charge density was close to the Manning limit.

4.1 INTRODUCTION

As shown in Table 1.2 of Chapter 1, the seafood processing industry produces large quantities of shell waste, which is approximately 30% by weight in chitin (1), a linear polysaccharide composed of β-(1-4) linked 2-deoxy-2-acetamido-D-glucose units (Glu-$NHCOCH_3$) (2) (see Fig. 1.1). On a worldwide basis, about 10^5 metric tons of chitin waste is available annually for industrial use (3) with crab and shrimp waste as the principal

sources (4). As described in Chapter 1, chitin is biosynthesized by chitin synthetase (5) and it is reported that deacetylation is due to a chitin deacetylase (6, 7). Partial removal of acetyl groups to leave amine groups on the backbone has a profound effect on chitin properties such as solubility. Chitin with a degree of deacetylation of 75% or above (4) is usually called chitosan and will be referred to as: Glu-NH_2.

Typical applications for chitin and chitosan include water purification, paper wet web strength enhancement, cosmetics additive, and pharmaceutical adjuvant (8). Medical gauzes, ointments and wound dressings have been made from chitin or its derivatives (9) because of its antibacterial, moisture retaining and healing characteristics.

Nascent chitin is a crystalline microfibrillar material usually having the α-polymorphic form such as occurs in crab and shrimp shell waste, etc. as discussed in Chapter 1. It usually exhibits a degree of deacetylation (DD) of approximately 5% "as received" (6). Both the degree of crystallinity and the DD of chitin depend on the source and the method of purification. The crystallographic unit cell parameters and three dimensional crystalline structure were reported by Carlstrŏm (10) for α-chitin and the same information for β-chitin from *Pogonophora* was derived by Blackwell (11), see Chapter 1 for detailed information.

When purified chitin isolated from crab shell is heterogeneously acid hydrolysed, the product, fragmented microfibrils or chitin crystallites, can be called hydrochitin by analogy with hydrocellulose. These crystallites are rod-like colloids from chain scission occurring at random locations along microfibrils. The colloidal stabilization is due to protonation of amino groups on the crystallites which provide a positive surface charge hence repulsive forces between particles (12, 13, 14). Above a certain concentration, chitin crystallite suspensions spontaneously separate into an isotropic and an anisotropic phase (13, 14) with the surface charge influencing the relative amount of the two phases. The anisotropic phase was shown to be chiral nematic and dries down to a film whose texture

mimics the naturally occurring organization of chitin microfibrils in arthropods (13). The effect of electrolyte on the boundary concentration for phase separation: isotropic to anisotropic, has been reported (13, 14). The electrostatic effect due to the surface charge of rodlike particles on phase separation was discussed by Onsager (15) and Stroobants (16). The latter (16) predicted that the boundary concentration for phase separation decreased with increasing surface charge density.

In the present study, chitin samples with a range of DD have been prepared under conditions used to prepare chitosan. Changes in crystallinity of the samples were monitored using x-ray diffraction. Solid state NMR (CP-MAS ^{13}C-NMR) and conductimetric titration were used to measure the DD and the surface amino groups (SAG). The weight loss of the samples having different DD due to acid hydrolysis under standard conditions (14) was recorded. The surface charge density was calculated from the titration data. The actual surface potentials for the suspensions of chitin crystallites having various DD at pH 4 were evaluated. The phase separation behaviour of crystallite suspensions have been compared using phase diagrams. Finally, the optical anisotropy of concentrated suspensions with a high degree of deacetylation was explored.

4.2 EXPERIMENTAL

Technical grade crab shell was ground to 20 mesh in a Wiley mill. Then, the shell was deproteinized in 1% (w/v) NaOH at 60 ^{0}C and demineralized using 1% (w/v) HCl at room temperature overnight. In both cases, the ratio of the shell material to the 1% (w/v) NaOH or 1% (w/v) HCl was 1 g per 10 ml. Treatment of samples with 50% (w/v) NaOH provided material corresponding to various levels of DD by treating crab chitin using 50% (w/v) NaOH with a ratio of liquor to solid (L/S), 4/1, for various length of time at 87-99^{0}C. The overall reaction time ranged from one hour to seven hours. One of the samples was treated with 50% (w/v) NaOH (L/S, 4/1) at 87-99 ^{0}C in a capped jar in an incubator

for seven hours in the presence of 3% $NaBH_4$ (by weight based on the chitin) in order to prevent alkali provoked depolymerization and weight loss. All the alkali-treated samples were washed to neutrality and air dried.

4.2.1 ACID HYDROLYSIS OF CHITIN AND WEIGHT LOSS

Chitin was hydrolysed as described in Chapter 2. For weight loss measurements, the weight of the suspension after hydrolysis was determined by the volume and concentration of the colloidal suspension. The weight loss of the samples due to acid hydrolysis was measured by the weight difference before and after acid hydrolysis.

4.2.2 X-RAY DIFFRACTION OBSERVATIONS

Powder diffractograms for alkali-treated chitin samples were recorded using a Rigaku D/MAX 2400 automated powder diffractometer with rotating anode and equipped with a single crystal monochromator and scintillator detector. CuK_α radiation with a voltage of 40 kV and a current of 120 mA was obtained using a graphite monochromator. The wavelength λ was 1.541 Å. Approximately 0.25 gram of sample was used in the measurement. The measurement was controlled by a Pentium PC using the *Rigmeas* program. A typical $\theta/2\theta$ scan range was from 2^0 to 69.9^0. The degree of crystallinity of the sample based on the $\theta/2\theta$ scan from 5^0 to 50^0 was calculated according to the method suggested by Challa et al. (17) which requires separation of the crystalline peaks from the diffuse background.

4.2.3 DETERMINATION OF DD OF CHITIN SAMPLES

Two methods were used: solid state NMR and conductimetric titration (18). The former provides the average amino group content in the sample. The latter provides only the surface amino content (14). As described in Chapter 2, a Fisher Scientific pH Meter

(Accumet, pH Meter 50) was used to monitor the pH change during titration. The conductance of the suspension was plotted as a function of the volume of 0.01 N NaOH used in the titration. The volume of alkali, needed to neutralize the protonated surface amino groups in the sample, was calculated from the points corresponding to the sharp change in the slope of the titration curve. The calculation of the surface charge density was discussed in Chapter 2.

4.2.4 ZETA POTENTIAL MEASUREMENTS

Zeta potentials for the suspensions of chitin crystallites from blank and alkali-treated material (treated with NaOH for 1 h and 3 h prior to acid hydrolysis) at pH 4 were obtained using a Lazer Zee Meter as described in Chapter 2.

4.2.5 PHASE SEPARATION AND MICROSCOPY

As described in Chapter 2 and Chapter 3, phase separation observations were made using NMR tubes of 5 mm internal diameter. Several ml of the concentrated suspensions at pH 4 were first transferred into 10 ml vials and then diluted with a pH 4 solution of HCl. The vials were shaken vigorously followed by transfer of some suspension into NMR tubes which were stoppered. The height of isotropic phase was recorded by viewing between crossed polarizers after a week standing at room temperature. The volume fraction of the anisotropic phase was determined by dividing the height of that phase by the total height. All the crystallite suspension samples were examined in a Nikon Microphoto-FAX optical microscope.

A transmission electron microscope (Phillip EM 400T) was used to obtain high magnification images of the chitin crystallites. The samples were prepared by contacting a drop of a dilute suspension (around 0.01% w/w) with a carbon coated carbon grid for about 30 seconds. The grid was then washed with deionized water and the water removed

from the grid with help of filter paper. For chitin samples exhibiting a positive charge, the carbon coated microscope grids were used as such. In this case, the carbon support being naturally negatively charged, the chitin crystallites are readily adsorbed onto it.

4.3 RESULTS AND DISCUSSION

The objective of this work was to control the surface charge density of chitin crystallites by varying the time of NaOH deacetylation. Ideally the axial ratio of the crystallites in the suspensions should remain unchanged thereby allowing a study of the effect of surface charge on the cholesteric phase formation of chitin crystallite suspensions.

The resistance of solid chitin to deacetylation can be overcome by using temperature, L/S, and the aqueous NaOH concentration as variables and assuming the following reaction:

$$\text{Glu-NHCOCH}_3 + \text{NaOH} \rightarrow \text{Glu-NH}_2 + \text{NaOCOCH}_3 \qquad (4.1)$$

This treatment was performed in a pilot reactor from which samples were periodically removed. It was observed that the viscosity of the reaction mixture increased with time. This is attributed to the development of microfibril fragments dispersed in a partially deacetylated chitin or chitosan matrix. However, this treatment changes the properties of chitin including crystallinity, surface charge, swelling and interfacial properties. Most notable among these changes is the degree of crystalline perfection as measured using x-ray diffraction.

X-ray powder diffractograms of chitin and alkali-treated chitin samples are shown in Fig. 4.1. Comparing with the d-spacings reported by Carlström (8), the x-ray pattern in Fig. 4.1 can be identified as α-chitin. The same peaks occur in each spectrum including the sample hydrolysed in 50% (w/v) NaOH for seven hours in the presence of $NaBH_4$. It

Fig. 4.1. X-ray diffractometer scans of α-chitin and alkali-treated chitin samples from crab shell, (1) starting chitin (2) chitin sample hydrolysed in 50% NaOH for three hours (3) chitin sample hydrolysed in 50% NaOH for seven hours (4) chitin sample hydrolysed in 50% NaOH for seven hours in the presence of $NaBH_4$. The reaction temperature was 87-99^{0}C.

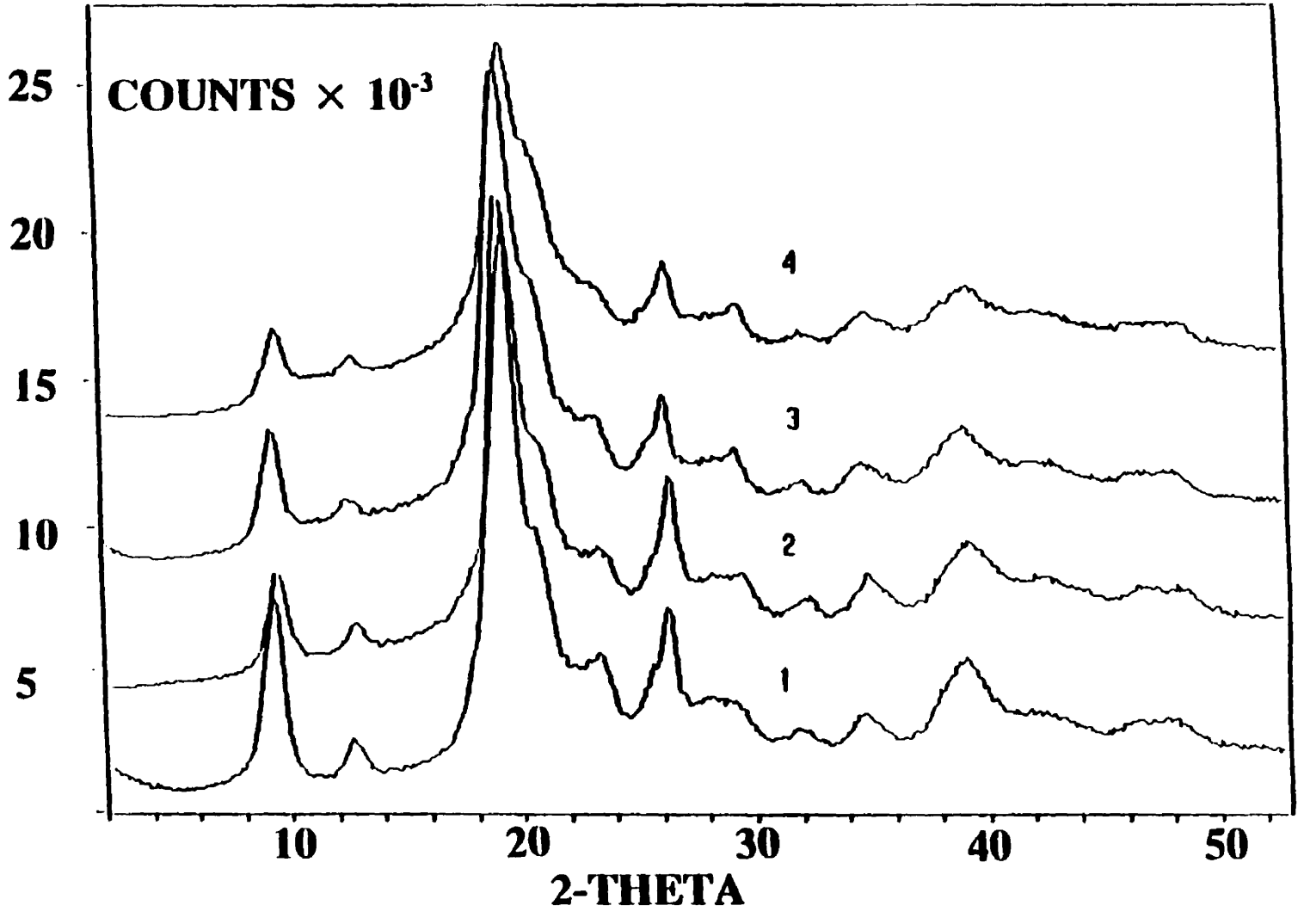
COUNTS × 10-3
25
20
15
10
5
4
3
2
1
10
20
30
40
50
2-THETA

was found that the line broadening and width at half maximum intensity (WHMI) of the composite peak at 20^0(2θ) increases with an increase of reaction time. For the sample hydrolysed in 50% (w/v) NaOH for seven hours in the presence of $NaBH_4$, the WHMI is larger than the others.

4.3.1 CHITIN DEACETYLATION

In concentrated solutions of NaOH (above 43%, w/v), chitin crystallites swell followed by formation of alkali-chitin; thus sodium hydroxide penetrates into the crystalline structure of chitin and more than 0.75 equivalents of sodium can combine with each N-acetylglucosamine (6). Alkali-chitin is partially crystalline (20), disperses rapidly in ice water (21), and regains its original crystalline structure (α form) after washing to neutrality. When the temperature increases, deacetylation takes place. For each swollen crystallite, the reaction can be considered as pseudo homogenous since the lattice of alkali-chitin is nematic-like when swollen, and the sodium hydroxide accesses all the acetamide group as in a reaction vessel. The deacetylation reaction depends on acetamide and OH^- concentrations. The reaction is pseudo first order when sodium hydroxide is in excess as in this case. The kinetic equation (22) is:

$$kt = 2.303\ Log(c_0/c) \qquad (4.2)$$

where t is reaction time, k is a constant, c is the fractional concentration of acetamide groups at time t, c_0 is the original concentration of acetamide group.

In Fig. 4.2, *Log c* is plotted as a function of reaction time t. A straight line is obtained, showing that the reaction is pseudo first order.The acetamide concentration extrapolated to 18 hour, that is when the reaction was terminated, is 73% deacetylation.

Fig. 4.2. Plot of log c, where c is the fractional concentration of acetamide, vs. deacetylation time at 87-99 ^{0}C. The value for 18 hours treatment (■) as a reference was measured by Vanson Inc. using a UV method.

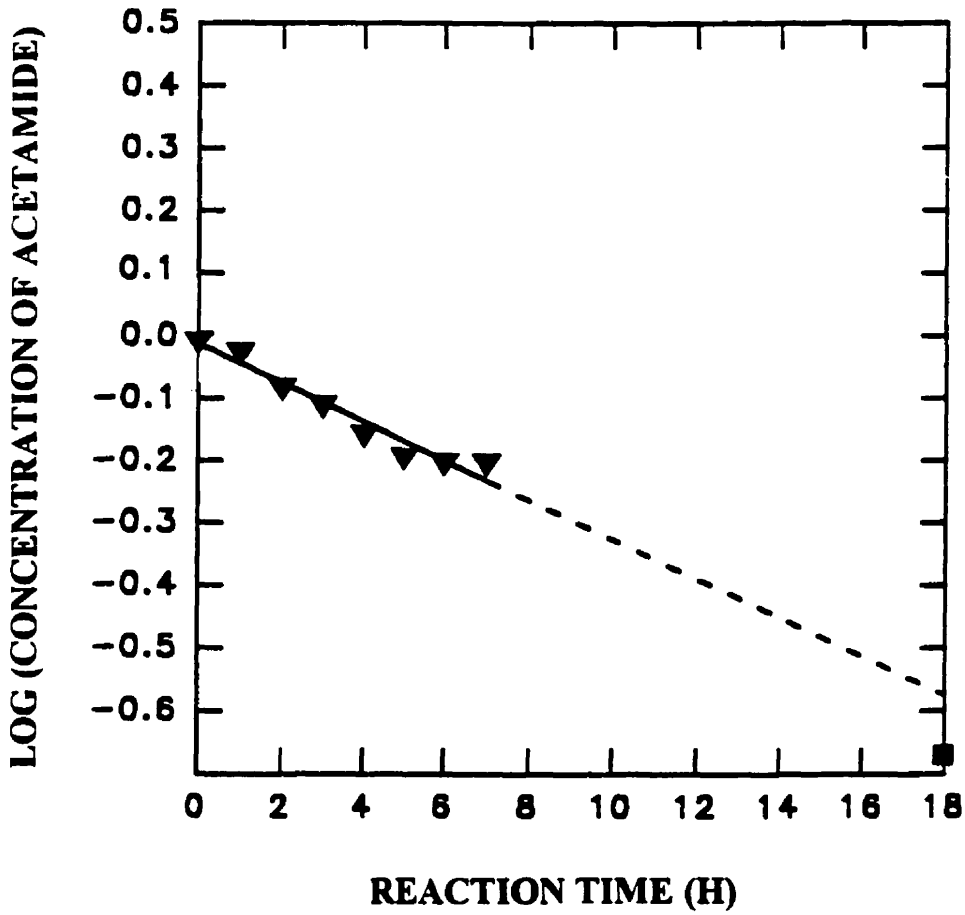
LOG (CONCENTRATION OF ACETAMIDE)
0.5
0.4
0.3
0.2
0.1
0.0
−0.1
−0.2
−0.3
−0.4
−0.5
−0.6
0
2
4
6
8
10
12
14
16
18
REACTION TIME (H)

This is comparable to the observed DD, using an UV method, which was found to be 80% (23).

Fig. 4.3 shows the crystallinity of the alkali-treated samples after washing and drying as a function of alkali hydrolysis time in 50% (w/v) NaOH. It was found that the alkali treatment reduced the crystallinity of the samples until a plateau was reached at 37.4% DD. The crystallinity change as a function of hydrolysis time is due to deacetylation taking place in the swollen crystallites in the samples. Alternatively, one can think in terms of a distribution of crystallite perfection and the less perfect ones are converted to chitosan which cease to count as crystalline chitin and are ultimately dissolved. The loss of the crystalline structure of chitin depends on deacetylation which prevents the intermolecular hydrogen bonding characteristic of α-chitin and breaks the regularity of lateral packing between chains.

For the sample hydrolysed using 50% (w/v) NaOH in the presence of $NaBH_4$, the crystallinity of the sample was 47% (see Table 4.1) which was significantly lower than the other samples and the DD was 49% which was much higher than the other samples (see Table 4.2). This is attributed to the effect of $NaBH_4$ as a reducing reagent which accelerates the deacetylation process, although $NaBH_4$ itself does not reduce the amide groups (24).

Fig. 4.3. Percent crystallinity of the alkali-treated chitin samples after washing and air drying.

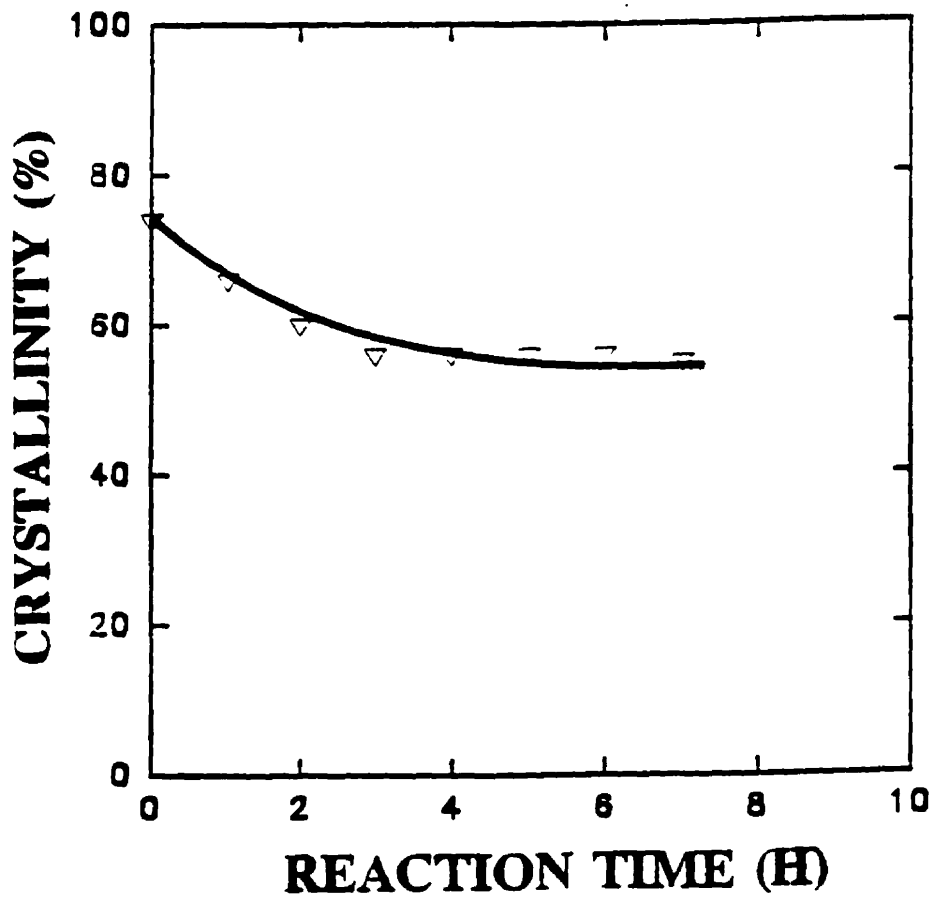
100
80
60
40
20
0
CRYSTALLINITY (%)
0
2
4
6
8
10
REACTION TIME (H)

TABLE 4.1 Crystallinity of the Alkali-Treated Chitin Samples Before and After Acid Hydrolysis

Reaction time (h)	Crystallinity before HCl hydrolysis (%)	Crystallinity after HCl hydrolysis (%)
0	74	-
2	60	78
4	56	76
5	56	64
7	55	61
7+ $NaBH_4$	47	-

TABLE 4.2 DD of the Alkali-Treated Chitin Samples Before and After Acid Hydrolysis

Reaction time (h)	DD before HCl hydrolysis from CP-MAS(%)	DD after HCl hydrolysis from CP-MAS (%)
2	17.6	2.3
4	30.5	6.1
5	36.1	5.7
7	37.4	8.4
7 + $NaBH_4$	49	-

4.3.2 EFFECT OF HCl HYDROLYSIS ON PARTIALLY DEACETYLATED CHITIN

Acid hydrolysis of chitin should follow first-order kinetics if all glycosidic bonds were equally accessible and reactive (25, 26). In fact, the kinetic behaviour is affected by the physical state of the chitin chains, which pack anti-parallel and are linked through interchain hydrogen bonding between the acetyl groups. In Fig. 4.4, the weight loss of the chitin and alkali-treated chitin samples from acid hydrolysis is plotted as a function of DD. It is found that the weight loss increases linearly with increasing DD, an expected result since the accessibility of glycosidic linkages to H^+ is influenced by disruption of chain packing. However, after acid hydrolysis, the remaining chitin crystallites have a higher crystallinity (see Table 4.1) due to removal of the noncrystalline fraction which is mostly the partially deacetylated material. In fact, some recrystallization may take place as a result of acid hydrolysis.

Fig. 4.4. Weight loss of the purified and dried alkali-treated chitin samples after acid hydrolysis at the boil vs. DD.

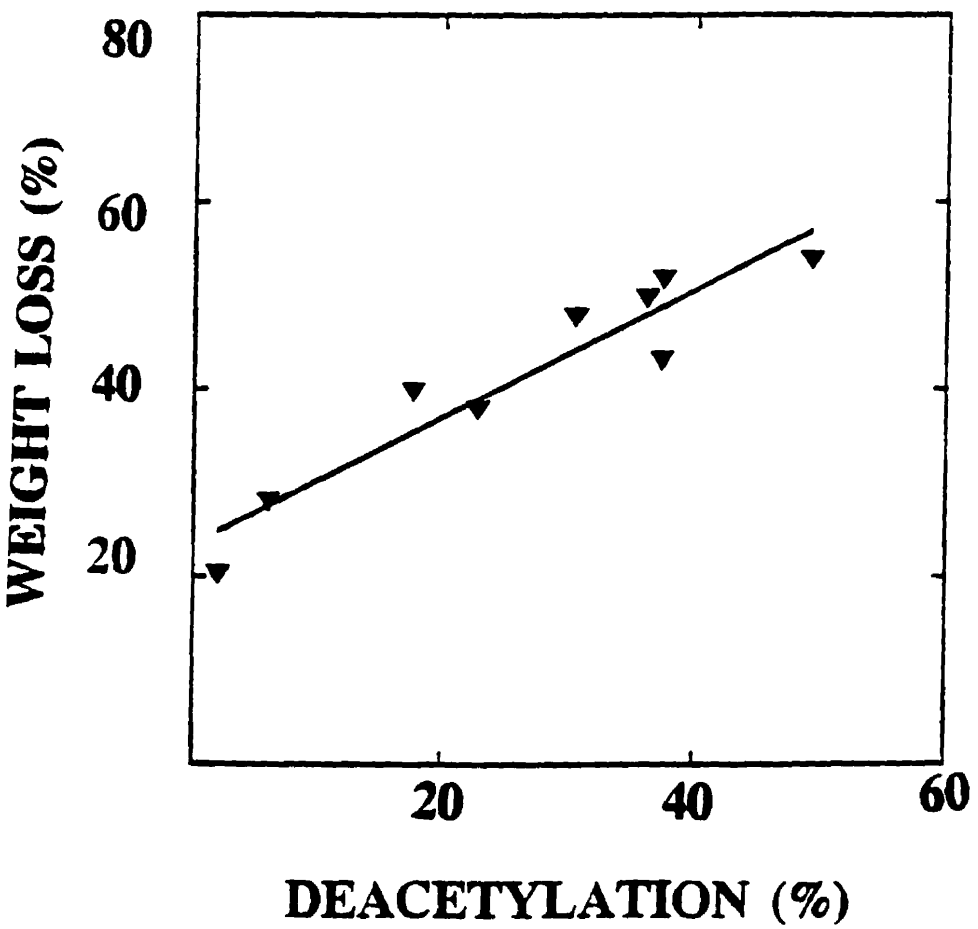
80
60
40
20
WEIGHT LOSS (%)
20
40
60
DEACETYLATION (%)

The DD of the samples after acid hydrolysis was measured using solid state NMR (see Table 4.2). It is found that the DD of the alkali-treated samples after acid hydrolysis is significantly lower than that before the acid hydrolysis. This supports the conclusion that acid hydrolysis preferentially removes chitosan blocks of repeating units especially if they were at the crystallite surface. The recovered hydrochitin is almost like original chitin in composition and degree of crystallinity.

After acid hydrolysis, the surface amino groups (SAG) of the chitin samples, which determined the surface charge property of the hydrochitin in suspension, were measured using conductimetric titration (18). Fig. 4.5 plots the SAG of chitin samples as a function of deacetylation time. It was found that SAG of alkali-treated and acid hydrolysed chitin samples increased with time.

4.3.3 EFFECT OF SURFACE CHARGE ON PHASE SEPARATION

In acidic media, the protonation of the surface amino groups of chitin crystallites provides positive surface charges which affect the phase behaviour of suspensions of chitin crystallites. The surface charge density of crystallites therefore increases with increasing SAG (see Table 4.3), assuming that the crystallite texture persists and the surface area does not change significantly, as confirmed by a TEM study (see Fig. 4.6). Fig. 4.6 shows that the rod-like character of the particles is retained and there is no significant change of the crystallite size after NaOH treatment. The TEM study also indicates that the crystallites from the sample treated with NaOH in the presence of $NaBH_4$ is the same as that without $NaBH_4$. Table 4.4 shows that for the suspensions at pH 4, the zeta potential increases with an increase of surface charge density resulting from deacetylation. This change in the zeta potential ultimately changes the boundary concentration for the phase separation of the suspensions if other factors remain unchanged.

Fig. 4.5. Surface amino groups of the alkali-treated chitin samples vs. reaction time.

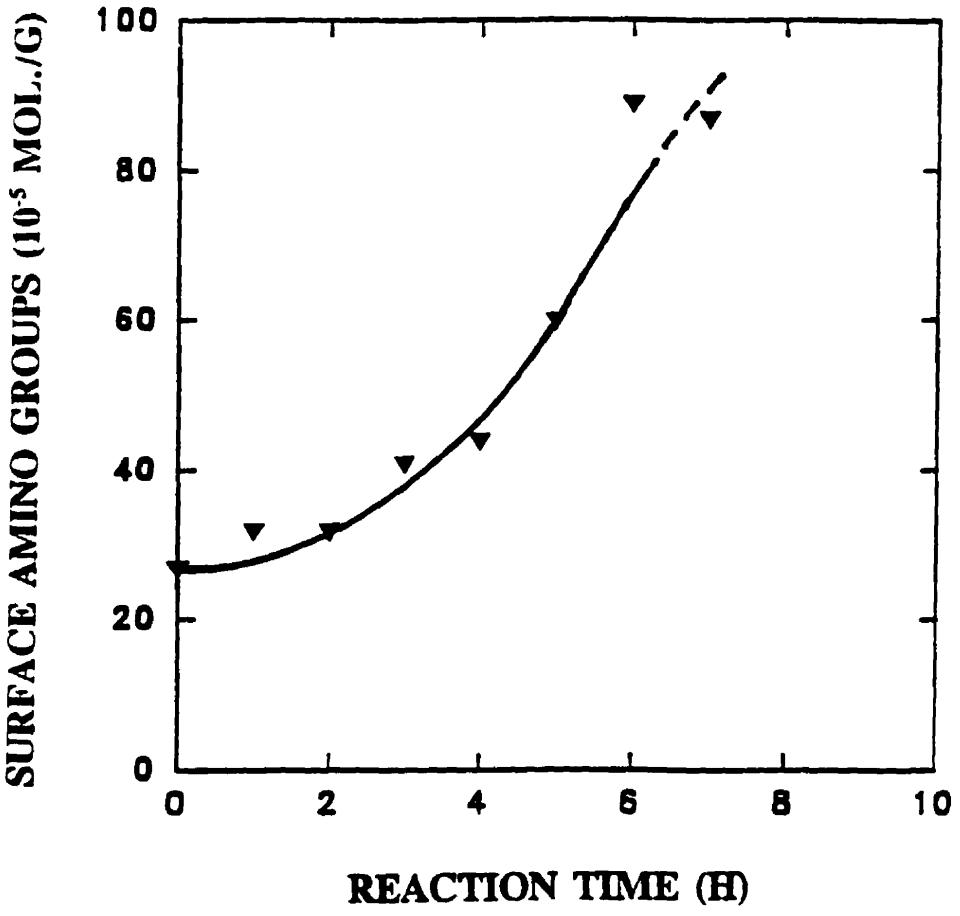
SURFACE AMINO GROUPS (10^{-5} MOL./G)
100
80
60
40
20
0
0
2
4
6
8
10
REACTION TIME (H)

TABLE 4.3 Surface Charge Density of Chitin and Alkali-Treated Chitin Samples Calculated from Conductimetric Titration Data

Reaction time (h)	Surface charge density (e/nm^2)	Surface amino group (10^{-5} Mol./G)
0	0.45	27
1	0.53	32
3	0.69	41
6	1.58	89
7 +$NaBH_4$	1.58	89

TABLE 4.4 Zeta Potentials of Chitin Suspensions at pH 4 and the Boundary Concentrations for Phase Separation

Reaction time (h)	Surface charge density (e/nm^2)	Zeta potential at pH 4 (mV)	Boundary concentration for phase separation (%)
0	0.45	32	2.18
1	0.53	41	3.84
3	0.69	44	4.43

As shown in our previous papers (13, 14), the chitin crystallites in the suspensions self-assemble into a chiral nematic phase above a critical concentration. As mentioned in the **Introduction**, the boundary concentration for phase separation depends on both the surface charge of the crystallites, i.e. surface charge density and zeta potential, and the electrolyte concentration of the suspensions. Fig. 4.7 is a phase separation diagram for the suspensions at pH 4 prepared from chitin and alkali-treated chitin samples, demonstrating that the boundary concentration increases with increasing treatment time in 50% (w/v) NaOH; the boundary concentration for phase separation increases with increasing surface charge. This is opposite to theoretical predictions (17). In the present work, the alkali-treated chitin crystallites are highly charged and their contribution to the ionic strength of the suspensions is significant thereby causing a double layer compression. In addition, since we are working close to the Manning limit i.e. the apparent linear charge density where condensation of counterions starts to occur, and the charge density remains constant (27). Table 4.4 shows that the boundary concentration for phase separation increases with increasing zeta potential. This is opposite to what is observed for the suspensions prepared from untreated chitin (14). The reason is that the zeta potentials were measured in diluted suspensions (less than 0.1%, w/w) where the contribution of the crystallites to the ionic strength of the suspensions was negligible. On the other hand, when phase separation occurs, the concentration is well above 1% and the contribution of the crystallites to the ionic strength should be taken into account (28).

For the suspensions prepared from the samples hydrolysed in 50% (w/v) NaOH for five hours or above, the suspensions are too viscous to phase separate. For the suspensions prepared from alkali-treated chitin samples for less than three hours, chiral nematic patterns similar to those of the suspensions prepared from untreated chitin samples were observed in optical polarized microscopy. For the suspensions prepared from the chitin

Fig. 4.6. A TEM micrograph of the chitin crystallite sample after seven hours alkali treatment in the presence of $NaBH_4$.

Fig. 4.7. Phase separation diagrams for biphasic region of chitin crystallite suspensions prepared from chitin and alkali-treated chitin samples with a different charge density, (▲) starting chitin, (□) alkali-treated chitin (1 h) and (■) alkali-treated chitin (3 h). The boundary concentration is obtained by extrapolating to 0% anisotropic phase.

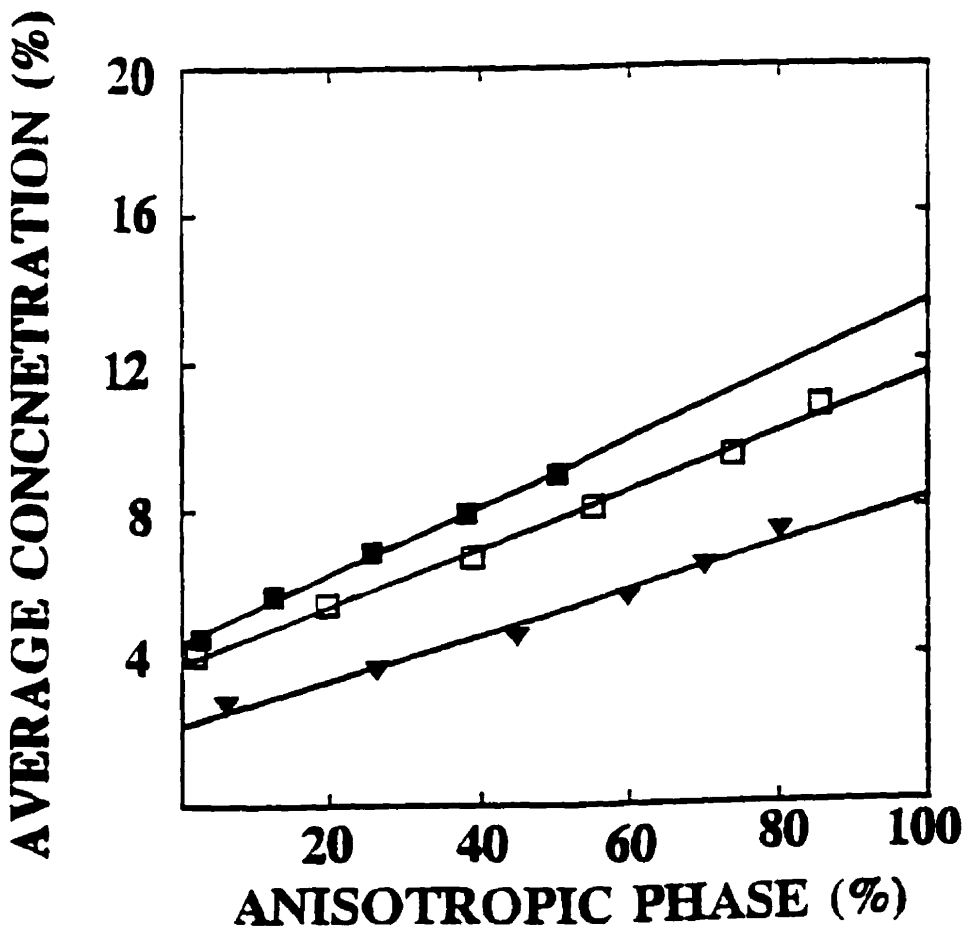
AVERAGE CONCNETRATION (%)
20
16
12
8
4
20
40
60
80
100
ANISOTROPIC PHASE (%)

samples hydrolysed in 50% (w/v) NaOH for more than four hours, the higher viscosity prevents formation of the chiral nematic texture. Interestingly, the suspension hydrolysed in 50% (w/v) NaOH for six hours has less birefringence than the one hydrolysed in 50% (w/v) NaOH for seven hours in the presence of $NaBH_4$ although the SAG from conductimetric titration show that both have same degree of surface deacetylation. We propose that the presence of $NaBH_4$ speeds up the deacetylation reaction and minimizes the degradation of chitin chains thereby leading to a higher effective axial ratio.

4.4 CONCLUSIONS

In the present work chitin samples with different DD were prepared by base hydrolysis through control of the reaction time. It was found that the treatment using a constant strength of alkali reduced the crystallinity of the sample, but the crystalline structure of α-chitin was retained after washing to neutrality and drying. Considering NaOH is in excess within each alkali-chitin crystallite, the reaction is pseudo first order. Both DD and SAG, from solid state NMR and conductimetric titration respectively increase with hydrolysis time. The increase of surface charge density resulting from the increased SAG is found to affect the boundary concentration for the formation of the anisotropic phase. However, the observed change of boundary concentration with surface charge is opposite to that predicted by theories (17). This is attributed to the contribution of the charged crystallites to the ionic strength. The suspensions of crystallites prepared from the samples treated with alkali for six and seven hours do not phase separate due to their high viscosity and chiral nematic structures were not observed beyond the four hour treatments.

4.5 REFERENCES

1. Shahidi, F., *Can. Chem. News*, September, 25 (1995)
2. Herrera-Ruiz, J., *in Cellulose and other Natural Polymer Systems: Biogenesis, Structure and Degradation*, pp 207-220, Edited by R. M. Brown Jr, Plenum Press, New York (1982).
3. Knorr, D., *Food Technology*, January, 114 (1991).
4. Robert, G. A., *Chitin Chemistry*, Macmillan Press Ltd, London (1992).
5. Muzzarelli, R. A. A., *Chitin Enzymology: Proceedings of the International Symposium on Chitin Enzymology*, European Chitin Society-Lyon and Ancona University of Ancona, Faculty of Medicine, IT-60100 Ancona, Italy (1993).
6. Muzzarelli, R. A. A., *Chitin*, Pergamon Press, New York (1977).
7. Kafetzopoulos, D., Martinou, A. and Bouriotis, V., *Proc. Natl. Acad. Sci*, USA, **90**, 2564-2568 (1993).
8. Rathke, T. D. and Hudson, S., J. M. S.-*Review. Macromol. Chem. Phys.*, C3 (3), 375-437 (1994).
9. Hirano, S., *Fragrance Journal* (Japanese), **10**, 70-73 (1990).
10. Carlström, D., *J. Biophys. and Biochem. Cytol.*, **3** (5), 669-682 (1957).
11. Blackwell, J., *Biopolymer*, **7**, 281-289 (1969).
12. Marchessault, R. H., Morehead, F. F. and Walter, N. M., *Nature*, **184**, 623 (1959).
13. Revol. J.-F. and Marchessault, R. H., *Int. J. Biol. Macromol.* **15**, 329 (1993).
14. Li, J., Revol, J.-F., Naraujo. E. and Marchessault, R. H., *Int. J. Biol. Macromol.* **18** (3), 177-187 (1996).
15. Onsager, L., *Ann. N.Y. Acad. Sci.* **51**, 627 (1949).

16. Stroobants, A. and Lekkerkerker, H. N. W., Odijk, Th., *Macromolecules*, **19**, 2232-2238 (1986)

17. Challa, G., Hermans P. H. and Weidinger, A., *Makromol. Chem.* **56**, 169 (1962).

18. Raymond, L., Morin, F. G. and Marchessault, R. H., *Carbohydrate Research*, **246**, 331-336 (1993).

19. Li, J., Revol, J.-F. and Marchessault, R. H., *J. Coll. and Interface Sci.*, in press.

20. Tokurs, S., Yoshida, J. and Nishi, N., *Polymer J.*, **14**, 527-536 (1982).

21. Thor, C. J. B. and Henderson, W. F., Am. Dyestuff Rep., **29**, 461-464 (1940).

22. Sannan, T., Kurita, K. and Iwakura, Y., *Polymer Journal*, **9**, 649-651 (1977).

23. Johnson, L., Private Communication, Vanson Chemical Inc. Washington (1996).

24. Brown, H. C., *Boranes in Organic Chemistry*, Cornell University Press, Ithaca, New York (1972).

25. Rupley, J. A., *Biochim. Biophys. Acta*, **83**, 245-255 (1964).

26. Corner, A. H., Wood, B. F., Hill, C. G. and Harris, J. F., *In Cellulose: Structure, Modification and Hydrolysis*, pp 281- 296, Ed. by Yong, R. A. and Rowell, R. M., A Wiley-Interscience Publication, New York (1986).

27. Manning, G. S. *J. Chem. Phys.*, **51**, 924 (1969).

28. Dong. X., Kimura, T., Revol, J.-F. and Gray, D.G., *Langmuir*, **12**, 2076-2082 (1996).

Chapter 5

EFFECT OF N-SULFONATION ON THE COLLOIDAL AND LIQUID CRYSTAL BEHAVIOUR OF CHITIN CRYSTALLITES

5.0 ABSTRACT

Chitin crystallites were heterogeneously N-sulfonated in an aqueous medium using triethylamine/sulfur trioxide (TEA/SO_3) or pyridine/sulfur trioxide. The extent of N-sulfonation of the crystallites has been controlled by the amount of TEA/SO_3 added in the reaction. The concentration of sulfur in the crystallites after N-sulfonation was quantified using conductimetric titration and elemental analysis. The ratio of N-sulfonated amino groups to amino groups (S/N) was calculated based on the titration data. The presence of N-S bond at crystallite surfaces was proved by x-ray photoelectron spectroscopy (XPS). After N-sulfonation, the crystallites have two ionizable groups at their surface: $-NH_3^+$ and $-NHSO_3H$ (Na). The former is pH dependent.

The colloidal properties of the N-sulfonated crystallites having different S/N were investigated by plotting the zeta potential as a function of the pH of the suspension. The isoelectric point was found to change with the level of N-sulfonation. Transmission electron microscopy shows that the aggregation of crystallites depends strongly on the extent of N-sulfonation. Above a certain concentration, the original chitin crystallites form tactoids (chiral nematic domains) in an aqueous medium. This phenomenon was not observed for the crystallites with a low extent of N-sulfonation (below 70%). At about 80% N-sulfonation, the formation of tactoids was once again observed.

5.1 INTRODUCTION

Chitin is the second most abundant carbohydrate polymer in nature, mainly existing in the skeletal materials of crustaceans and insects as well as in the cell walls of yeast and

fungi (1). Chemically, chitin is a homopolymer consisting of β(1-4) linked N-acetylglucosamine where a minority of acetyl groups have been lost due to deacetylation by chitin deacetylase (2). Chitin has potential as a versatile specialty material since it has three different kinds of substituents: amino, hydroxyl, and amino acetyl (3).

The applications of chitin and chitosan in health science are attractive due to their antibacterial, biocompatible, and biodegradable properties (4). Chitin and its derivatives have been used as suture materials in medicine, additives in cosmetics, and ingredients in the food industry. Oral sustained release tablets and microspheres based on chitosan containing chitin blocks have been prepared (5,6). Chitosan and other chitin derivatives are candidates for making hydrogels for the controlled delivery of drugs including antibiotics, steroids, and others (7. 8, 9. 10, 11, 12).

Although a variety of modification reactions have been reported, the difficulty for preparing chitin derivatives with well defined structures is due to its multi-functionality and its poor solubility in conventional solvents (13). Therefore, the development of controlled modification reactions is becoming increasingly important for the full exploitation of this biomass. In theory, it is feasible to modify chitin regioselectively based on the reactivity difference of these functional groups in different media. This has increased activities for the preparation of chitin derivatives using selective chemical reactions. Historically chitosan was the first derivative made from chitin using base hydrolysis (1). Following this, many O- and N- chitin derivatives have been reported (14, 15). The discovery of sulfonated amino groups in heparin, a naturally occurring sulfonated polysaccharide and anticoagulation agent having alternating glucosamine and glucuronic acid units, has stimulated considerable interest in the preparation of synthetic compounds having similar constituents starting from chitosan (16, 17).

The preparation of aqueous colloidal suspensions of nanosize chitin crystallites by HCl hydrolysis was reported previously (18, 19, 20). It is the presence of a positive charge

at the crystallite surface, resulting from protonation of the minority glucosamine (Glu-NH_2) at the crystallite surface in acidic media (see Eq. 5.1), that is responsible for the colloidal stability.

$$Glu + H^+ \rightleftharpoons Glu\text{-}NH_3^+ \qquad (5.1)$$

In suspension, these nano-crystallites are surrounded by negatively charged chloride ions to form an electrical double layer. When pH is between 2 and 6 the electrostatic repulsive force between the crystallites is strong enough to prevent coagulation at which point a colloidal state develops.

Above a critical concentration, such suspensions separate into a top (isotropic) and bottom (anisotropic) phase which exhibits a chiral nematic (CN) texture (19, 20). Upon drying this mesophase, solid films are produced in which the CN arrangement is preserved (19). This phase separation depends on the surface charge of the crystallites, the ionic strength of the suspensions, and the crystallite concentration.

In the present study, the surface amino groups of the chitin crystallites (Glu-NH_2) have been partially converted to sulfonated amino groups (Glu-$NHSO_3H$), which enhances the anti-bacterial properties of this material. The extent of N-sulfonation was determined using conductimetric titration and elemental analysis respectively. The presence of N-S bonds in the N-sulfonated samples has been demonstrated using X-ray photoelectron spectroscopy (XPS). The electrical properties of the N-sulfonated chitin crystallites in the suspensions were evaluated by a zeta potential study. Finally, the effect of the surface charge on phase separation and the formation of a chiral nematic organization was investigated.

5.2 EXPERIMENTAL

The suspensions of chitin crystallites were prepared as described in Chapter 2. Following acid hydrolysis in 3 N HCl at the boil for 1.5 h, the chitin hydrolysate was

repeatedly washed with deionized water followed by a centrifugation-decantation cycle until a pH of about 1.6 was reached. These suspensions were dialysed against deionized water until the pH was close to neutrality. To achieve a better dispersion of the chitin crystallites, a 10 ml aliquot of a 1% (w/w) suspension was then ultrasound treated in a Branson Sonifier (model 350) for one minute.

5.2.1 MATERIALS

The complexes of triethylamine sulfur trioxide (TEA/SO_3) and pyridine sulfur trioxide ($Pyr./SO_3$) were purchased from Sigma Chemical Co. (St. Louis, MO). An Avicel sample (cellulose crystallites prepared by HCl hydrolysis) was provided by FMC Co. (Philadelphia, PA).

5.2.2 SULFONATION OF CHITIN CRYSTALLITES

5.2.2.1 METHOD ONE

Approximately, 60-80 ml of the suspension of chitin crystallites with a concentration of 5% (w/w) at pH 5 was transferred into a three-neck round bottom flask followed by dilution with 100 ml of deionized water. Various quantities of Na_2CO_3 (indicated in Table 1) were dissolved in 50 ml of deionized water and transferred to the three-neck flask. The mixture of Na_2CO_3 and chitin crystallites was then shaken vigorously and stirred for half an hour. Similarly, different quantities of TEA/SO_3 or 10 g of $Pyr./SO_3$ were first dissolved in 50 ml of deionized water followed by gradual mixing with the mixture of Na_2CO_3 and chitin crystallites. This mixture was heated to 65 ^{0}C in a water bath for time ranging from 20 h to 100 h. Upon completion of the reaction, the product was diluted with deionized water followed by centrifugation (6000 RPM) and decantation cycles until the suspension spontaneously reached a colloidal state. Following this, the suspension was transferred into a dialysis bag and dialysed against deionized water until the pH of the

suspension was 8.

5.2.2.2 METHOD TWO

The process described in the method 1 was repeated for three times, with reaction time of 48 hours for each cycle (see Table 1). In the second and third cycles, the product from the previous cycle was used as a suspension for N-sulfonation.

5.2.2.3 METHOD THREE

Na_2CO_3 and TEA/SO_3 was premixed in 80 ml of deionized water before gradually adding 60 ml of 5% (w/w) colloidal suspension of chitin crystallites or 20 ml of 5% (w/w) Avicel suspension with good stirring at 65 °C. The reaction continued at this temperature for 100 h. The "clean-up" process was the same as described above.

5.2.3 CHARACTERIZATION OF SULFUR CONTENT

5.2.3.1 CONDUCTIMETRIC TITRATION

The sulfur concentration in the N-sulfonated samples was quantitatively determined by titrating the amino groups of the chitin crystallites in suspension before and after N-sulfonation; the decrease of the surface amino groups' concentration during N-sulfonation corresponds to the formation of -$NHSO_3^-$ groups at the surface of the crystallites. Approximately, 25 ml of the 4% (w/w) N-sulfonated chitin crystallite suspension was first dispersed in a basic medium (pH=10) using ultrasound and the concentration was accurately measured. Then, 6 ml of 0.1 N HCl was added to the suspension followed by dilution with 150 ml of deionized water. The suspension was first shaken vigorously and conductimetric titration of this sample was performed as described in the previous paper (20) with vigorous stirring.

5.2.3.2 ELEMENTAL ANALYSIS OF SULFUR

Microanalysis of sulfur in the N-sulfonated samples was done using a combustion method followed by titration. A weighed sample was combusted in an oxygen rich atmosphere in a Schodinger oxygen flask containing distilled water with H_2O_2 as the absorbing solution. An aliquot was then passed through a cation exchange column to remove any interfering substances. A portion of this solution was then titrated with a standardized barium perchlorate solution using thorin as an indicator. The analysis was performed by Guelph Chemical Laboratory Ltd.(Guelph, ON).

5.2.4 X-RAY PHOTOELECTRON SPECTROSCOPY (XPS)

The chemical composition of the crystallites for both the original and the N-sulfonated chitin samples were analysed using a VG ESCALAB 3 MKII instrument. The MgK_α X-ray source (1254.6 eV) was operated at 240 W (12 kV, 20 mA) to produce photoelectrons. The pressure inside the analytical chamber was 10^{-9} torr. The analyzer was positioned perpendicular to the specimen surface and the incident beam was oriented at 45^0. The analyzer was operated at a passing energy of 50 eV for survey scans and 20 eV for high resolution scans. The analysed surface was 2X3 mm. All peak positions were corrected for adventitious carbon, at 285.0 eV in binding energy, to adjust for charging effect.

5.2.5 X-RAY DIFFRACTION (XRD)

Powder diffractograms for the N-sulfonated chitin crystallites and non-sulfonated original sample were obtained as described in Chapter 4.

5.2.6 ELECTRON AND OPTICAL MICROSCOPY

A transmission electron microscope (TEM) (Phillip EM 400T) was used to obtain

high magnification images of the chitin crystallites (see Chapter 4 for detailed discussion). For the N-sulfonated crystallites exhibiting a negative charge, the carbon film was first reacted with a solution of poly-L-Lysine (M.W. 33000-44000). In this case, a drop of 1% (w/w) aqueous solution of poly-L-Lysine was placed onto the supporting film for 1 min. and rinsed with deionized water. The carbon film was thus covered by a thin layer of the protein which is positively charged over a large pH range (21). Images were obtained by diffraction contrast in the bright field mode.

The optical pictures of the anisotropic suspensions were taken using a Nikon Microphot-FXA optical microscope (see Chapter 2 for detailed description).

5.2.7 ZETA POTENTIAL MEASUREMENTS

All the zeta potential measurements were done on a Pen Kem Model 501 Lazer Zee Meter. The detailed procedure has been described in Chapter 2 (20).

5.3 RESULTS AND DISCUSSION

The objective of this work was to study how the surface charge of the chitin crystallites affects the formation of the chiral nematic phase. This involves two steps: (a) changing the surface charge from positive to negative through N-sulfonation of the amino groups at the surface of the chitin crystallites without affecting the axial ratio of the crystallites, and (b) studying the colloidal and liquid crystal properties of the chitin crystallites having a different surface charge densities. The schematic of N-sulfonation is shown in Fig. 5.1.

TEA/SO_3 and Pyr./SO_3 were used as reagents for selective N-sulfonation of the chitin crystallites in aqueous suspensions due to their high selectivity over O-sulfonation in aqueous media (22,23) compared with chlorosulfonic acid and other reagents (24, 25). N-sulfonation of chitin crystallites was performed heterogeneously in aqueous suspensions

Fig. 5.1. Schematic of N-sulfonation reaction of chitin crystallites in suspension.

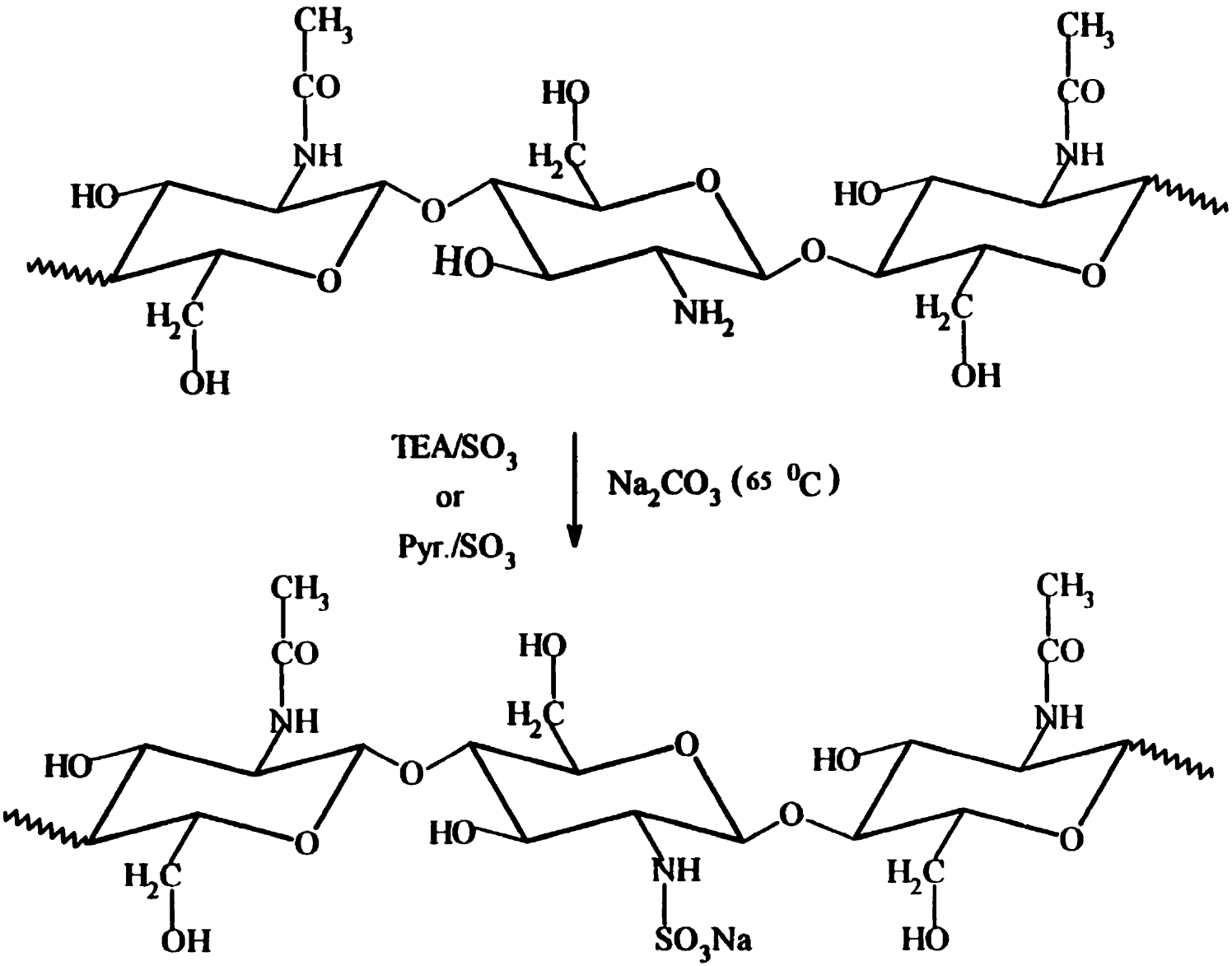
CH3
CO
NH
HO
O
H2C
OH
HO
NH2
TEA/SO3
or
Pyr./SO3
Na2CO3 (65 0C)
SO3Na

at pH 9-10 which was adjusted using Na_2CO_3. In this pH range, the surface amino groups (Glu-NH_2) remain unprotonated in the suspension, which react with TEA/SO_3 or Pyr./SO_3 effectively (see Fig. 5.1). Because in this range of pH, the suspension is coagulated due to lack of electrostatic repulsive forces between particles, deionized water was added to reduce the viscosity of the suspension and so increase the accessibility of the surface amino groups to TEA/SO_3 or Pyr./SO_3. This reaction has been reported to depend on the surface conditions of the sample and a mechanism involving nucleophilic attack has been suggested (26).

The N-sulfonated chitin crystallites were characterized using conductimetric titration and elemental analysis respectively. The results from both techniques are comparable. The sulfur content increases with the amount of TEA/SO_3 used in the reaction (see Table 5.1), although it is difficult to achieve a complete conversion of Glu-NH_2 to Glu-NH-SO_3^-. Pyr./SO_3 is less reactive (see Table 5.1) by a factor of two. This result is expected because Pyr./SO_3 has a lower solubility in aqueous media (27). Once chitin crystallites are partially N-sulfonated and isolated, they form a stable suspension at basic pH. Further addition of more Na_2CO_3 and TEA/SO_3 to this suspension according to *method two* does not improve the extent of N-sulfonation (see Table 5.1). Surprisingly, when the crystallites are added to a premixed solution of Na_2CO_3 and TEA/SO_3, as a possible way of increasing the N-sulfonation level, no N-sulfonation is obtained (see Table 5.2) according to the results from conductimetric titration. However, sulfur elemental analysis indicates that a significant amount of sulfur is present in the sample. The zeta potential of the colloidal suspension prepared from this sample at pH 10 is - 33 mV. This suggests that hydroxyl groups were sulfonated. In this case, as the premixed solution of Na_2CO_3 and TEA/SO_3 is a relatively rich medium in organics, compared to *method one* in which the reactant TEA/SO_3 is added to a more water-rich buffered suspension, O-sulfonation may be favoured. The possibility for O-sulfonation was further supported by sulfonating an Avicel

cellulose suspension (see Table 5.2). The reacted Avicel particles show a higher negative charge in terms of zeta potential (-27 mV) compared with the original charge (-17 mV). However, the XPS evidence for O-sulfonation is ambiguous. Clearly further investigation is required to resolve this ambiguity.

Table 5.1 Reaction Conditions of N-sulfonation of Chitin Crystallites Using TEA/SO_3 or $Pyr./SO_3$ (*method one and method two*)

Reaction Time (h)	Temp. and pH	Na_2CO_3 (g/g chitin)	TEA/SO_3 (g/g chitin)	[S] from Conducti-metric Titration (mM/g)	[S] from El. Anal. (mM/g)	S/N and Conver-sion
20	65°C/10	0.4	0.3	4.67×10^{-2}	3.13×10^{-2}	0.3/23%
20	65°C/10	0.5	0.8	13.3×10^{-2}	6.25×10^{-2}	0.9/47%
20	65°C/10	0.8	1.1	15.3×10^{-2}	9.38×10^{-2}	1.1/52%
72	65°C/10	0.98	1.64	16.8×10^{-2}	9.4×10^{-2}	1.5/60%
100	65°C/10	1.89	3.14	21.8×10^{-2}	30×10^{-2}	3.0/75%
100	65°C/10	3.16	6.33	25.3×10^{-2}	30×10^{-2}	5.0/83%
48*	65°C/10	1.10	1.10	12.8×10^{-2}	7.2×10^{-2}	0.8/44%
100*	65°C/10	1.89	2.76	10×10^{-2}	6.0×10^{-2}	0.5/33%

* After three cycles of N-sulfonation.

** $Pyr./SO_3$ was used as a N-sulfonation reagent.

Note: Both sulfur elemental analysis and conductimetric titration are $\pm10\%$.

TABLE 5.2 N-sulfonation of Chitin Crystallites and Avicel Particles

(method three)

Materials	Reaction time (h)	Temp. and pH	Na_2CO_3 (g/g reacting material)	TEA/SO_3 (g/g reacting material)	[S] from conducti metric titration (mM/g)	[S] from El.Anal. (mM/g)	Zeta potential at pH 10 (mV)
Chitin crystalli-te	72	65°C/10	0.98	1.64	Not detected	9.4×10^{-2}	-33
Avicel	72	65°C/10	3	3	-	1.9×10^{-3}	-27

5.3.1 X-RAY PHOTOELECTRON SPECTROSCOPY OF THE N-SULFONATED CHITIN CRYSTALLITES

The XPS spectrum (survey scan) of the N-sulfonated chitin crystallites including the peaks of C_{1s} (285 eV), N_{1s} (399 eV), O_{1s} (531 eV), and S_{2p} (168 eV) is shown in Fig. 5.2. The S_{2p} peak is very small in the survey scan due to its low concentration. An accumulated spectrum for the S_{2p} peak is shown in Fig. 5.3. Assuming the XPS peak area has a Gaussian line shape, the S_{2p} peak is resolved into four components, two of them correspond to Glu-NH-SO_3H (acid form), and the other two correspond to Glu-NH-SO_3Na (sodium salt form). The higher peak of each doublet is attributed to the $2p^{3/2}$ orbital and the smaller peak is ascribed to the $2p^{1/2}$. The major component (more than 70%) corresponds to -$NHSO_3Na$ with a $S_{2p(3/2)}$ peak position at 168.4 eV. In comparison, the binding energy ($S_{2p(3/2)}$) of O-S in the R-OSO_3Na groups is at 169.7 eV (28), which is

Fig. 5.2. XPS survey scans of N-sulfonated chitin crystallites. The full line is the recorded spectrum and the dotted line represents a amplified region (0-280 eV). All elements are easily accounted for except for fluorine which is a impurity.

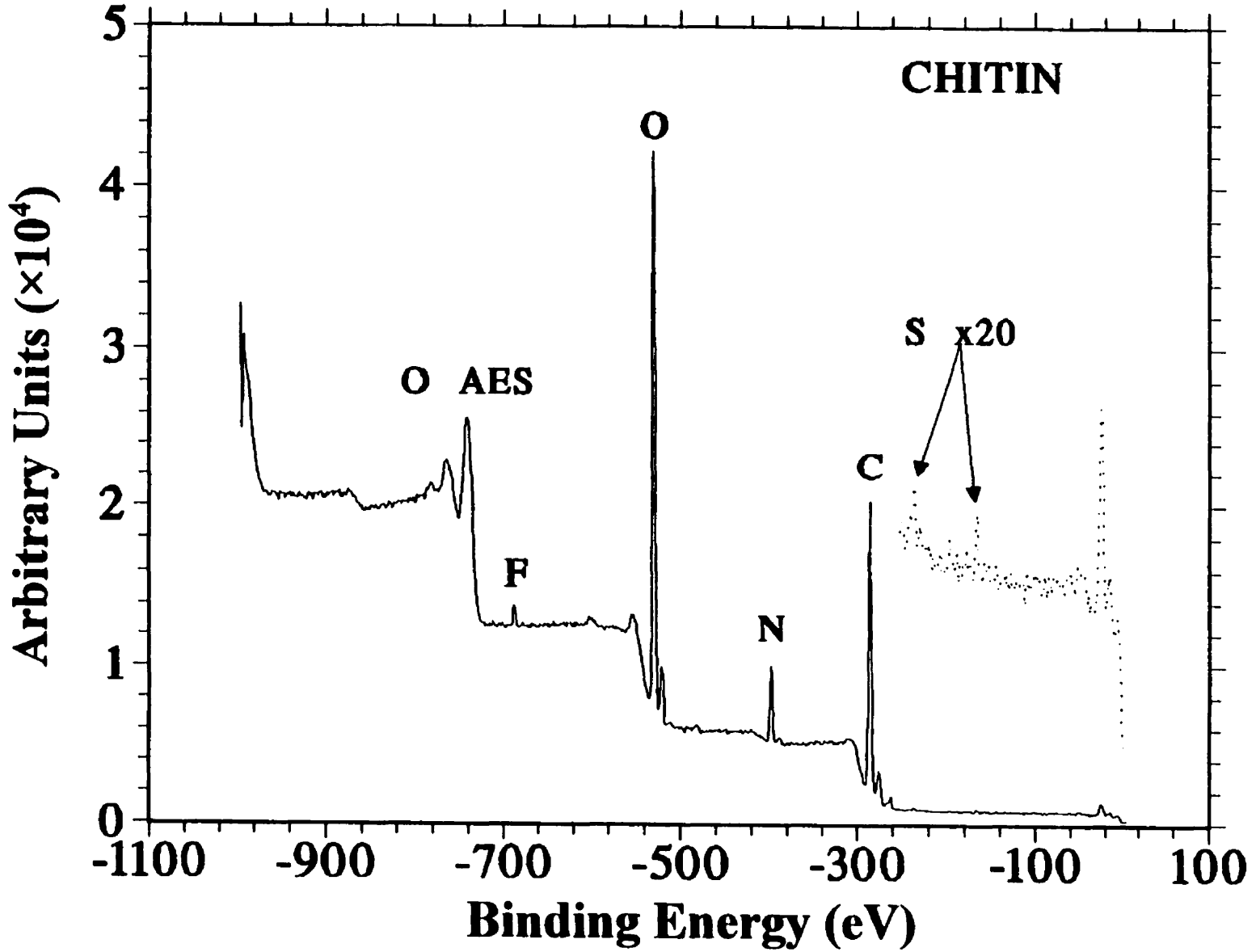
CHITIN
O
O AES
F
N
C
S x20
Arbitrary Units (×10⁴)
Binding Energy (eV)
0
1
2
3
4
5
-1100
-900
-700
-500
-300
-100
100

Fig. 5.3. High resolution XPS scans of S_{2p} peak.

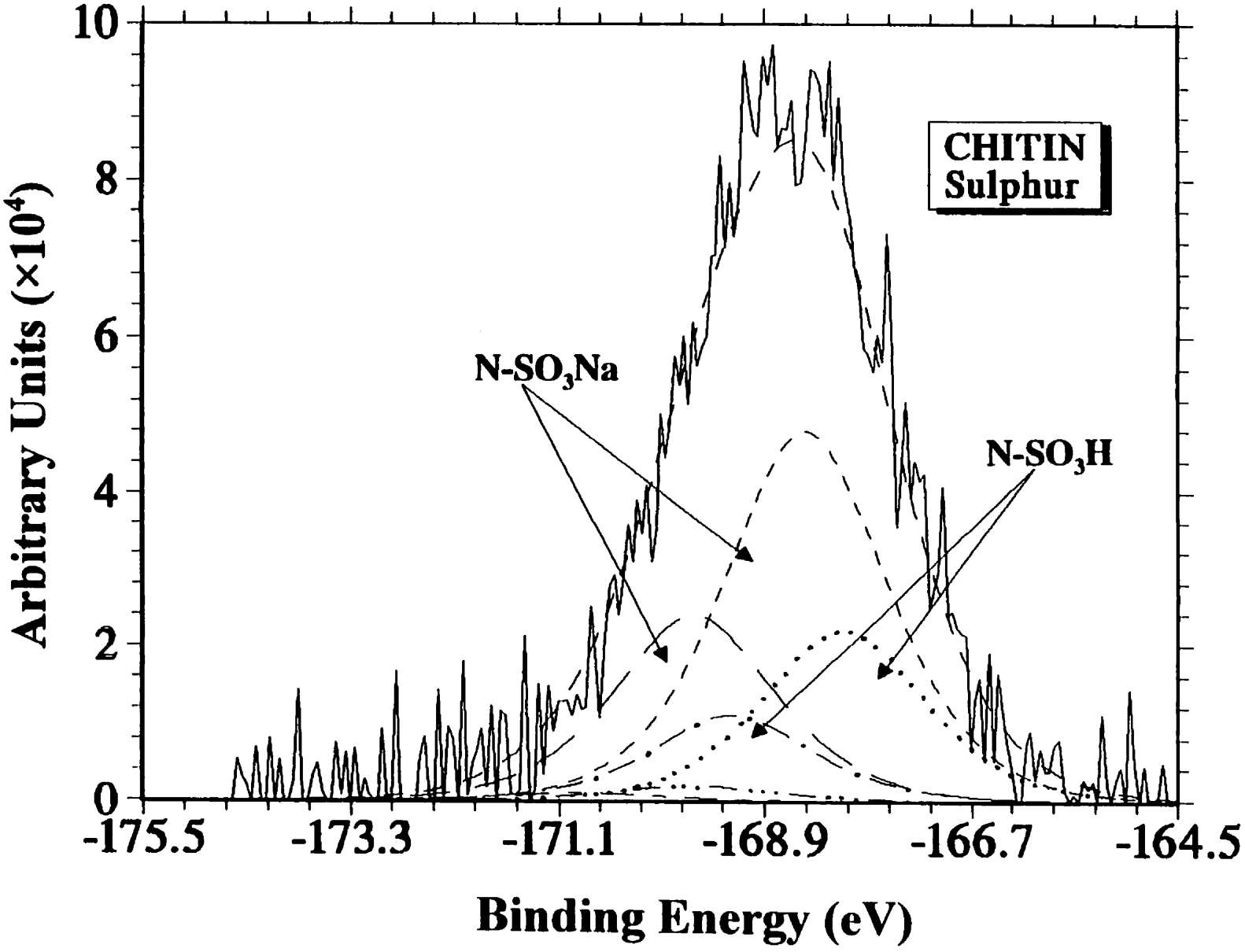
CHITIN
Sulphur
N-SO3Na
N-SO3H
Arbitrary Units (×10^4)
10
8
6
4
2
0
-175.5
-173.3
-171.1
-168.9
-166.7
-164.5
Binding Energy (eV)

confirmed by using sodium dodecyl sulfate (SDS) as standard (see Fig. 5.4). These results support our conclusion from the conductimetric titration that with *method one* the reaction occurs mainly on the amino groups. Similarly, the O_{1s} peak (see Fig. 5.5) can be resolved into three components, corresponding to C-O-C, -OH, and -$NHC(O)CH_3$ respectively, the three types of oxygen present in chitin.

5.3.2 X-RAY DIFFRACTION (XRD)

X-ray powder diffractograms of N-sulfonated chitin crystallites and the original chitin are shown in Fig. 5.6. In comparison with the d-spacings reported by Carlström (29), the X-ray patterns are identified as α-chitin. It is also clearly shown that the crystallinity of the crystallites remains unchanged after N-sulfonation. This is expected because the treatment is very mild and the N-sulfonation reaction only occurs at the surface.

5.3.3 COLLOIDAL PROPERTIES OF THE N-SULFONATED CRYSTALLITES

Chitin crystallites with various extents of N-sulfonation were obtained by controlling the amount of reagent, TEA/SO_3. After N-sulfonation, chitin crystallites have two kinds of functional groups:Glu-$NHSO_3^-$ and Glu-NH_2, and the ratio Glu-$NHSO_3^-$/Glu-NH_2 is referred as the S/N ratio. The mechanism of the surface charge generation for these two ionizable groups is different. Glu-NH_2, which is a weak base, can be protonated to form Glu-NH_3^+ in acidic media and the degree of protonation varies with the pH. Glu-$NHSO_3^-$ is a strong acid which exhibits a negative charge regardless of the pH of the suspension. The electrical properties of N-sulfonated chitin crystallites are determined by the charge balance between Glu-$NHSO_3^-$ and Glu-NH_3^+. Hence, the colloidal behaviour of the crystallites depends upon both the extent of N-sulfonation (S/N) and the pH of the suspension. In Fig. 5.7, the zeta potential of chitin crystallites with different S/N is plotted

Fig. 5.4. High resolution XPS scans of S_{2p} from a SDS sample showing the binding energy of O-S. The big and small peaks are ascribed to $S_{2p(3/2)}$ and $S_{2p(1/2)}$ of O-S respectively.

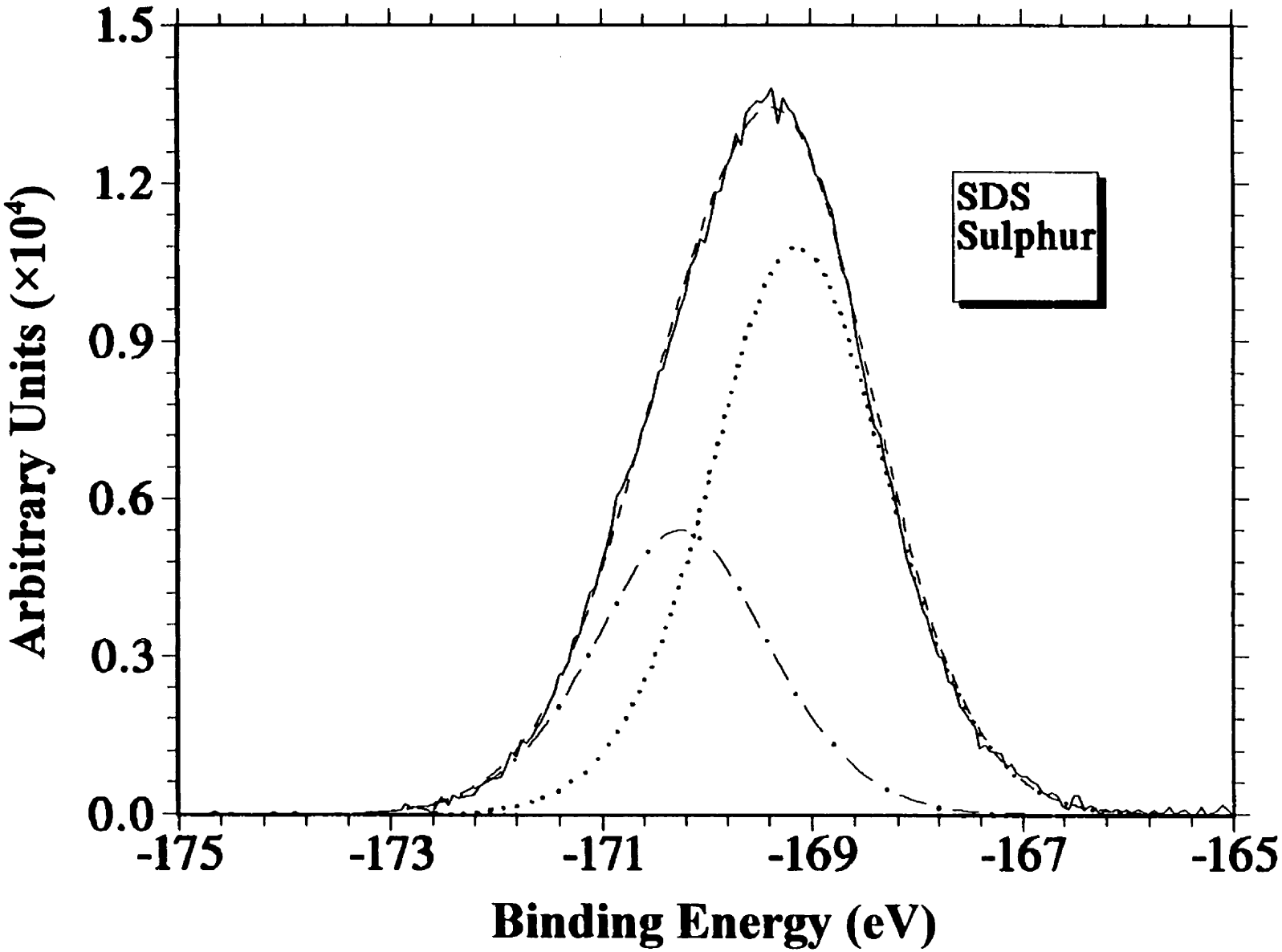
1.5
1.2
0.9
0.6
0.3
0.0
Arbitrary Units (×10⁴)
-175
-173
-171
-169
-167
-165
Binding Energy (eV)
SDS
Sulphur

Fig. 5.5. High resolution XPS scans of O_{1s} peak. The peak is deconvoluted into three components corresponding to the three kinds of oxygen in chitin.

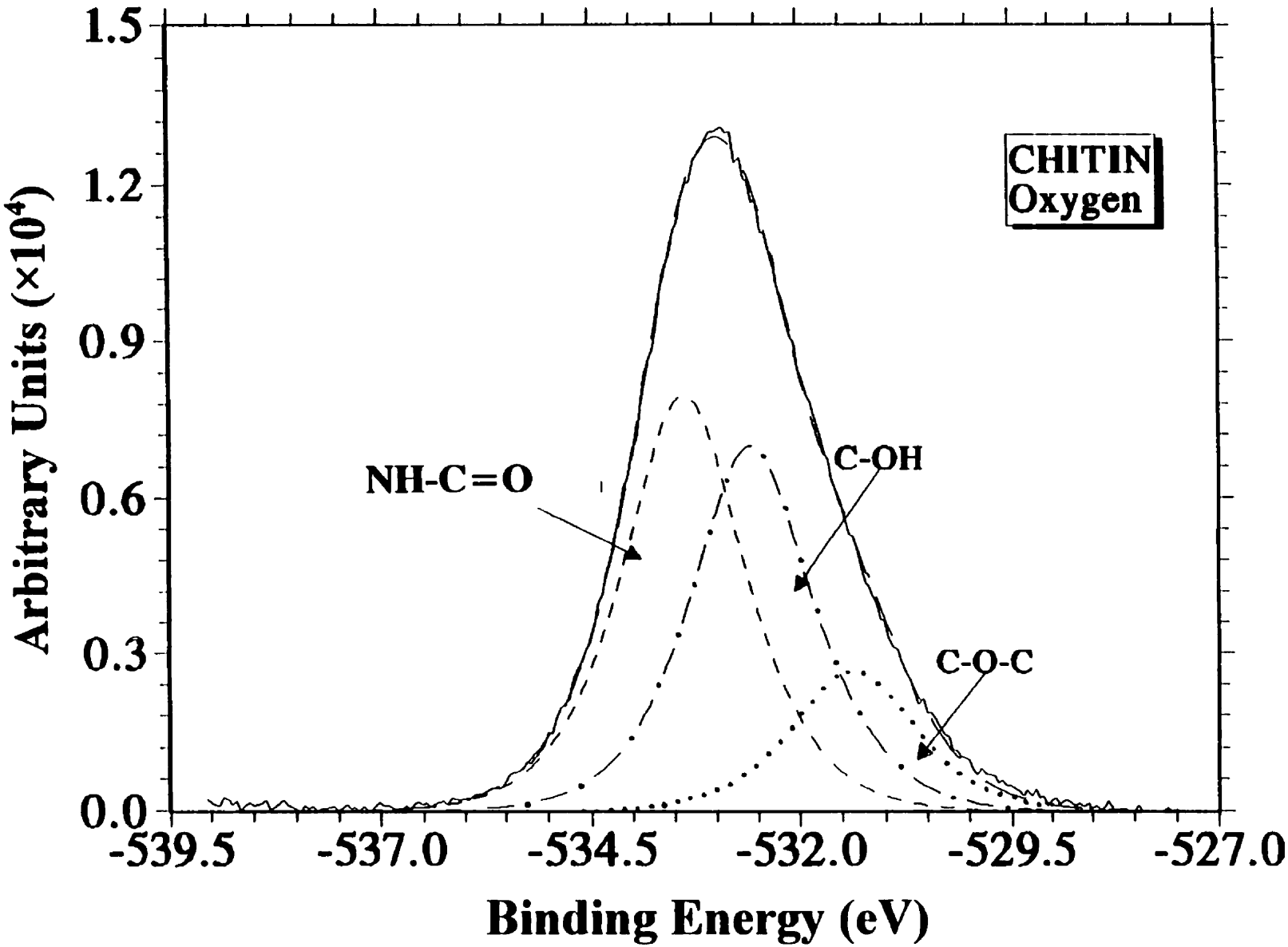
CHITIN
Oxygen
NH-C=O
C-OH
C-O-C
Arbitrary Units (×10⁴)
1.5
1.2
0.9
0.6
0.3
0.0
-539.5
-537.0
-534.5
-532.0
-529.5
-527.0
Binding Energy (eV)

Fig. 5.6. X-ray powder diffractograms of the N-sulfonated chitin crystallites (2) and the original chitin sample (1).

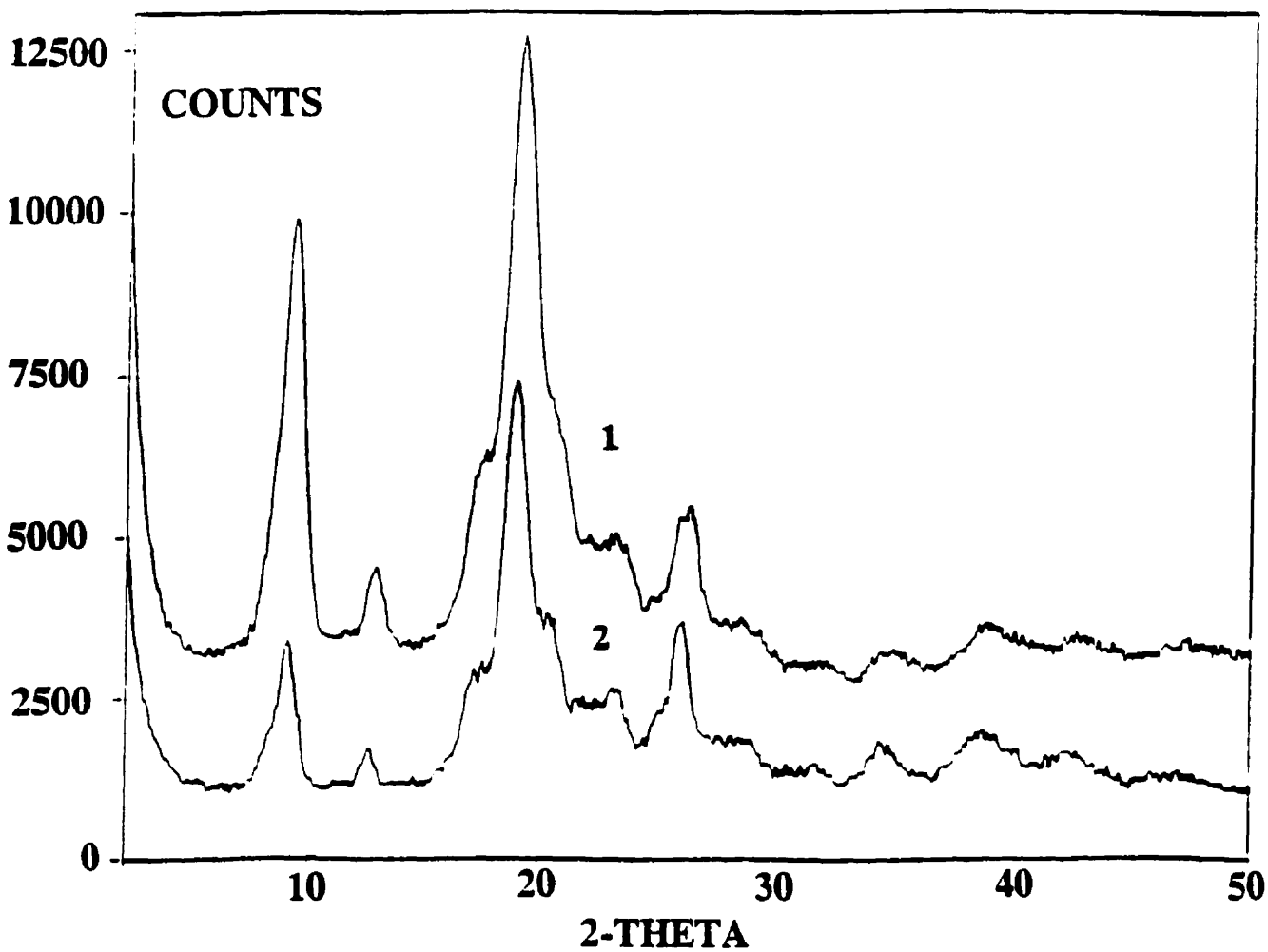
12500
COUNTS
10000
7500
5000
2500
0
1
2
10
20
30
40
50
2-THETA

Fig. 5.7. Zeta potentials of chitin crystallites and N-sulfonated chitin crystallites in suspensions with 10^{-3} N NaCl as a function of pH; S/N=0 is for the original chitin crystallites.

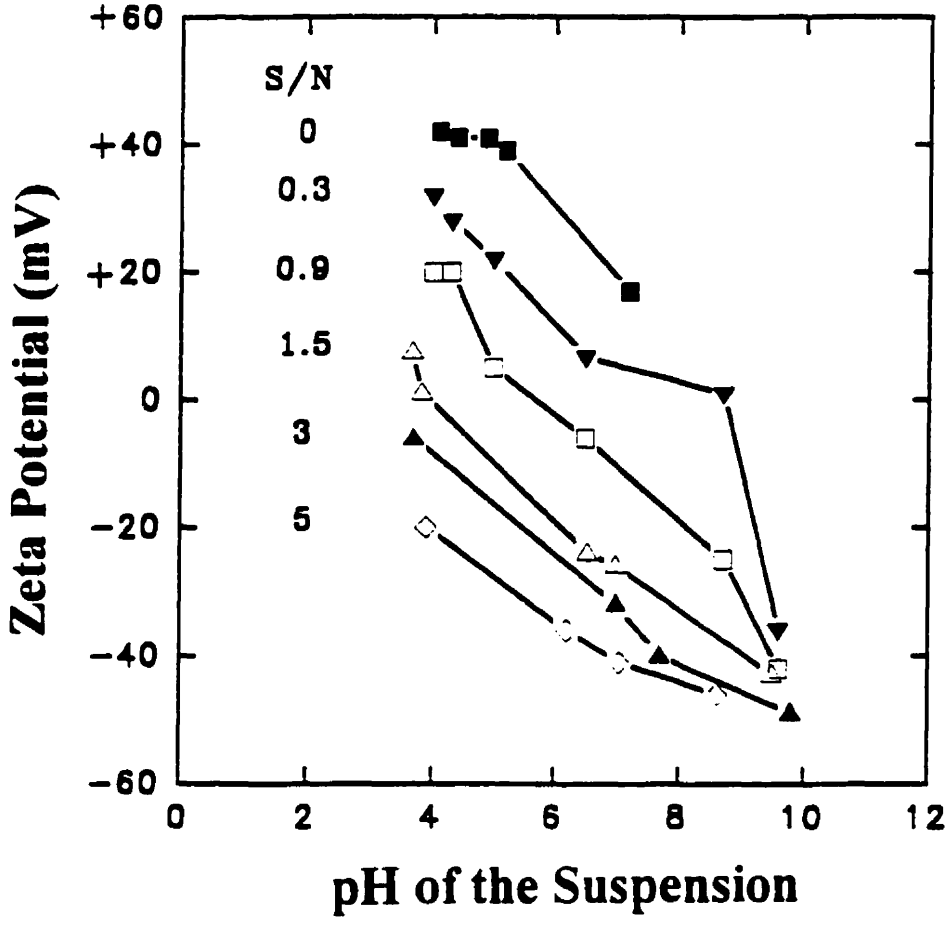
+60
+40
+20
0
−20
−40
−60
0
2
4
6
8
10
12
S/N
0
0.3
0.9
1.5
3
5
Zeta Potential (mV)
pH of the Suspension

as a function of the pH of the suspension. For the untreated chitin crystallites, the crystallites always show a positive charge and the suspension is stable at pH < 7 up to a pH value at which the suspension is salting out. For the suspension of chitin crystallites with a low extent of N-sulfonation (S/N = 0.3), the suspension is stable at either acidic pH (pH close to 4) or basic pH (pH > 9). When the pH of the suspension is less than 4, more than 90% of Glu-NH_2 is protonated (20) and as a consequence the positive charges are dominant. On the other hand, for pH >9 the Glu-NH_2 is not protonated and only the negative charge of the sulfate groups provides the electrostatic repulsive force between particles. When the pH of the suspension is between 4 and 8, the number of Glu-NH_3^+ is of the same order as the number of Glu-$NHSO_3^+$ groups, which results in a charge neutralization and coagulation of the system. This is reflected in the zeta potential results where high positive and negative values were observed only at pH close to 4 and >9 respectively (see Fig. 5.7). For the suspension of crystallites with S/N close to 1, the suspension is only stable at pH >9. Fig. 5.7 shows that it is only at this pH that the zeta potential is strong enough to maintain a colloidal stability. For the suspension of crystallites with a high extent of N-sulfonation (S/N >>1), the crystallites always show a negative charge in the range of pH studied, but the suspension is stable from pH 6 onward when the negative charge is sufficiently high. These crystallites are very much like cellulose crystallites prepared from a sulfuric acid hydrolysis of cellulose (30).

In addition, it is noted that the isoelectric point is shifted from pH 9 for the crystallites with S/N=0.3 to pH = 4 for the crystallites with S/N =1.5. For the crystallites with S/N > 3 and the untreated chitin crystallites, no isoelectric point is observed in the range of pH studied.

The colloidal properties of the N-sulfonated crystallites discussed above will inevitably change the liquid crystal properties of these crystallites in suspensions. This is discussed in the next section.

5.3.4 LIQUID CRYSTAL PROPERTIES OF N-SULFONATED CHITIN CRYSTALLITES AS A FUNCTION OF S/N

As shown in Fig. 5.7, the apparent charge of N-sulfonated chitin crystallites depends upon both the extent of N-sulfonation and the pH of the suspension. As previously reported (20), liquid crystal formation from aqueous chitin crystallite suspensions depends on the surface charge of the crystallites, the ionic strength, and the chitin concentration. For the suspension of crystallites with S/N = 0.3 at pH 4 and for a concentration of chitin > 4% (w/w), the suspension separates into an isotropic (top) and an anisotropic phase (bottom) in which a chiral-nematic structure is observed. For the same sample, no anisotropy is observed at pH >6 due to rapid coagulation of the crystallites. For the suspension of crystallites with S/N close to 1, anisotropy can hardly be detected at both acidic and basic pH. When the extent of N-sulfonation increases to S/N = 1.5, a weak birefrigence showing a nematic texture (31) is observed for a suspension with a concentration of 5% (w/w) and a pH of 10.5 (see Fig. 5.8). This suggests that the surface charge density at this level of N-sulfonation is strong enough to prevent particles from completely coagulating. The particles have enough mobility to align with each other in parallel, forming large nematic domains as shown in Fig. 5.8. However, such a suspension does not phase separate probably because of some degree of aggregation resulting in gelation. From Fig. 5.9 TEM micrographs suggest that the axial ratio of the chitin crystallites of this sample remains the same as in the original sample (20) but most of the crystallites are nevertheless strongly aggregated, forming bundles of parallel crystallites.

With increasing N-sulfonation the electrostactic repulsive force beween particles increases also and at a given concentration the suspension is more fluid. For a 5% (w/w) suspension with S/N = 3 and a pH of 7, a phase separation into a top isotropic layer and a bottom anisotropic layer is observed after a mild

Fig. 5.8. Optical micrograph (viewed between crossed polarizers) of a 5% suspension (pH=10.5) of N-sulfonated chitin crystallites with S/N=1.5 viewed between crossed polarizers. The magnification is 200.

Fig. 5.9. A TEM micrograph of N-sulfonated chitin crystallites with S/N=1.5.

centrifugation. In this case, the TEM micrograph (Fig. 5.10) shows that the crystallites are well dispersed with a low degree of aggregation. When the crystallites have a degree of N-sulfonation of S/N=5, the suspensions behave much like the suspensions of the non-sulfonated crystallites, but over a different pH range. As previously seen, this sample always exhibits a negative charge (see Fig. 5.7), but it is only above a pH of 6 to 7 that the charge is sufficiently strong to provide good colloidal stability that allows a spontaneous separation into a chiral nematic phase. In the present case, such a phenomenon was observed at a pH of 7 and at a chitin concentration of 5% (w/w). Fig. 5.11 shows the early stage of the phase separation. Typical tactoids, i.e. chiral nematic domains (19) are already formed in the suspension. The successive periodic birefringent bands corresponding to half the CN pitch are clearly visible in these tactoids. The value of the CN pitch in this case is ~40 μm. Eventually, these individual mesomorphic drops will continue to grow, to coalesce and sediment to form a continuous CN phase at the bottom of the suspension, as previously reported for the non-sulfonated crystallites (20) if the suspension is fluid enough.

The effect of surface charge on the phase separation of rodlike particles has been treated theoretically by Onsager (32) followed by Stroobants et al.(33). Onsager indicated that the effect of electrostatic repulsion was equivalent to an increase of the effective diameter which depended on the thickness of the electrical double layer. The increase of the effective diameter will ultimately change the axial ratio and the concentration for phase separation. Stroobants et al. (21) extended the Onsager theory to include a twisting effect to minimize the free energy of the electrostatic interaction. The results from Stroobants' study show that the surface charge density has a strong effect on the phase separation concentration of rodlike particles. The Onsager theory has been confirmed by the experimental study of both positive (chitin crystallites) (20) and negative charged rodlike particles (cellulose crystallites) (30). In this work, the positive charge of chitin crystallites

Fig. 5.10. A TEM micrograph of N-sulfonated chitin crystallites with S/N=3.

1 μm

Fig. 5.11. Optical micrograph (viewed between crossed polarizers) of a 5% suspension (pH=7) of N-sulfonated chitin crystallites with S/N=5 showing tactoids viewed between crossed polarizers. The magnification is 250.

has been changed to negative while the formation of a chiral nematic phase was still observed. This is consistent with the theoretical prediction. Furthermore, we have found in this study that a critical surface charge density ($\approx$0.40 e/nm^2) is required to form chiral-nematic phase. Below this critical surface charge density, only the nematic phase is observed because of a low particle mobility.

5.4 CONCLUSIONS

In the present study, chitin crystallites were heterogeneously N-sulfonated using TEA/SO_3 or Pyr./SO_3. The former was a more effective reagent. The level of N-sulfonation was quantified using conductimetric titration and elemental analysis. The presence of N-S bonds was demonstrated by XPS. The colloidal properties of the N-sulfonated crystallites were examined using zeta potential measurements, which were found to be dependent on the pH of the suspension and the level of N-sulfonation. TEM micrographs have shown that the reaction does not change the rod-like shape of the crystallites and the homogeneity of the crystallite suspensions depends on the level of N-sulfonation. When N-sulfonation has reached S/N > 3, the suspension can phase separate after centrifugation to yield a CN phase. The tactoids formed from the 5% (w/w) crystallite suspension with S/N=5 at pH 7 was found to have a pitch of ~40μm. However, N-sulfonation of the crystallites is incomplete and probably non-uniform, thereby also causing some degree of aggregation in the colloidal suspension.

5.5 REFERENCES

1. Muzzarelli, R. A. A., *Chitin*, Pergamon Press, New York (1977).
2. Martinou, A., Kafetzopoulos, D. and Bouriotis, V., *Carbohydrate Res.*, 273, 235-242 (1995).

3. Kurita, K., In *Chitin in Nature and Technology*, Ed by Muzzarelli, R. A. A., Jeuniaux, C. and Goodway, G. W., Plenum, New York (1986).

4. Murta, J., Saiki, I., et al, *Jpn. J., Cancer Res.*, 80, 866-872 (1989).

5. Miyazaki, S., Yamaguchi, H., Yokouchi, C., Takada, M. and Hou, W. *J. Pharm. Pharmacol.*, 40, 642-643 (1988).

6. Li, Y. P., Machida, Y., Sannan, T. and Nagai, T., S. T. P. *Pharma Science*, 1, 363-368 (1991).

7. Nakatsuka, S. and Andrady, A. L., *J. Applied Polymer Science*, 44, 17 (1992).

8. Hirano, S. and Ohe, Y., *Agricultural and Biol. Chem.*, 39 (6), 1337 (1975).

9. Hirano, S., Kondo, S. and Ohe, Y., *Polymer*, 16, 622 (1975).

10. Kim, J. H., Kim, J. Y., Lee, Y. M. and Kim, K. Y., *J. Applied Polymer Science*, 45, 1711 (1992).

11. Yao, K. D., Peng, T., Feng, H. B. and He, Y. Y., *J. Applied Polymer Science*, 32, 1213 (1994).

12. Guan, Y. L., Shao, L. and Yao, K. D., *J. Applied Polymer Science*, 61, 2325 (1996).

13. Kurita, K., Ishii, S., Nishimura, S.-I., Yoshino, H. and Hashimota, S. In *Chitin Enzymology*, Ed by Muzzarelli, R. A. A.,European Chitin Society, Universiy of Ancona, Faculty of Medicine, IT-60100 Ancona, Italy.

14. Hirano, S., in *Chitin and Chitosan: Sources, Chemistry, Biochemistry, Physical Properties and Applications. Proceeding from the 4th International Conference on Chitin and Chitosan*, Ed. by Skjak-braek, G., Anthonsen, T. and Sandford, P., Elsevier Applied Science, New York (1989).

15. Ishihara, C., Shimakawa, S., Tsuji, M., Arikawa, J., and Tokura, S., *Immunopharmacology*, 29, 65 (1995).

16. Jorpes, J. E., Bostrom, H. and Mutt, V., *J. Biol. Chem.*, 183, 607 (1950).

17. Meyer, K. H. and Schwartz, D. E., *Helv. Chim. Acta*, 33, 1651 (1950).

18. Marchessault, R. H., Morehead, F. F. and Walter, N. M.,Nature, 184, 632 (1959).

19. Revol, J.-F. and Marchessault, R. H., *Int. J. Biol. Macromol.*, 15, 329 (1993).

20. Li. J., Revol, J.-F., Naranjo, E. and Marchessault, R. H., *Int. J. Biol. Macromol.* 18(3), 177 (1996).

21. Revol, J.-F., Godbout, L. and Farvier, V., PACIFICHEM "95, Honolulu, Hawai, Dec. 17-22 (1995).

22. Warner, D. and Coleman, L. L., *J. Organic Chemistry*, 23, 1133 (1958).

23. Holme, K. and Perlin, A. S., *Carbohydrate*, In press.

24. Wolfrom, M. L., Shen, T. M. and Summers, C. G., *J. Am. Chem. Soc.*, 75, 1519 (1953).

25. Wolfrom, M. L. and Shen, T. M., *J. Am. Chem. Soc.*, 81, 1764 (1959).

26. Stache, H. W., *Anionic Surfactants: Organic Chemistry*, Surfactant Science Series, 56, Marcel Dekker, Inc., New York (1995).

27. Sandler, S. R. and Karo, W., *Organic Functional Group Preparations*, Vol. 3, pp 147, Academic Press, New York (1989).

28. Idage, S. B., Badrinarayanan, Vernekar, S. P., and Sivaram, S., *Langmuir*, 12, 1018 (1996).

29. Carlström, D., *J. Biophys. Biochem. Cytol.*, 3, 669 (1957).

30. Dong. X, Kimura, T., Revol, J.-F., Gray, D. G., *Langmuir*, 12, 2076 (1996).

31. Collings, P. J., *Liquid Crystals; Nature's Delicate Phase of Matter*, Princeton University Press, Princeton, New Jersey (1990).

32. Onsager, L., *Ann. N. Y. Acad. Sci.* 51,627 (1949).

33. Stroobants, A., Lekkerkerker, H. N. W. and Odijk, Th., *Macromolecules*, 19, 2232 (1986).

Chapter 6
GENERAL CONCLUSIONS

6.1 SUMMARY

In this dissertation the self-assembly of chitin crystallites in suspensions which mimics the natural organization in arthropod shells has been investigated (1). The formation of a chiral nematic phase in chitin and surface modified chitin crystallite suspensions, and the phase separation of the suspensions of these crystallites under different experimental conditions have been explored using FFTEM, phase diagrams, a polarised optical microscope study, etc.

In Chapter 2, chitin crystallites prepared from crab chitin by HCl hydrolysis were found to be positively charged by conductimetric titration and zeta potential measurements. FFTEM revealed that the crystallites, having an average size of 200 nm in length by 8 nm in width in suspensions, were partially aggregated. The study by polarised optical microscopy showed that chitin crystallites in suspension first formed tactoids and then sedimented to form a chiral nematic phase.The phase diagrams of the suspensions of chitin crystallites with different ionic strengths indicated that the effect of the ionic strength in the suspensions on the boundary concentrations of phase separation was not significant. The thicknesses of the effective repulsive layer estimated both from the phase diagrams according to Onsager's theory and from the computed interaction energy curves derived from the Poisson-Boltzmann equation using the experimental zeta potential as the surface potential were comparable. When the contribution of crystallites to the ionic strength was taken into account and an hypothetical linear charge density close to the Manning limit was assumed, there was good agreement with the Debye length.

Chapter 3 showed that the flow properties of isotropic, biphasic ,and anisotropic suspensions of chitin crystallites could be studied rheologically. Shear thinning behaviour and a two-regime flow curve were observed for isotropic and biphasic suspensions of chitin crystallites respectively. A typical flow behaviour for LCPs: the three-regime flow curve, is observed for the anisotropic suspension of chitin crystallites. Compared with the dry diameters of chitin crystallites reported in Chapter 2, the average hydrodynamic diameter of chitin crystallites in a pH 4 suspension was determined to be 80 nm by dynamic light scattering. The maximum viscosity in the viscosity-concentration curve was found at the concentration of the phase transition from isotropic to biphasic. It was found that the secondary electroviscous effect due to electrostatic interactions between particles influenced the viscosity at higher concentrations.

In Chapter 4, chitin crystallites were systematically modified using NaOH hydrolysis. The reaction was found to be pseudo first order. Swollen crystallites were suggested as a reaction system. The crystallinity of the crystallites decreased after alkali treatment. After acid hydrolysis, a linear relationship was observed between the weight loss and the degree of deacetylation of the samples. Compared with the original chitin, the modified chitin crystallites showed a higher surface charge density by conductimetric titration. The phase diagrams showed that the suspension of the crystallites with a lower surface charge density separated first. This observation contradicts the theoretical prediction by Stroobants (2). The explanation for this observation is that the contribution of the highly charged chitin crystallites to the ionic strength of the suspension was not negligible, especially when it is close to Manning limit.

Chapter 5 covers the surface N-sulfonation of chitin crystallites, the characterization of the N-sulfonated chitin crystallites, and the study of the colloidal and liquid crystal properties of N-sulfonated chitin crystallites. Chitin crystallites were heterogeneously N-sulfonated in an aqueous medium using TEA/SO_3. The extent of N-sulfonation was

controlled by the amount of TEA/SO_3 used in the reaction. The sulfur concentration in the N-sulfonated crystallites was determined by conductimetric titration and elemental analysis. The results from both methods were comparable. The colloidal properties of N-sulfonated chitin crystallites were investigated by plotting the zeta potential of the suspension as a function of the pH of the suspension. It was found that zeta potential depended on both the pH of the suspension and the extent of N-sulfonation. The formation of tactoids was observed when the extent of N-sulfonation reached above 80%. Below this level, only nematic liquid crystals were observed in the suspension of N-sulfonated chitin crystallites. TEM micrographs showed that there was less aggregation for the highly N-sulfonated crystallites.

The freeze-fracture and freeze-etching transmission electron microscopy (FF/FETEM) study suggests that in an anisotropic phase, chitin crystallites first orient in parallel to form sheets and these sheets stack over each other helicoidally. This supports the model that Nevill proposed for the organization of chitin crystallites in natural systems such as in crab shells and cuticles.

Finally, does the self-assembly of chitin crystallites in nature go through a liquid crystalline phase? Although there is no direct evidence found, the study from this thesis shows that it is possible for chitin crystallites to self-organize through a liquid crystalline phase because only a small amount of charge is needed to maintain the mobility of crystallites and nature provides this through deacetylation.

6.2 CLAIMS TO ORIGINAL RESEARCH

1) The dynamic process of phase separation of chitin crystallites in suspensions showing that tactoids formed first and then sedimented to form a chiral nematic phase was observed under a polarized optical microscope.

2) The FFTEM study revealed that the chitin crystallites were slightly aggregated in

parallel in suspensions.

3) The charge properties of chitin crystallites under different experimental conditions have been characterized using zeta potential measurements.

4) The surface charge density of the crystallites when fully protonated was calculated to be 0.5 e/nm^2 based on conductimetric titration data.

5) The effect of the ionic strength in the suspension on the boundary concentration of phase separation for crystallite suspensions was studied through phase diagrams of suspensions with different ionic strengths.

6) The thickness of the repulsive layers has been estimated both from phase diagrams according to Onsager's theory (3) and from the interaction energy curves derived from the Poisson-Boltzmann equation using the experimental zeta potential as the surface potential.

7) Shear thinning behaviour and a two-regime flow curve were found for isotropic and biphasic suspensions of chitin crystallites respectively.

8) A typical three-regime flow curve for LCPs is found for the anisotropic suspension of chitin crystallites.

9) A viscosity maximum in the viscosity-concentration curve was observed at the concentration of phase separation.

10) The effect of the secondary electroviscous factor on the viscosity of the suspension has been investigated.

11) The pK_a and pK_0 of the crystallites were determined to be 6.3 and 7.5 respectively based on the conductimetric and pH titration data.

12) The reaction of NaOH hydrolysis of chitin was found to be pseudo first order.

13) The swollen crystallites has been suggested as a reaction system.

14) The weight of the crystallites after HCl hydrolysis was found to increase with the DD of the samples linearly.

15) The phase diagrams of the suspensions of the modified chitin crystallites were constructed.

16) It was shown that for the highly charged crystallites the contribution of the crystallites to the ionic strength of the suspensions was significant.

17) The chitin crystallites were N-sulfonated in an aqueous medium using TEA/SO_3.

18) The formation of tactoids was observed for the highly N-sulfonated crystallites.

19) The colloidal properties of the N-sulfonated crystallites were investigated by plotting the zeta potential of the suspension as a function of the pH.

20) The results are compared with the theoretical predictions by Onsager (3).

21) That a critical surface charge density is needed for the formation of a chiral nematic phase. It has been suggested.

22) The helicoidal stacking of chitin crystallite sheets has been observed in the anisotropic phase of chitin crystallite suspensions

6.3 SUGGESTIONS FOR FUTURE WORK

1) The freeze-fracture TEM study has revealed the *in situ* texture, aggregation level, etc. of chitin crystallites in suspensions. More study is needed to focus on examination of the replicas from the chiral nematic phase and to show the *in situ* organization of a chiral nematic phase and the distance between the rods. In addition, cryo-TEM is another technique to examine the texture of the chiral nematic phase.

2) Rheologically the suspensions of the different phases: isotropic, biphasic, and anisotropic, has been investigated. Experimentally, the structural transformation of chiral nematic domains during shear needs to be investigated. Several experiments can be done to demonstrate this. Neutron scattering under shear can reveal the change of the order parameter of chitin crystallites with shear rate and the distance

between crystallites. Furthermore, a rheo-optical system with different light sources can be built to study the texture change of the anisotropic domains of chitin crystallites during shear. It would also be of interest to investigate the elastic relaxation of the biphasic and anisotropic suspensions.

3) As for N-sulfonated chitin crystallites, photoacoustic infrared spectroscopy can be used as a complementary technique to prove the presence of N-S bonding in the sample.

4) Colloidal crystals are very interesting to many researchers. The colloidal crystals of chitin crystallites can be prepared from a suspension of chitin crystallites by applying an electrical field to the platinum electrode cell containing the crystallites.

5) N-sulfonated chitin crystallites have shown some antibacterial activities. This material can be a candidate for drug delivery applications. Further tests of chitin crystallites as a drug releasing agent is needed. In addition, a composite membrane of chitin crystallites, cellulose crystallites, N-sulfonated chitin crystallites, and chitosan can be prepared for wound dressing applications. Chitin crystallites have potential to replace the cellulose crystallites in many applications including suspension stabilizer, viscosity modifier for gels. More research is required to explore this area.

6) The crystalline structure of chitin crystallites in concentrated NaOH (above 40%) needs to be explored using X-ray diffraction.

6.4 REFERENCES

1. Revol, J.-F. and Marchessault, R. H., *Int. J. Biol. Macromol.*, **15**, 329 (1993).

2. Stroobants, A., Lekkerkerker, H. N. W. and Odijik, Th., *Macromolecules*, **19**, 2232 (1986).

3. Onsager, L., *Ann. N. Y. Acad. Sci.*, **51**, 627 (1949).

Appendix 1

EXPERIMENTAL TECHNIQUES: PRINCIPLES AND INSTRUMENTATION

A1.1 ZETA POTENTIAL MEASUREMENT (1,2,3)

Surface potential is an electrostatic potential between the surface of charged particles and the bulk of suspensions. The governing equation for charged particles in a electrolyte solution is the Poisson-Boltzmann (P-B) equation. Using the Debye-Hückel approximation, the P-B equation can be simplified to an ordinary differential equation. The solution of this equation gives a potential, ψ, which is a function of distance from the particle surface. Surface potential, ψ_0, is the potential at zero distance. Because adsorption of counterions at the surface is so strong that they become part of the surface, normally the potential, ψ_s, at the surface of the adsorbed counterion layer (Stern layer) is taken as the surface potential. In practice, only the ζ potential, a potential at the slipping plane, can be determined electrokinetically. It is generally assumed in tests of double-layer theory that the ζ potential and ψ_s are the same.

The ζ potential can be determined using several methods including electrophoresis, electro-osmosis, streaming potential, etc. Electrophoresis is by far the most common procedure for determining ζ. What is electrophoresis? When an electric field is applied to a suspension of particles, the particles migrate with the field owing to the presence of the surface charge. This phenomenon is called electrophoresis. The electrophoretic mobility of particles is defined as:

$$\mu \equiv \mathbf{V/E} \qquad \text{(A1.1)}$$

where V is the velocity of the particles and E is the field strength. Based on Henry's Equation (1,2):

$$\mu = V/E = 2\zeta\epsilon/3\eta \times F(\kappa a, K') \qquad (A1.2)$$

where ζ is the zeta potential, ϵ is the dielectric constant, a is the radius of particles, η is the viscosity of the suspension, and F is a factor depending the double layer thickness(κ^{-1}) and particle shape. For non-conducting cylinders, F = 1.5 for all κa values and the equation A1.2 is reduced to:

$$\mu = \zeta\epsilon/\eta \qquad (A1.3)$$

$$\text{or} \quad \zeta = \mu\eta/\epsilon \qquad (A1.4)$$

Experimentally, the measurement of the electrophoretic mobility of colloidal particles requires the preparation of the colloidal suspension, transferring the suspension into the measuring cell, applying an external field, and determining the velocity of the particles. Most modern instruments measure the velocity of particles based on monitoring individual particles by visualizing the particles using a laser light scattering technique. For the experiments in this thesis, The Lazer Zee meter (Model 501) with a rectangular cell from Pen Kem Inc.was used. This instrument incorporates a prism which rotates with a speed controlled manually by the observer, so that the motion of the particles is just compensated by the prism rotation and the particles appear to be stationary. The zeta potential calculated using Eq.1.4 (Smoluchowski equation) is displayed on a digital voltmeter. The instrument was calibrated using latex colloid standard (-55 mV at pH 9).

A1.2 MEASUREMENTS OF RHEOLOGICAL PROPERTIES (4,5)

Rheology is the science or study of how things flow under the influence of external forces. The basic law of rheology is:

$$\tau = \eta \times \dot{\gamma} \qquad \text{(A1.4)}$$

where τ is shear stress, η is viscosity, and $\dot{\gamma}$ is shear rate. Shear stress is a force (F) per unit of area (A), which is expressed as:

$$\tau = F/A \qquad \text{Newton/ M}^2 \text{ (Pascal)} \qquad \text{(A1.5)}$$

Shear rate is a velocity change with distance between parallel measuring surfaces that one of which moves at a velocity V while separated by a distance y from the other (see the *schematic* below). It is expressed as follows:

$$\dot{\gamma} = dV/dy \text{ (1/s)} \qquad \text{(A1.6)}$$

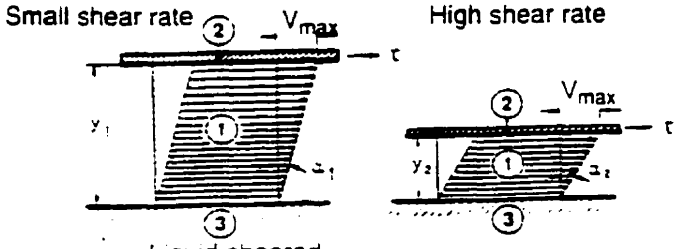

1 Liquid sheared
2 Moving plate with shear area A to contact the liquid below
3 Stationary plate

***Schematic* showing the flow between two plate**

For Newtonian liquids including water, mineral oil, bitumen, etc., η is a constant regardless of changes in $\dot{\gamma}$. For non-Newtonian liquids such as solution of rodlike polymers, polymer suspensions, etc. η varies with γ in Eq. A1.5.

The rheometer used was a Bohlin VOR system with a Couette configuration that was based on rotating the sample and measuring its response to the applied stress by a variety of sensors (see Fig. A1.1 for schematic). In this system, the outer cylinder rotates at a defined speed and the torque is transmitted to the inner cylinder, and the measuring sensor measures the force required to hold the inner cylinder at still. The inner cylinder is connected to a torsion bar and a device monitors the deflection of the torsion bar by an electronic transducer. The shear rate and shear stress for this system are expressed as:

$$\dot{\gamma} = P \cdot V \tag{A1.7}$$

where P is the geometric constant depending the radius of the outer and inner cylinders.

$$\tau_i = K \cdot S \tag{A1.8}$$

where K is a constant depending on the shape of the inner cylinder and the torsion bar, and S is a signal from the instrument. Therefore, viscosity is:

$$\eta = \tau_i / \dot{\gamma}_i = KS/PV = (K/P)(S/V) \tag{A1.9}$$

The instrument was calibrated using silicon oil standard with a viscosity of 8.9 cP (Brookfield standard) before measuring the samples. A straight horizontal line was obtained. The measurment parameters including shear rate, temperature, delay time, etc. are controlled by a computer program.

A1.3 ^{13}C SOLID STATE NMR (7)

Solid state ^{13}C NMR spectra were recorded using cross polarization magic angle-spinning (CP/MAS) at 75 MHz on a Chemagnetics CMX-300 Spectrometer. Powder samples of chitin were first inserted into a 7.5 mm zirconia rotor. A contact time of ~2.0 ms and a recycle delay of 2s were employed. A magic angle spinning rate of 5 kHz was used. A typical spectrum of chitin is shown in Fig. A1.2. The degree of acetylation of chitin (%), defined as the percentage of -$NHCOCH_3$ per glucose ring, can be evaluated by comparing the integrated peak area of the methyl group with the integrated area of the glucose ring carbon peaks in the ^{13}C NMR spectrum (C_1, C_2, C_3, C_4, C_5, and C_6), as shown in Fig. 1.1, with the integrated area of the glucose ring carbon peaks set to 600 (8). For complete acetylation, The peak area for the methyl group is 100. The degree of deacetylation is expressed as:Degree of Deacetylation (%) = 100 - Degree of Acetylation (%).

A1.4 TRANSMISSION ELECTRON MICROSCOPY (TEM)

The TEM instrument used was a Philips EM 400 operated at 120 kV for imaging by diffraction contrast in the bright field mode. The optics system of the TEM is shown in Fig. A1.3 (9). The electron beam is collimated onto the sample by two condenser lenses. A real magnified image is formed by the objective lens and is further magnified to form an image on a screen or on a Kodak photographic film. In the bright field mode, only the direct unscattered beam is used to form the image (see Fig. A1.4).

A1.5 REFERENCES

1. Hunter, R. J., *Zeta Potential in Colloid Science: Principles and Applications*, Academic Press, New York (1988).
2. Masliy, J. H., *Electrokinetic Transport Phenomena*, Alberta Oil Sands

Technology and Research Authority, Edmonton (1994).

3. Myers, D., *Surfaces, Interfaces, and Colloids: Principles and Applications*, VCH Publishers, Inc., New York (1991).
4. Laba, D., *Rheological Properties of Cosmetics and Toiletries*, Marcel Dekker, Inc., New York (1993).
5. Macosko, c., *Rheology: Principles, Measurements and Applications*, VCH Publishers, Inc., New York (1994).
6. Alexander, L. F., *X-ray Diffraction Methods in Polymer Science*, Wiley-Interscience, Toronto (1969).
7. Fyfe, C. A., *Solid State NMR for Chemists*, C.F.C. Press, Guelph, Ontario (1983).
8. Pelletier, A., Lemire, I., Sygusch, J., Chornet, E. and Overend, R. P., *Biotechnol. Bioeng.*, **36**, 310 (1990).
9. Raymond, L. M., *Nanocomposite Cellulosics Prepared by the In Situ Synthesis of Ferrites*, Ph.D Thesis, Department of Chemsitry, McGill University (1995).

Fig. A1.1. Schematic diagram of the Bohlin VOR rheometer. A DC motor with tachometer A drives gear box B, which drives the timing belt to provide steady rotation of the shaft. When the electromagnetic clutch C is activated, the eccentric arm D can oscillate the shaft sinusoidally. The sample cell is surrounded by a temperature control bath E. An air bearing F centres a torsion bar H, whose rotation is sensed by linear variable differential transformer.

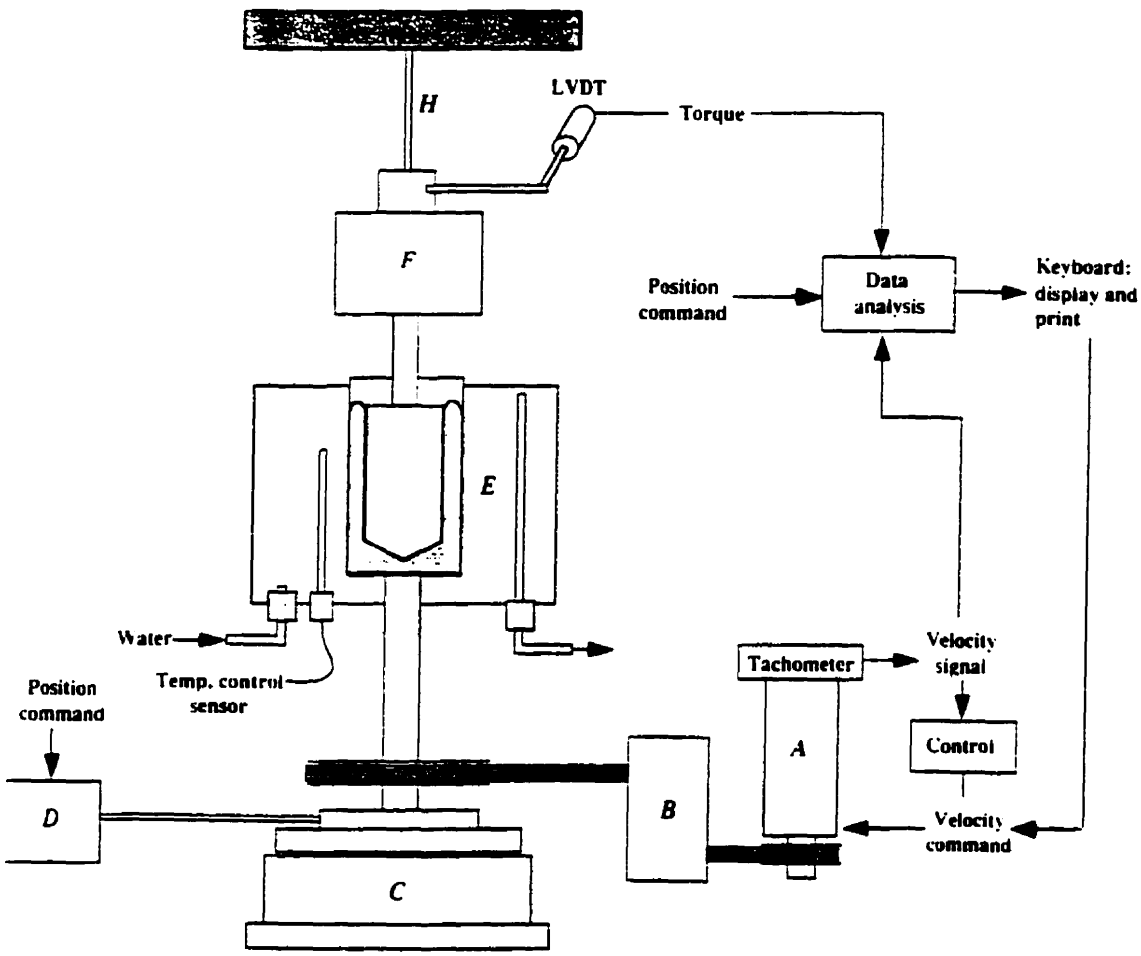
H
LVDT
Torque
F
Position command
Data analysis
Keyboard: display and print
E
Water
Temp. control sensor
Position command
Tachometer
Velocity signal
A
Control
D
B
Velocity command
C

Fig. A1.2. A typical CP-MAS ^{13}C NMR spectrum of chitin.

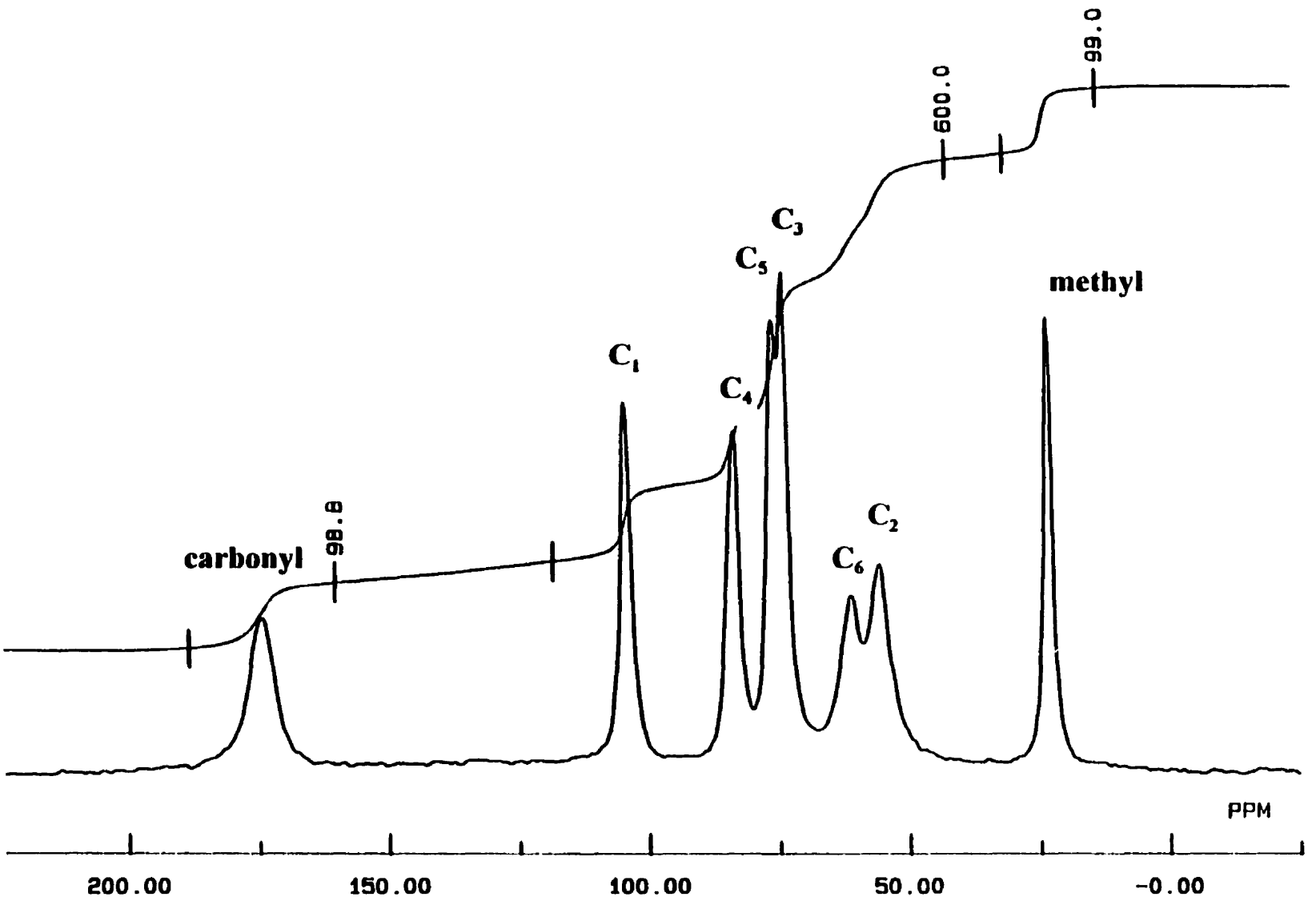
99.0
600.0
98.8
carbonyl
C1
C4
C5
C3
C2
C6
methyl
PPM
200.00
150.00
100.00
50.00
-0.00

Fig. A1.3. The optics system in TEM.

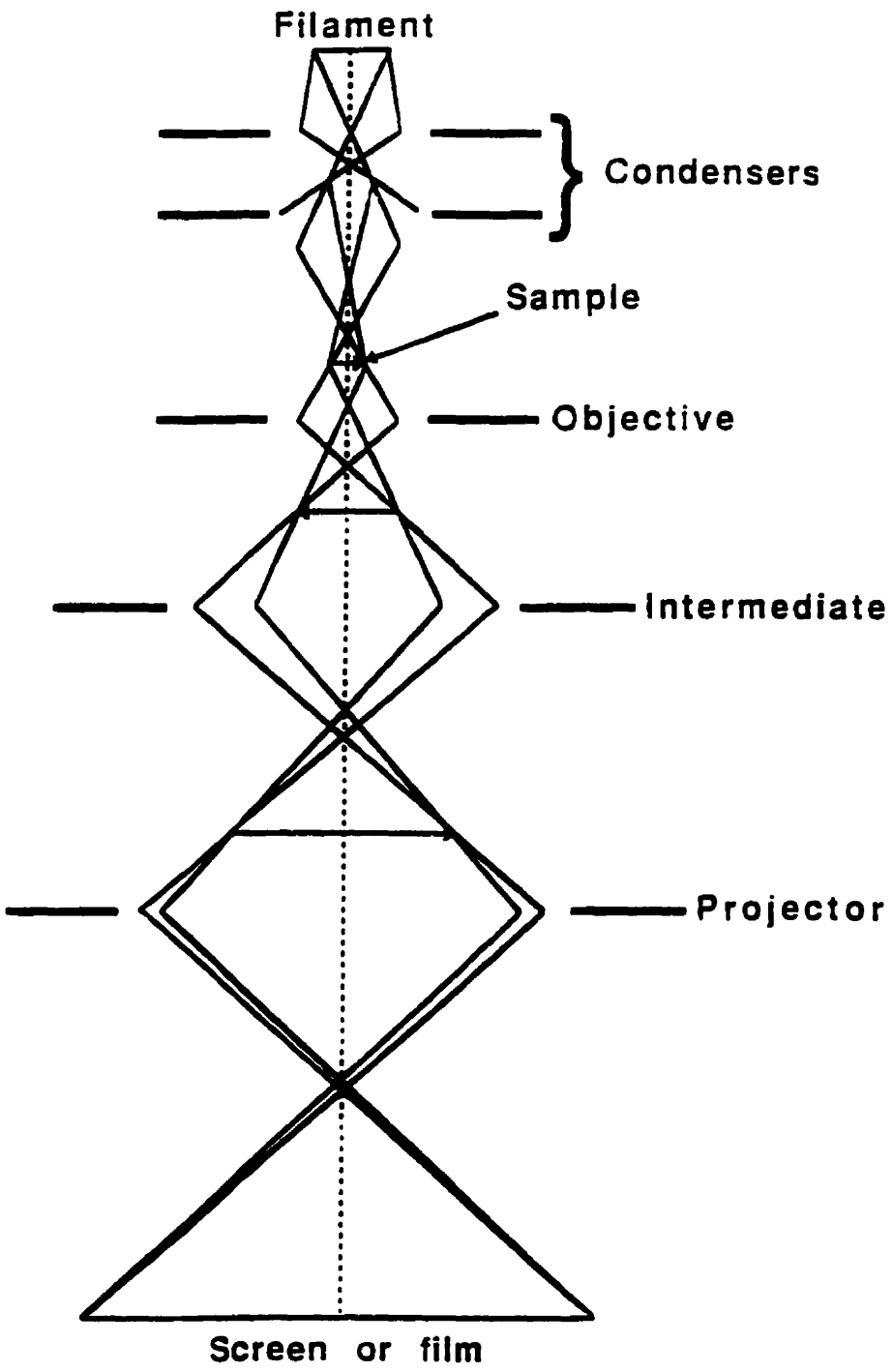
Filament
Condensers
Sample
Objective
Intermediate
Projector
Screen or film

Fig. A1.4. Imaging by diffraction contrast in TEM.

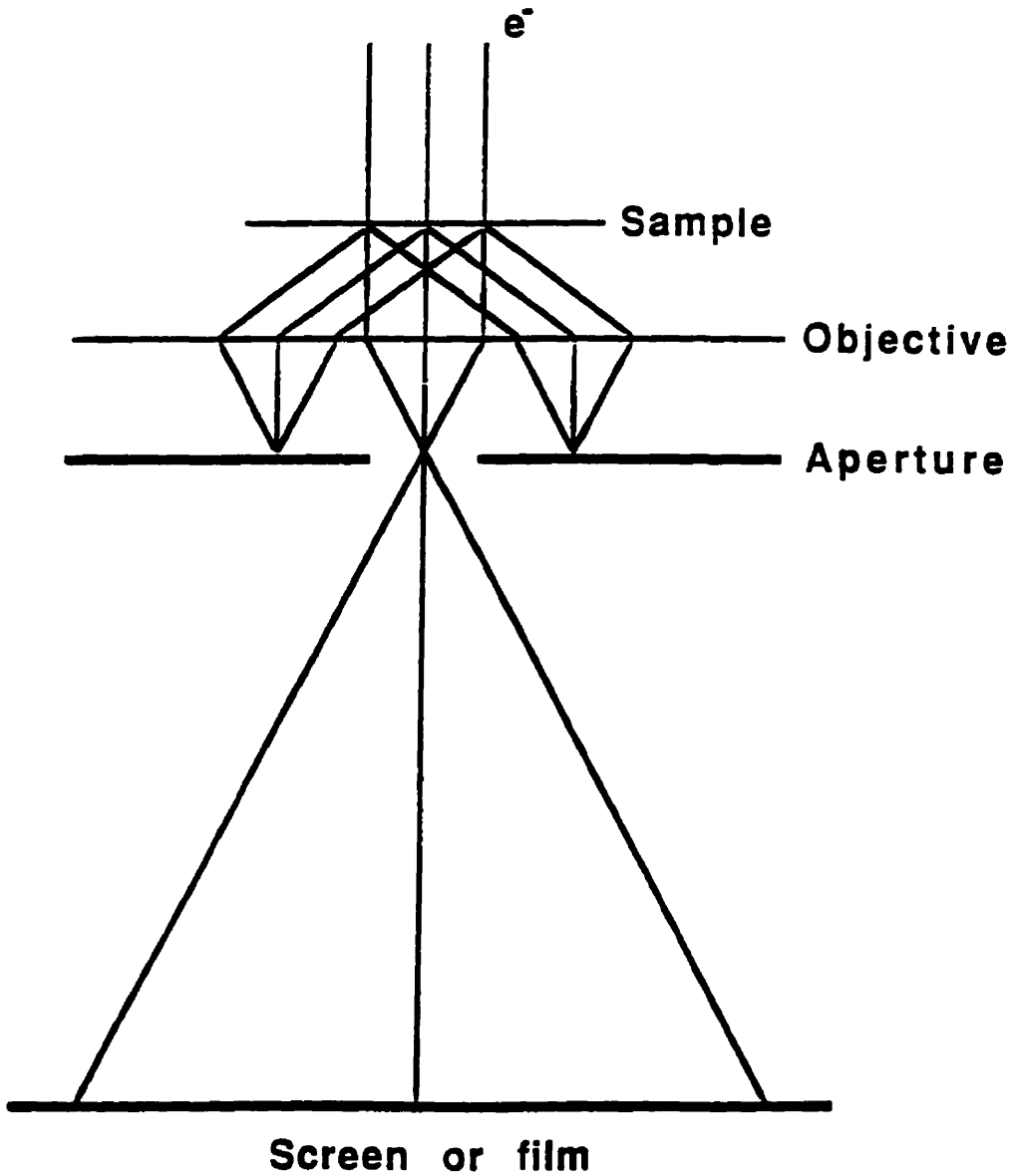
e⁻
Sample
Objective
Aperture
Screen or film

Appendix 2

ESTIMATION OF THE SURFACE CHARGE DENSITY OF CHITIN CRYSTALLITES

The surface charge density of chitin crystallites is estimated from the density of chitin, the average size of the crystallites and the amount of surface charge for 1 g of hydrolysed chitin derived from conductmetric titration. The calculation is as follows:

Chitin density: 1.425 g/(cm)^3.

The average size of a chitin crystallite is 200 nm in length and 8 nm in width.

The volume of 0.01 M NaOH required for titrating 1 g of hydrolyzed chitin is 30 ml.

The volume of one chitin crystallite is:

$$V_{crystallite} = 200 \times 8 \times 8 = 12800\ (nm)^3 = 12800 \times (10^{-7})^3\ (cm)^3 \quad (A2.1)$$

The number of crystallites per g sample is:

$$N = 10^{21}/(1.425 \times 12800) = 5.483 \times 10^{16} \quad (A2.2)$$

Hence, the surface area of one crystallite is:

$$A_{crystallite} = 200 \times 8 \times 4 + 128 = 6528\ (nm)^2 \quad (A2.3)$$

The overall surface area for one gram sample is:

$$A = 5.483 \times 10^{16} \times 6528 = 3.579 \times 10^{20}\ (nm)^2 \quad (A2.4)$$

Therefore, the surface charge density is:

$$\sigma = 30 \times 0.01 \times 10^{-3} \times 6.023 \times 10^{23}/(3.579\ 10^{20}) = 0.5049\ (1/nm^2)$$

Appendix 3

FREEZE-FRACTURE AND FREEZE -ETCH TRANSMISSION ELECTRON MICROSCOPY (FF/FETEM) RESULTS OF ISOTROPIC AND ANISOTROPIC PHASES OF CHITIN CRYSTALLITES

In a preliminary experiment conducted under the close supervision of Dr. Vali (Department of Earth and Planetary Science) at the Department of Anatomy, both isotropic and anisotropic phases of chitin crystallites have been examined using FF/FETEM instrument in the Department of Anatomy and Cell Biology, McGill University. Results are shown in Fig.A3. 1. For the isotropic phase, the results are comparable with those obtained Using the FFTEM instrument of the Department of Chemical and Nuclear Engineering, the University of California, Santa Barbara (see Chapter 2 for discussion). For the anisotropic phase, twisted and possibly stacked layers of crystallite sheets are observed (see Fig.A3.1). In each layer, crystallites are oriented in parallel to form a sheet, thus direction of the crystallites changes through a small angle from one layer to another. This is consistent with the current model for the structure of self-assembled chitin crystallites in natural systems including crab shells and cuticles (see Chapter 1). In addition, some crystallites are found twisted along the fibre axis.

A3.1 EXPERIMENTAL PROCEDURE

A 4% chitin suspension with a pH of 4 was left in a refrigerator for a week. After phase separation, the top isotropic (3.3%, w/w) and bottom anisotropic phases (4.8%, w/w) were transferred into 10 ml vials using syringe respectively. Freeze-fracture and freeze-etch was performed using a Balzers 300 apparatus. Small drops (1-2 μl) of suspensions were transferred to the gold sample holders followed by plunging into liquid

nitrogen-cooled liquid Freon 22 (monochlorodifluoromethane, -160°C). For the anisotropic phase, the suspension was allowed to equilibrate for 5 minutes before freezing to minimize the shear effects due to sample transfer. After 3-4 seconds, the samples were transferred onto a specimen holder immersed in liquid nitrogen prior to insertion into the freeze-fracture apparatus (-100 to -120 °C specimen holder). The samples were fractured with a liquid N_2-cooled (-196°C) knife under high vacuum. Freeze-fracture and freeze-etch replicas were obtained using an etching time (-100°C) of 60 s. The fractured plane was shadowed with 2.5 nm of platinum/carbon at an angle of 30° and subsequently coated with 25 nm carbon at an angle of 90° to strengthen the replica. The Pt/C replicas were floated off onto a distilled water followed by cleaning with 10% HF solution, transferred to uncoated Cu TEM grids and carefully washed with $CHCl_3$. The replicas were examined using a Philips EM400 microscope operating at 80 kV accelerating voltage.

Fig.A3.1 Freeze-fracture and freeze-etch TEM micrographs of isotropic (3.3%, w/w) and anisotropic phases (4.8%, w/w) of chitin crystallites with a pH of 4. The micrograph at top is for the isotropic phase and the micrograph at bottom is for the chiral nematic phase. The magnification is 30000.